E.O. Paton Electric Welding Institute of the National Academy of Sciences of Ukraine

International Scientific-Technical and Production Journal

# The Paton WELDING JOURNAL

**January 2013**
**No.1**

**Published since 2000**

English translation of the monthly «Avtomaticheskaya Svarka» (Automatic Welding) journal published in Russian since 1948



**Founders**
E.O. Paton Electric Welding Institute of the NAS of Ukraine, International Association «Welding»

**Publisher**
International Association «Welding»

*Translators:*
A.A.Fomin, O.S.Kurochko, I.N.Kutianova, T.K.Vasilenko
*Editor*
N.A.Dmitrieva
*Electron galley*
D.I.Sereda, T.Yu.Snegiryova

**Address**
E.O. Paton Electric Welding Institute, International Association «Welding»
11, Bozhenko str., 03680, Kyiv, Ukraine
Tel.: (38044) 200 82 77
Fax: (38044) 200 81 45
E-mail: journal@paton.kiev.ua
www.paton.kiev.ua
URL: www.rucont.ru

State Registration Certificate
KV 4790 of 09.01.2001
ISSN 0957-798X

**Subscriptions**
$348, 12 issues per year, air postage and packaging included.
Back issues available.



## CONTENTS

# FEATURES OF CURRENT PROTECTION OF POWER SOURCES FOR EBW

**O.K. NAZARENKO, O.A. GURIN** and **E.I. BOLGOV**
E.O. Paton Electric Welding Institute, NASU
11 Bozhenko Str., 03680, Kiev, Ukraine. E-mail: office@paton.kiev.ua

The purpose of investigations was elaboration of recommendations to reduce disturbances of weld formation during EBW, if current protection of accelerating voltage source has operated because of vacuum breakdown in the welding gun, or if specified value of beam current was exceeded because of short-circuiting in the control electrode–cathode circuit. In view of the random nature of development of the mentioned transient processes, normally-open shorting plug of control electrode–cathode circuit and discharger with adjustable interelectrode gap were temporarily built into the accelerating voltage source between the cable conductor connected to control electrode and ground. This allowed closing any of the circuits and recording load current and accelerating voltage directly during welding, which was followed by comparison of oscillograms with the occurring disturbance of weld formation. It is found that in order to reduce the disturbances of weld formation at breakdown in the gun, the high-voltage source should go into the mode of automatic re-starting during the time of about 0.1 ms. The current threshold of this transition should 3–4 times exceed the maximum load current of the source, allowing for starting current at asynchronous switching on of the power source, and charging currents of capacitances of high-voltage cable and output filter. At short-circuiting in the control electrode–cathode circuit, the accelerating voltage source should automatically go into the mode of beam current stabilization after exceeding its set value by 20–30 % for 3–5 ms. 3 Ref., 1 Table, 4 Figures.

***Keywords:*** *electron beam welding, accelerating voltage source, three-electrode emission system, accelerating gap breakdowns, short-circuiting of control electrode to the cathode, physical modelling, requirements to current protection*

In welding gun emission system breakdowns can develop in vacuum insulation between control electrode and anode. Gap between control electrode and cathode is often bridged by drops of molten metal from the weld pool. Violation of electrical insulation between the high-voltage cable conductors connected to cathode and control electrode is also possible. In all these cases an uncontrolled beam current rise takes place, disturbing weld formation.

Abrupt switching off of accelerating voltage source at operation of maximum current protection is highly undesirable, as it causes a serious weld defect in the form of a through-thickness crater, unfilled with liquid metal. Therefore, it is first of all necessary to minimize disturbance of weld formation, and only after that disconnect accelerating voltage source. If the source was switched off, then in case of its asynchronous restarting current protection operation is inadmissible, because of power source starting current, which is much higher than the operating current, because of a surge of magnetization current of the power source [1], and charging current of capacitances of high-voltage cable and output filter. These are exactly the currents, which at automatic re-starting of the source, even in the mode of the so-called soft, i.e. delayed start, can cause false operation of current protection, if its time delay is absent and too low operation threshold is set.

This work is devoted to experimental study of algorithms and dynamics of current protection operation at breakdowns and current overload in the gun, in order to reduce disturbances of weld formation.

**Investigation procedure.** High-voltage inverter power source of 6 kW power with 60 kV accelerating voltage was used in the study. It was created as a result of cooperation of the teams of PWI and «Torsion» Company (Kharkov). At up to 0.1 A load currents the source operates in the mode of accelerating voltage stabilization. Because of the presence of current sensor in the load circuit, at short-circuiting the voltage stabilizer can go into current stabilization mode, thus limiting the load current. Connected at high-voltage filter output is a ballast resistor, limiting the maximum amplitude of current through output high-voltage rectifier at short-circuiting in the load and preventing development of parasitic resonance processes in output cable [2].

Random nature of vacuum breakdown development makes it difficult to record its electric

and time parameters to compare them with weld formation disturbances. Therefore, normally-open shorting plug of control electrode–cathode circuit and discharger with adjustable interelectrode gap were temporarily built into the high-voltage power source between the cable conductor connected to control electrode and ground (Figure 1). This allows directly during welding of the sample closing any of the circuits, recording the oscillograms of load current and accelerating voltage at a selected moment, and comparing them with the occurring disturbance of weld formation. Used as a recorder was digital electronic oscillograph Tektronix TDS-2014 with the bandwidth of 100 MHz and sampling frequency of 1 Gsamp/s.

**Results and their discussion.** Experimental studies revealed the need for applying various approaches to operating algorithms of power source current protection, in order to enable performance of EBW at simulation of breakdowns in the gun and at short-circuiting of control electrode–cathode circuit (diode mode of gun operation).

Figure 2 gives oscillograms of beam current and accelerating voltage at simulation of electric breakdown between the control electrode and anode of the gun directly during welding. Accelerating voltage source is forcedly switched into the mode of automatic re-starting, in order to prevent any serious disturbance of weld formation or malfunction of the source [3]. Duration of fronts of accelerating voltage cutting off and respective load current surge is equal to about 0.1 ms. Accelerating voltage is absent for 7.5 ms, that allows recovering the electric strength of vacuum gap of gun emission system. Then accelerating voltage is recovered slowly enough — in 2.5 ms — by the linear law.

Recovery of accelerating voltage can be performed much faster, but then metal splashing out of the weld pool can take place, because of the respective increase of beam current rising speed. Moreover, a soft start of accelerating voltage lowers the source starting current, and also slows down charging of capacitances of the filter and high-voltage cable, that enables a certain lowering of requirements to power source maximum current. Nonetheless, as follows from Figure 2, the value of load current surge at the moment of accelerating voltage re-starting reaches 0.35 A, i.e. it exceeds the maximum operating current of the source (0.1 A), by at least 3–4 times. Naturally, if the threshold of exceeding the admissible current is lowered, then even if the electric strength of the vacuum gap has already been recovered, false operations of source protection will be occurring for an unlimited time, and the welding process will not be able to recover. Note that

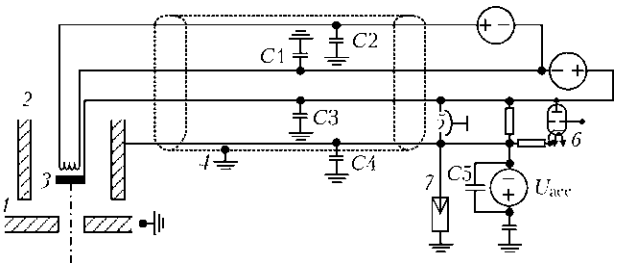


**Figure 1.** Schematic of experimental set-up: *1* — anode; *2* — control electrode; *3* — cathode; *4* — high-voltage cable; *5* — short-circuiting plug of control electrode–cathode circuit; *6* — beam current regulator; *7* — discharger with adjustable interelectrode distance; $U_{acc}$ — accelerating voltage source; *C*1–*C*4 — distributed capacitances of cable conductors relative to the ground; *C*5 — filter capacitance

in the absence of accelerating voltage the oscillogram records running of a certain load current, in all probability, between the cathode, which is at residual negative potential, and control electrode. At increase of accelerating voltage the transient current rises, its value being affected by beam current stabilization circuit. In the absence of serious malfunctions of instrumentation, total duration of recovery of normal operation of equipment is not more than fractions of a second and in the worst case, a repair welding pass over the region of weld formation disturbance is required.

In the considered case, switching the accelerating voltage source into the mode of automatic re-starting is much more efficient that forced switching of the accelerating voltage source into the current source mode, as current flowing results in maintaining of ionization processes in the vacuum gap, which prevent recovery of its electric strength.

Contrarily, as will be shown below, at emission system transition into the diode mode, forced switching of accelerating voltage source into current source mode turns out to be beneficial because of short-circuiting of control electrode–cathode circuit. At closing of this circuit, current rises up to a level, corresponding to completely

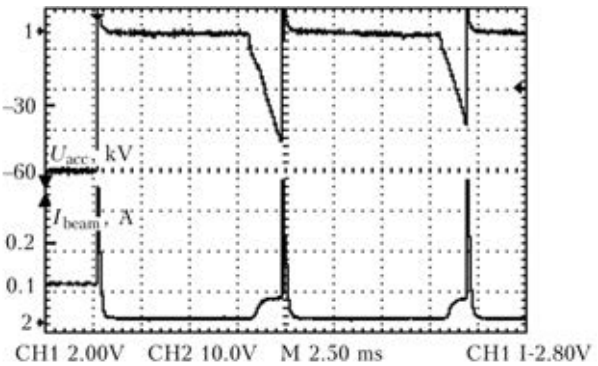


**Figure 2.** Dynamics of variation of beam current $I_{beam}$ and accelerating voltage $U_{acc}$ at simulation of electric breakdown in the gun in the vacuum gap of control electrode–cathode directly during EBW

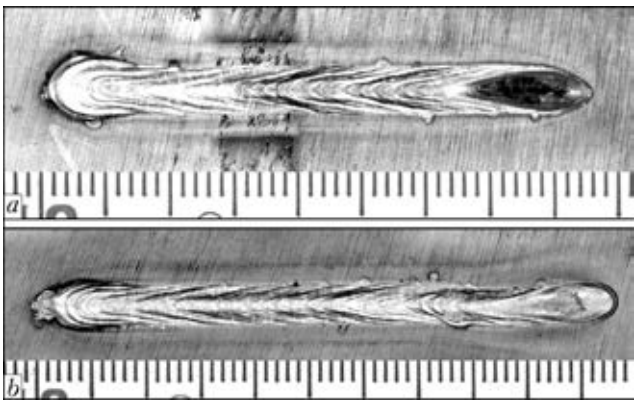

**Figure 3.** Appearance of welds interrupted at the moment of short-circuiting in control electrode–cathode circuit: *a* — formation of defect in the form of crater at cutting off of accelerating voltage by maximum current protection; *b* — defectfree completion of weld owing to source going from accelerating voltage stabilization mode into beam current stabilization mode

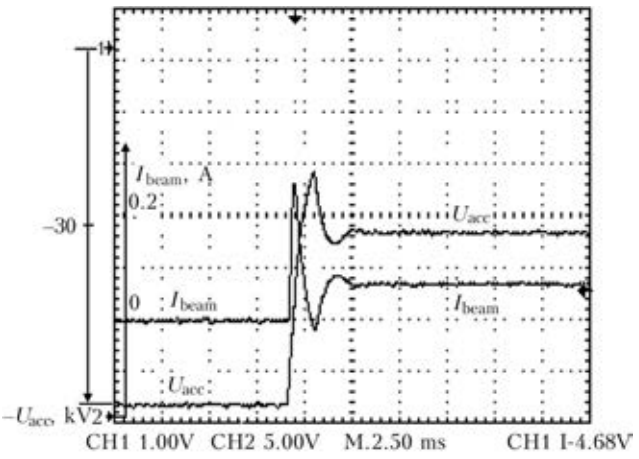


**Figure 4.** Dynamics of variation of beam current $I_{beam}$ and accelerating voltage $U_{acc}$ at simulation of short-circuiting of control electrode to cathode directly during EBW

Characteristics of current protection of power source for EBW

| Welding mode disturbance | Cause for disturbance | Algorithm of current protection operation | Operating time, ms |
|---|---|---|---|
| Beam current 3–4 times exceeded maximum load current of the source | Electric breakdown between the control electrode and anode | Forced switching of accelerating voltage source into the mode of its automatic re-starting | ~0.1 |
| Beam current reached the value corresponding to diode mode of gun emission system | Short-circuiting in control electrode–cathode circuit | Forced switching of the source from voltage stabilization mode into current stabilization mode | 2–5 |

unblocked emission system. Cutting off accelerating voltage at this moment leads to defect formation in the form of a deep crater unfilled with liquid metal and having numerous shrinkage cracks (Figure 3, *a*).

Switching accelerating voltage source into current source mode with respective lowering of accelerating voltage allows avoiding formation of this defect (Figure 3, *b*).

Figure 4 gives oscillograms of beam current and accelerating voltage at simulation of electric breakdown between control electrode and cathode of the gun. At the moment of short-circuiting of control electrode to the cathode, when the emission system goes into diode mode, beam current rises from the set value of 0.1 up to 0.25 A. After 3–5 ms current protection operates, in which programmed threshold is 0.13 A, i.e. is by 30 % higher than beam current level, and the voltage source goes into the mode of stabilization of this value. In order to maintain such current, the source generates a voltage of about 30 kV. Thus, beam power decreases from 6 to 3.9 kW, and, most importantly, at lowering of accelerating voltage the beam is refocused significantly (focal spot rises relative to item surface), that results in a considerable reduction of molten metal volume. A defect-free completion of weld formation without fixing of the crater takes place, after which the source can be switched off to perform the required reconditioning operations.

The Table gives optimum characteristics of current protection of accelerating voltage source.

## Conclusions

1. At breakdown in welding gun emission system, the high-voltage source should within about 0.1 ms go into the mode of automatic re-starting. Current threshold of this transition should be 3–4 times higher than the maximum load current of the source, allowing for starting current at asynchronous starting of the power source and charging currents of capacitances of the high-voltage cable and output filter.

2. At short-circuiting of control electrode–cathode circuit, the accelerating voltage source should automatically go into the mode of beam current stabilization after 20–30 % exceeding of its set value for 3–5 ms.

1. Shabad, M.A. (2011) *Maximum current protection*. Leningrad: Energoatomizdat.
2. Nazarenko, O.K., Matvejchuk, V.A. (2011) Limitation of overvoltages in high-voltage circuits after discharges in welding gun. *The Paton Welding J.*, **10**, 32–35.
3. Lebedev, V.K., Nazarenko, O.K., Lokshin, V.E. et al. *Method and apparatus for electron beam welding*. Pat. 3042652 DE. Publ. 02.04.82.

Received 15.10.2012

# INVESTIGATION OF STRESS-STRAIN STATE OF WELDED STRUCTURES FROM AUSTENITIC STEEL AT RADIOACTIVE IRRADIATION

**O.V. MAKHNENKO** and **I.V. MIRZOV**
E.O. Paton Electric Welding Institute, NASU
11 Bozhenko Str., 03480, Kiev, Ukraine. E-mail: office@paton.kiev.ua

Nuclear reactor reflection shield is exposed to high doses of radiation, leading to its noticeable deformation and closing of the clearance between the reflection shield and cavity wall. This leads to a change of heat exchange in the reactor core that may have hazardous consequences in terms of violation of temperature mode of reactor operation. To evaluate the radiative swelling of the reflection shield, a 2D finite element model was constructed, using calculation algorithms well-tested at the E.O. Paton Electric Welding Institute, in which isotropic volumetric deformations were assigned as radiative swelling. The model non-linearly takes into account the dependence of radiative swelling of the reflection shield material on irradiation temperature, stressed state and plastic deformations. The model also describes the change of yield limit of welded cavity wall, as a function of irradiation temperature and accumulated radiation dose. After 25 years of reactor operation the maximum value of swelling deformations in reflection shield material is equal to 1.3 %, reaching 1.8 after 40 years, and 3.7 after 60 years. Maximum radial displacements of the reflection shield outer surface during reactor operation are equal to 11.2 mm after 25 years, 12.9 mm after 40 years, and 16.1 mm after 60 years. In a more conservative model, not allowing for the history of volumetric deformation accumulation, reflection shield swells by 26 % over 60 years of operation that corresponds to even greater radial displacements of reflection shield outer surface in the outward direction. Results on swelling and radial deformations of the reflection shield derived allowing for the stressed state are indicative of a possible contact of reflection shield with the cavity welded wall during reactor operation. Such a contact can greatly affect the stress-strain state of the cavity welded structure, therefore, it requires a more detailed study. 9 Ref., 2 Tables, 14 Figures.

***Keywords:*** *welded metal structures, austenitic steel, stress-strain state, reflection shield, reactor service life, radiative swelling, numerical model, cavity wall*

In a nuclear reactor the energy source are rod-like radioactive fuel elements (FE). They are grouped into fuel element assemblies (FEA), forming the reactor core, which is surrounded by a steel shell of a cylindrical shape — the reflection shield (Figure 1), made from austenitic steel by forging. In its turn, FEA and reflection shield are placed into the welded structure of reactor cavity and are fastened to its faceted girth. The main purpose of the shield is FEA grouping into the core, reducing the intensity of neutron flux to reactor case, and ensuring core coolant circulation along the design circuit [1].

Height of reflection shield of WWER-1000 reactor (Figure 2) is 4070 mm. It consists of five rings of the same height pinned to each other. The ring inner surface is faceted. Shield radius in the place of ring joining is 1742.5 mm. The shield is cyclically symmetrical relative to a 60° sector that essentially simplifies the modelling process.



Shield cross-section (normal to the axis) is shown in Figure 3. Diameter of small channels is 70 mm, large channel diameter is 130 mm.

Reflection shield and wall of welded cavity of nuclear reactor are exposed to high doses of radiation, which causes a whole range of defects, leading to degradation of physico-mechanical properties. In chromium-nickel steels microstructural transformations take place under the conditions of heating up to 400–550 °C with partial transition from austenitic into ferritic state with formation of carbides of chromium, titanium, molybdenum and other impurity metals [2]. Nonetheless, the main phase (austenite) preserves about 90 % of the total volume. So, at high-temperature irradiation by intensive neutron fluxes, vacancy pores initiate and grow in austenitic steels and nickel-, titanium-, molybdenum- and beryllium-based alloys, leading to a noticeable increase of the metal volume — radiative swelling. This process largely depends on radiation dose, irradiation temperature and stresses and plastic deformations in the material caused by swelling [1–3].

Radiative swelling of reflection shield material leads to its deformation and closing of the

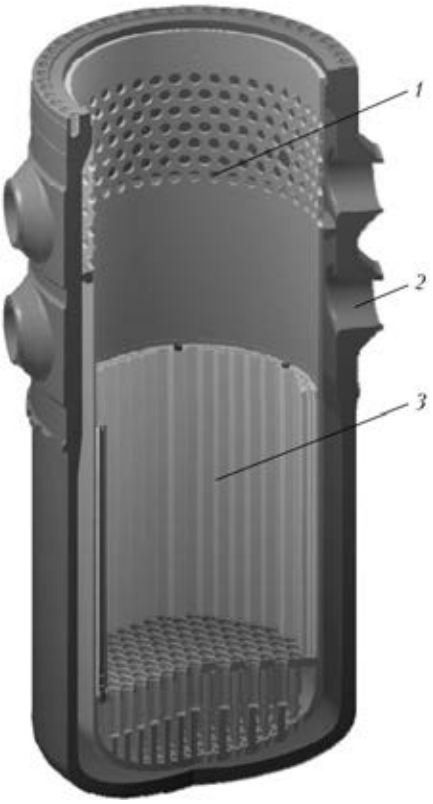


**Figure 1.** Reactor design: *1* — cavity; *2* — vessel; *3* — reflection shield

clearance between it and cavity wall, thus resulting in a change of heat exchange in the core, which may have hazardous consequences in terms of violation of temperature mode of reactor operation. Complete closing of the clearance between the reflection shield and cavity wall and further swelling of reflection shield leads to a considerable deformation of cavity wall and stress increase that may result in its failure. Prediction of the change of stress-strain state (SSS) of the reflection shield and welded structure of cavity wall in operation, in particular for substantiation of extension of service life of operating WWER-1000 reactors up to 60 years, is an extremely urgent task today.

**Figure 2.** General view of reflection shield

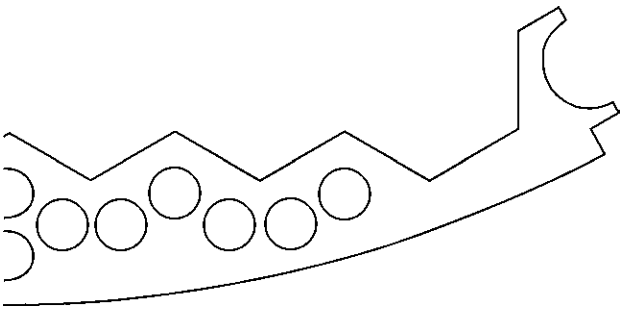

**Figure 3.** Section of reflection shield, 30° sector

Reflection shield material is austenitic steel 08Kh18N10T of the following composition, wt.%: 0.8 Si; 0.3 Cu; 2 Mn; 10 Ni; 0.4 Ti; 0.035 P; 18 Cr; 0.02 S. Physical properties of 08Kh18N10T steel, given in Table 1, correspond to the initial (nonirradiated) state.

In order to assess radiative swelling of the reflection shield, a 2D finite element model was constructed (Figure 4). A section, where the values of damaging dose and energy evolution are maximum, was specifically selected for shield behaviour modelling. Conditions of cyclic symmetry for shield sector of 60°, and symmetry relative to a straight line dividing this sector into two equal sectors of 30° were applied. Each of the respective mechanical problems was solved under the conditions of generalized plane strain. Model constructed from linear four- or three-node elements in the form of rectangles or triangles, contains 10486 nodes and 9748 elements.

Temperature distribution in the reflection shield during swelling calculation is constant and is determined by preliminary nonstationary thermodynamic calculation (reactor reaching maximum power mode). Assigned as boundary conditions are coolant temperatures in the channels and on free surfaces of reflection shield (Figure 5, Table 2), as well as respective heat transfer co-

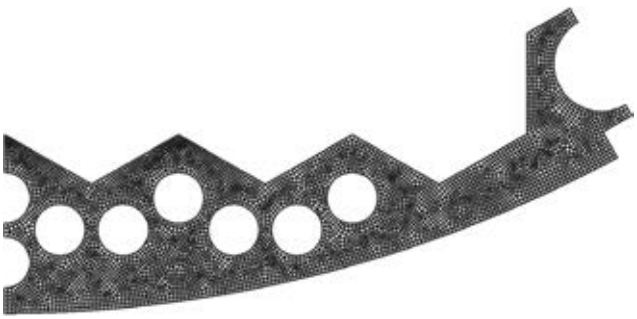

**Figure 4.** Two-dimensional finite element model of reflection shield, 30° sector

**Table 1.** Physical properties of 08Kh18N10T steel [4, 5]*

| Temperature $T$, °C | Young's modulus $E$, GPa | Coefficient of linear expansion $\alpha^t$, $\cdot 10^{-6}$ $K^{-1}$ | Heat conductivity λ, $W \cdot m^{-1} \cdot K^{-1}$ | Specific heat capacity $c_p$, $J \cdot kg^{-1} \cdot K^{-1}$ | Density ρ, $kg/m^3$ |
|---|---|---|---|---|---|
| 20 | 205 | – | 16.6 | 478 | 7900 |
| 100 | 200 | 16.6 | 17.2 | 495 | 7862 |
| 200 | 190 | 17.0 | 18.0 | 516 | 7821 |
| 300 | 180 | 17.4 | 18.7 | 537 | 7778 |
| 400 | 170 | 17.8 | 19.4 | 558 | 7732 |
| 500 | 165 | 18.2 | 20.1 | 579 | 7684 |
| 600 | 160 | 18.5 | 20.8 | 600 | 7634 |

*Poisson's ratio ν = 0.3 [1].

**Table 2.** Coolant temperature and values of heat exchange coefficients for different surfaces of reflection shield [1]

| Surface number acc. to Figure 5 | Surface temperature, °C | Heat exchange coefficient, $W/(m^2 \cdot K)$ |
|---|---|---|
| 1, 6, 8 | 291.7 | 2308 |
| 2–5, 2–7 | 292.1 | 1331 |
| 9 | 291.7 | 1115 |
| 10 | 291.7 | 15900 |
| 11 | 320.0 | 39017 |

efficients. Volumetric heat generation in reflection shield material is taken into account (Figure 6).

Heat flows ($q$, $W/m^2$) are determined by the formula

$$q = -h(\theta_{in} - \theta_{out}), \quad (1)$$

where $\theta_{in}$ is the surface temperature, °C; $h$ is the heat-transfer coefficient, $W/(m^2 \cdot K)$; $\theta_{out}$ is the coolant temperature, °C.

Calculation method is used to find the values of stresses and strains in the reflection shield, arising at reactor reaching the full power mode. This SSS is incorporated into swelling calculations as initial conditions.

Result of temperature field calculation is given in Figure 7. The pattern and absolute values of temperature are in complete agreement with the results given in [1].

Then, in order to evaluate the change of the shield shape during 60 years of reactor operation, tracing in time of initiation and development of radiative swelling deformations and of the respective SSS change under the conditions of constant temperature distribution was performed. Periodical cooling of the shield at reactor shutdowns was not taken into account, as it was determined by calculations for one cooling–heating cycle that this does not cause any redistribution of residual deformations. PWI has accumulated extensive experience of solving non-linear problems of tracing the initiation and development of plastic strains in welding and subsequent cooling [6]. Therefore, this problem was solved with application of well-tested calculation algorithms,

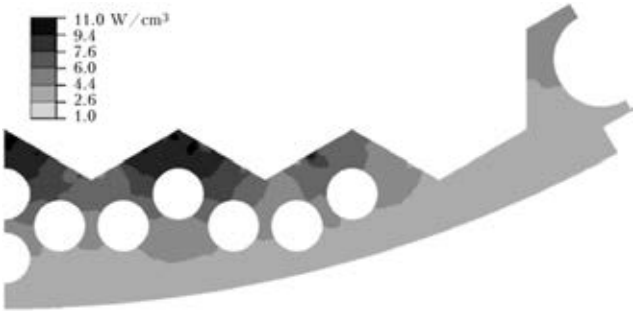


**Figure 6.** Volumetric heat evolution in reflection shield at reactor running at full power

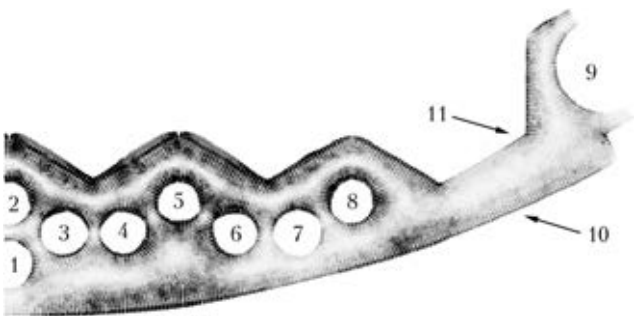


**Figure 5.** Heat flows in reflection shield: 1–9 — channel surfaces; 10, 11 — free surfaces


**Figure 7.** Temperature distribution in reactor reflection shield at operation at maximum power

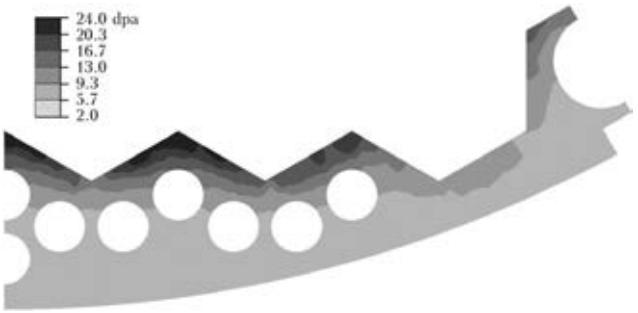


**Figure 8.** Damaging irradiation dose, 22nd fuel cycle

in which radiative swelling deformations in the form of isotropic volumetric deformations were assigned as bulk effects. Material swelling increment is calculated in each time step. Values of damaging dose (Figure 8), yield limit, average stresses and plastic strains in each finite element are recalculated at the same time. Size of time step is 1 year, that ensures sufficient accuracy at calculation of reflection shield swelling for the cases of 15, 40 and 60 years of reactor operation.

Dependence of swelling $S_i$ of the considered material at a certain moment of time can be presented in the following form [2, 7, 8].

$$S_i = C_D D_i^n f_0(T) f_1(\sigma_m) f_3(\kappa), \quad S_i > 0, \tag{2}$$

where $D_i^n$ is the irradiation dose, displacements per atom (dpa); $f_0(T) = \exp(-r(T - -T_{\max})^2)$; $f_1(\sigma_m) = 1 + P\sigma_m$; $f_3(\kappa) = \exp(-\eta\kappa)$; $C_D$, $n$, $r$, $P$, $\eta$ are the dimensionless constants ($C_D = 1.035 \cdot 10^4$, $n = 1.88$, $r = 1.1 \cdot 10^{-4}$, $P = 4 \cdot 10^{-3}$ MPa$^{-1}$. $\eta = 8.75$); $T_{\max} = 470$ °C; $T$ is the irradiation temperature, °C; $\sigma_m = \frac{1}{3}(\sigma_1 + \sigma_2 + \sigma_3)$ are the average stresses; $\kappa = \int_0^D d\varepsilon_i^p$, where $d\varepsilon_i^p$ is the intensity of plastic deformation increments equal to

$$d\varepsilon_i^p = \frac{\sqrt{3}}{2}\sqrt{d\varepsilon_{ij}^p d\varepsilon_{ij}^p}, \quad i, j = 1\text{–}3.$$

Total swelling in all $N$ time steps is sought as a sum of swelling increments in each step:

$$S_\Sigma = \sum_{i=1}^{N} dS_i, \quad dS_i > 0.$$

This model allows for the history of accumulation of volumetric deformations as a result of radioactive irradiation.

Yield limit of materials of reflection shield and cavity changes under the impact of temperature and radioactive irradiation by the following dependence [2]:

$$\sigma_{0.2} = 153 + 239 \exp(-2.22 \cdot 10^{-3}(T + 273)) + 365 \left(\frac{T}{T_{\text{ir}}}\right)^{-2.2} \left[1 - \exp\left(-0.47 \frac{D}{D_0}\right)\right]^{0.5}, \tag{3}$$

where $T_{\text{ir}} = 450$ °C; $D_0 = 4.55$ dpa.

So, after the reactor has reached full power mode, when the irradiation dose is still negligibly small, material yield limit decreases (Figure 9). At the same time, stressed state is intensified, thus leading to initiation of a plastic region in the reflection shield (Figure 10). At this stage the yield limit value is completely determined by the first two addends from dependence (3).

At increase of accumulated irradiation dose the influence of the third addend from dependence (3) on the yield limit is also increased. So, during the first year of reactor operation the yield limit of reflection shield material increased from 220 MPa in the region of the temperature maximum up to 480 MPa in the region of the maximum of accumulated damaging dose (Figure 11).

General pattern of volumetric swelling deformations in the reflection shield remains approximately the same during the entire operation period of the reactor (Figure 12), but the absolute value of swelling increases. After 25 years of reactor operation, the maximum value of swelling

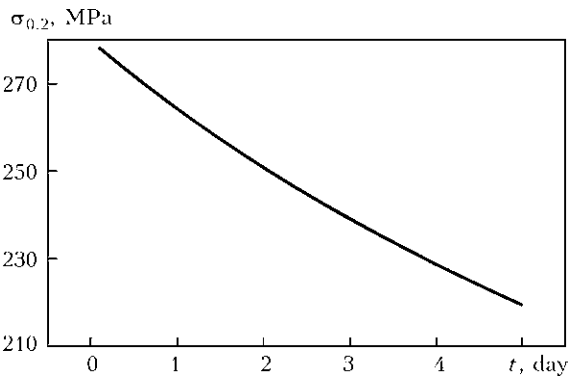


**Figure 9.** Lowering of yield limit at heating of reflection shield when reaching the working mode (maximum temperature mode)

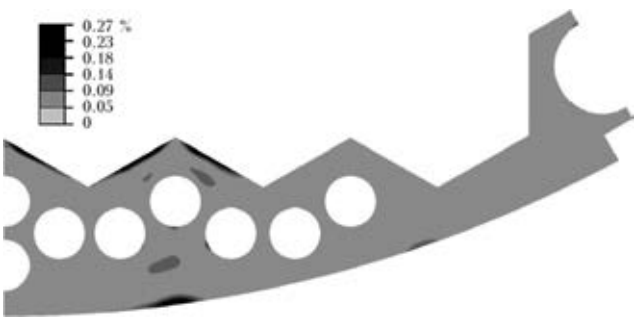


**Figure 10.** Intensity of plastic deformations in reflection shield after reactor reaching the required mode

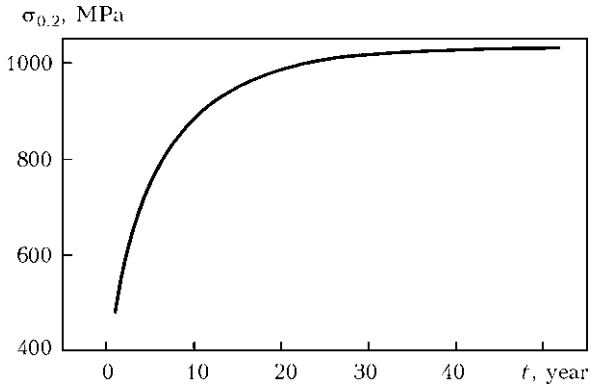


**Figure 11.** Increase of yield limit at accumulation of irradiation dose during reflection shield operation (in the zone of maximum of accumulated damaging dose)

deformations is equal to 1.3, after 40 years it is 1.8 and after 60 years — 3.7 %.

Because of non-uniform heating and swelling, radial deformations in the reflection shield are unequal. Radius increment is maximum in the region of large channel 9, and minimum in the region of channel 1 (Figure 13). Their difference is noticeable already when the reactor reaches full power mode, even when the swelling value is negligibly small. Increment of radius on the shield outer surface at reactor running at full capacity is positive everywhere, but at swelling accumulation the shield outer surface in the region of channel 1 moves inside, while the radius in the large channel mode continues growing.

Radial displacements of the shield outer surface after reactor going into normal operation mode are equal to 11.2 mm for the MAX region, and 9.4 mm for MIN region. After 25 years of operation MAX(MIN) radial displacements are equal to 12.9 (8.8 mm); after 40 years — 14.1 (7.9); and after 60 years — 16.1 (7.1), respectively.

In a number of currently available publications [1] it is proposed to perform calculation of volumetric deformations resulting from radiative swelling by the following formula:

$$S = \Delta V / V = 0.55(D + 0.1T - 67) \exp(-2.9 \cdot 10^{-4} (T - 485)^2), \quad (4)$$

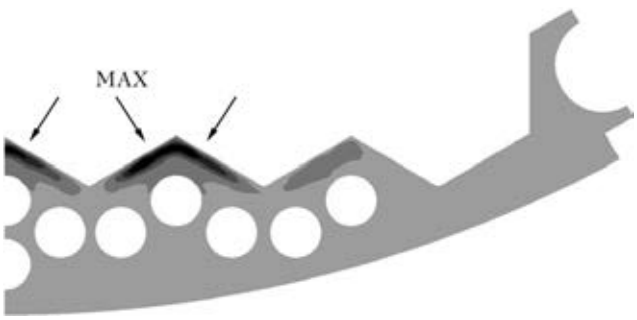


**Figure 12.** Total pattern of volumetric swelling deformations in reflection shield during the entire term of reactor operation

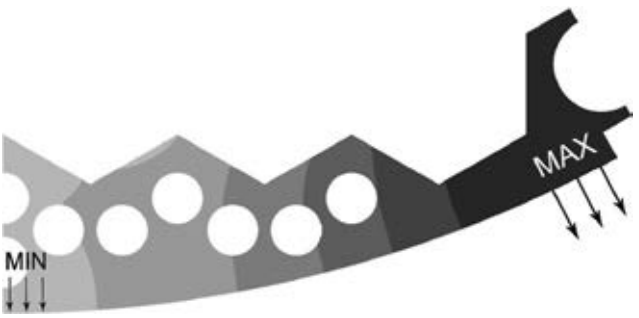


**Figure 13.** Regions of maximum and minimum increment of radius in the reflection shield during operation

where $S$ is the relative radiative swelling, %; $\Delta V / V$ is the volumetric swelling of the reflection shield, %; $D$ is the damaging irradiation dose, dpa.

Such a model does not allow for the stressed state, and it means that calculation does not depend on loading history. Expression $(D + 0.1T - 67)$ can take negative values, if irradiation dose has not reached a certain value, and in this case the swelling value is zeroed by the program. In keeping with this model, swelling begins in the 23rd year of reactor operation, when maximum value of the dose in the reflection shield $D = 67 - 0.1T = 25$ dpa. Incubation period [9], during which this dose will accumulate, is 23 years.

Evaluation of swelling by formula (4) over 60 years yields

$$S = 0.55(65.5 + 490/10 - 67) \exp[-2.9 \cdot 10^{-4} (490 - 485)^2] = 0.55 \cdot 47.5 \exp(-7.25 \cdot 10^{-3}) = 26\ \%.$$

Program calculation by formula (4) yields 17 %. Calculation result is given in Figure 14.

Calculation of volumetric deformations over 60 years of reactor operation performed in this work by a refined model (formulas (2) and (3)) allowing for SSS yields not 26 %, but a much lower value of 3.7 %. Thus, allowing for the loading history (stressed state) at evaluation of radiative swelling of the shield material and its radial deformations essentially influences the accuracy of the results.

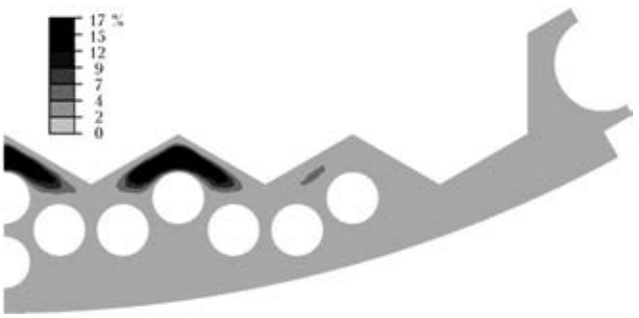


**Figure 14.** Volumetric swelling of reflection shield $\Delta V / V$ after 60 years of reactor operation found by formula (4)

Results on swelling and radial deformations of the reflection shell, obtained allowing for the stressed state, are indicative of the possible contact of the shield with the welded wall of the cavity during reactor operation period, with the initial minimum clearance between them being 2.5 mm. Such a contact can have an essential influence SSS of the cavity welded structure, so that it requires a more detailed study and construction of a 3D model of radiative swelling and contact interaction of the shield and cavity wall, allowing for distribution of irradiation dose and heating by structure height.


1. (2011) *Additional operations on assessment of technical state of reactor elements of power unit No.1 of OP Yuzhno-Ukrainskaya. Assessment of radiative swelling of reflection shield*: Report. NRI Rez.
2. Kursevich, I.P., Margolin, B.Z., Prokoshev, O.Yu. et al. (2006) Mechanical properties of austenitic steels in neutron irradiation: Influence of different factors. *Voprosy Materialovedeniya*, 48(**4**), 55–69.
3. Borodin, O.V., Bryk, V.V., Voevodin, V.N. et al. (2006) Microstructural mechanisms of low-temperature radiative swelling and embrittlement of materials of WWER-1000 reactor devices. In: *Problems of resource and safe service of structures, constructions and machines*. Kyiv: PWI.
4. (2008) *Determination of current values of mechanical properties of vessel internals elements*: Report. NRI Rez.
5. Shary, N.V., Semishkin, V.P., Piminov, V.A. et al. (2004) *Strength of main equipment and pipelines of WWER reactor facilities*. Moscow: IzdAT.
6. Makhnenko, V.I. (1976) *Computational methods of investigation of welding stress and strain kinetics*. Kiev: Naukova Dumka.
7. Margolin, B.Z., Kursevich, I.P., Sorokin, A.A. et al. (2009) On problem of radiative swelling and embrittlement of austenitic steels. Pt 2. Physical and mechanical principles of embrittlement. *Voprosy Materialovedeniya*, 51(**2**), 99–111.
8. Vasina, N.K., Margolin, B.Z., Gulenko, A.G. et al. (2006) Radiative swelling of austenitic steels: Influence of various factors. Processing of experimental data and formulation of determinant equations. *Ibid*., 48(**4**), 69–89.
9. Votinov, S.N., Prokhorov, V.I., Ostrovsky, Z.E. (1987) *Irradiated stainless steels*. Moscow: Nauka.


Received 10.09.2012

## *NEWS*

## *Technology and Equipment for Electroslag Welding of Busbars of Aluminium Electrolysers under Conditions of Service and Powerful Magnetic Fields*

At present, when assembling the busbars in electrolysis shops the welding-on of outlet chutes to busbars is one of the most complicated and labor-intensive operations. Welding is realized under the conditions of effect of high-power magnetic fields, influencing negatively the welding process stability. Moreover, the work with busbars is performed without switching-off of the technological current.

The technology of electroslag welding (ESW) with consumable wire electrode is offered for mastering, allowing making welding of joints of sections from 60 × 800 mm up to 140 × 1000 mm under the conditions of operating shops and powerful magnetic fields. A rolled aluminium wire of diameter of up to 10 mm and fluxes, not containing lithium, and which are available in sufficient amounts at any enterprise of this profile, are used as welding consumables. Specialized equipment, rigging and technological processes are designed and developed to suit the conditions of the Customer.

ESW can be performed both at the de-energized area of busbar and also on the busbar, along which the technological current of up to 7 kA is passed. Inspection of electrotechnical properties of joints showed that the voltage drop (allowable to 20 mV) in joints, produced by ESW, was 5.2 mV (while in manual arc welding the voltage drop is 30 mV), and it is 4.8 mV at a monolithic busbar.

The given technology allows decreasing the losses of electric power in welded joints, reducing the expenses for manufacture and repair of aluminium busbars, improving the welding process efficiency and quality of aluminium welded joint of above-mentioned sections, improving greatly the labor conditions of the welders.

A number of foreign companies resumed the application of mechanical joints in the busbar design. At aluminium plants of CIS the manual arc welding with carbon electrode and method of filling with a molten aluminium are used. All the applied technologies do not provide a stable required quality of busbar joints.

New technology of ESW has been successfully tested at maximum magnetic fields (vertical component of a magnetic induction was $30 \cdot 10^{-4}$ T) using laboratory equipment at operating shops of aluminium plants of the Russian Federation.

*Term of payback*: not more than 12 months.

# DEVELOPMENT OF FLUX-CORED WIRE OF THE FERRITIC GRADE FOR SURFACING OF HIGH-CARBON STEEL PARTS

**Ya.P. CHERNYAK**
E.O. Paton Electric Welding Institute, NASU
11 Bozhenko Str., 03680, Kiev, Ukraine. E-mail: office@paton.kiev.ua

The issue of current importance is reconditioning of parts with a carbon content of more than 0.5 %. Traditional methods for crack control, such as preliminary and concurrent heating, in surfacing of parts made from high-carbon steels are not always possible to apply, because of a large weight of the parts or economic inexpediency. The investigation results presented in the article allowed the development of a new surfacing consumable of the ferritic grade, which provides the defect-free deposited layer when using no preliminary and concurrent heating. The key element of the Fe–Ti–Mn–Si–Mo alloying system is titanium. Considering its affinity for carbon and stoichiometric ratio, this made it possible to produce a soft ferritic matrix in the deposited layer, the content of carbon in the base metal being up to 1 %. The positive result of experimental-industrial verification of the developed flux-cored wire in surfacing of tram rails made from steel M76 with a carbon content of up to 0.8 % permitted recommending this wire for commercial application. Specifications of Ukraine TUU 28.7.05416923.066–2002 were worked out for commercial manufacture of wire PP-Np-06T3GM (PP-AN203). Ferritic flux-cored wire PP-Np-T3SGM provides the absence of all types of cracks in the deposited metal and HAZ, including spalls, within a wide range of surfacing parameters. It is recommended for application in surfacing of parts made from high-carbon steels without preliminary and concurrent heating. 4 Ref., 2 Tables, 3 Figures.

***Keywords:*** *arc surfacing, surfacing consumables, high-carbon steels, flux-cored wire, ferritic deposited metal, preliminary and concurrent heating*

Many components of metallurgical equipment, railway transport, construction machinery, etc. are manufactured from high-carbon steels with a carbon content of more than 0.5 %. In surfacing of these components it is necessary to take measures to prevent formation of cold cracks in the deposited metal and HAZ. The most common method for prevention of cracks is still preliminary and concurrent heating followed by tempering, allowing a substantial decrease in residual surfacing stresses induced by formation of martensitic structure in the deposited metal and HAZ. If heating is impossible, surfacing is performed by using austenitic electrode materials, which is not always reasonable both from the technical and economic standpoints [1].

The purpose of this study was to develop a consumable for surfacing of parts made from high-carbon steels without or with minimal heating, providing the defect-free deposited metal corresponding in structure to alloyed steel of the ferritic grade [2]. To eliminate formation of martensite, carbon transferring from the base metal into the deposited one is fixed into strong carbides in such a proportion that it remains in matrix in the minimal amount. In this case, the matrix retains a relatively soft and ductile ferritic structure, and the deposited and base metals have close thermal expansion coefficients, this leading to decrease in residual surfacing stresses.

The Fe–Ti–Mn–Si–Mo alloying system of the deposited metal was selected for investigations. The titanium content of the deposited metal was chosen based on the following considerations. Titanium is known to actively react with carbon to form carbide TiC with stoichiometric ratio of 4:1. It was planned to perform surfacing on steel with a carbon content of 0.7–0.9 %. In penetration of the base metal equal to about 30–40 %, the carbon content of the first deposited layer may amount to 0.35 %. To fix this amount of carbon it is necessary to have about 2 % Ti, which should provide formation of a soft ferritic matrix and, as a result, the absence of cracks in the deposited metal.

Titanium is also known to strongly oxidise during the surfacing process. Experiments were carried out on surfacing of specimens of high-carbon steel with a carbon content of 0.8 % by using the 2.6 mm diameter self-shielding wire of the investigated alloying system to determine its required content in the deposited metal and, correspondingly, in the flux-cored wire charge. Surfacing was performed with the open arc under

**Table 1.** Content of titanium in metal of the first deposited layer depending on its content in the self-shielding flux-cored wire charge

| Calculated content of titanium in flux-cored wire charge, wt.% | Actual content of titanium in deposited metal, wt.% |
|---|---|
| 2.17 | 0.68 |
| 3.26 | 1.15 |
| 3.95 | 1.31 |
| 4.05 | 1.51 |
| 4.87 | 2.05 |
| 5.62 | 2.50 |
| 7.04 | 2.73 |

the following conditions: $I$ = 430–450 A, $U$ = = 24–26 V, and $v_s$ = 36.8 m/h. The use was made of the basic-type gas-slag system ($CaF_2$ + + $CaCO_3$ + [$SiO_2$ + $K_2O$ + $Al_2O_3$]). Titanium was added in the form of ferrotitanium FTi-70 with 69 % Ti.

The mean coefficient of transfer of titanium into the first deposited layer metal equal to about 40 % was calculated from the data of Table 1, which gives the investigation results. Therefore, to provide the required amount of titanium in the first deposited layer equal to 2 %, its content of the flux-cored wire charge should be approximately 5 %.

Based on the data on transfer of titanium into the deposited metal, experimental flux-cored wire PP-Np-T3SGM was made for the investigations, and surfacing was performed on steel with a carbon content of 0.8 % under the above conditions. The results of investigation of chemical composition and hardness of the deposited metal of the first and third beads are given in Table 2.

As shown by metallographic analysis, metal of the first and third layers had a ferritic structure (Figure 1). Its characteristic feature is the presence of disoriented fine crystalline grains with dispersed inclusions that precipitated along their boundaries and in their bulk, these inclusions being mostly carbonitrides of different compositions. Low hardness ($HV$ 170–195) is also indicative of the absence of martensite in matrix of the deposited metal of the first and third beads.

**Table 2.** Chemical composition and hardness of metal deposited with flux-cored wire PP-Np-T3SGM

| Bead number | Content of elements, wt.% | | | | | | | Hardness $HV$ |
|---|---|---|---|---|---|---|---|---|
| | C | Mn | Si | Cr | Ni | Ti | Mo | |
| 1 | 0.4 | 0.9 | 0.9 | – | – | 2.6 | 0.4 | 185–195 |
| 3 | 0.2 | 1.0 | 1.2 | – | – | 3.3 | 0.6 | 170–180 |

Structural and phase transformations occurring in the deposited metal during the heating and cooling process were studied by using a fast-response dilatometer designed by the E.O. Paton Electric Welding Institute [3, 4]. In this dilatometer the rates of heating and cooling of specimens simulate the thermal surfacing (welding) cycles. The specimens were made from metal of the first layer deposited by using wire PP-Np-T3SGM on steel with a carbon content of 0.8 % (see Table 2).

As seen from Figure 2, *a*, the specimens in cooling at a rate of 36 °C/s (according to the most rigid thermal surfacing cycle) retain their initial ferritic structure. This is evidenced by monotony and reversibility of the curves.

The plotted curves were compared with a dilatometry pattern of core iron containing 4–5 % Si and having a stable ferritic structure (bcc lattice) in a range from room temperature to melting point (Figure 2, *b*). It can be seen from comparison of dilatometry patterns of the T3SGM deposited metal and core iron that they are similar and have an identical slope, i.e. their struc-

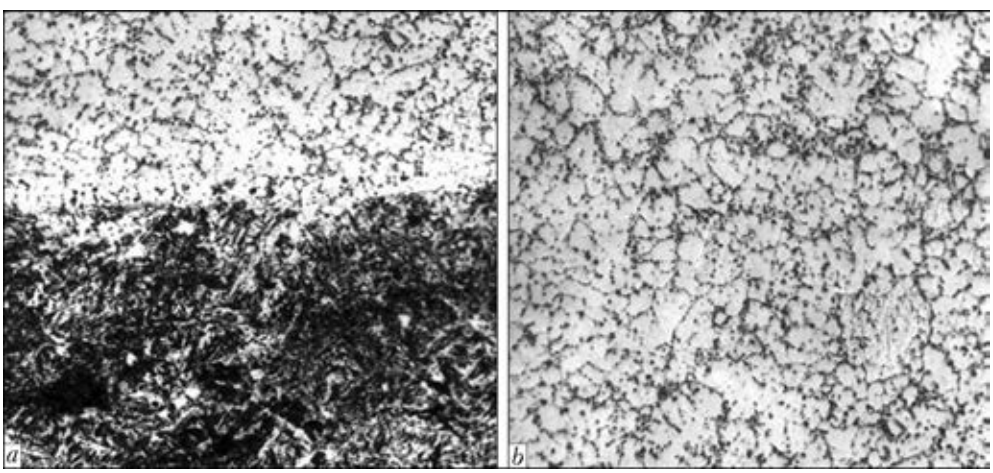


**Figure 1.** Microstructure (×500) of metal deposited with flux-cored wire PP-Np-T3SGM: *a* — fusion zone; *b* — first bead centre

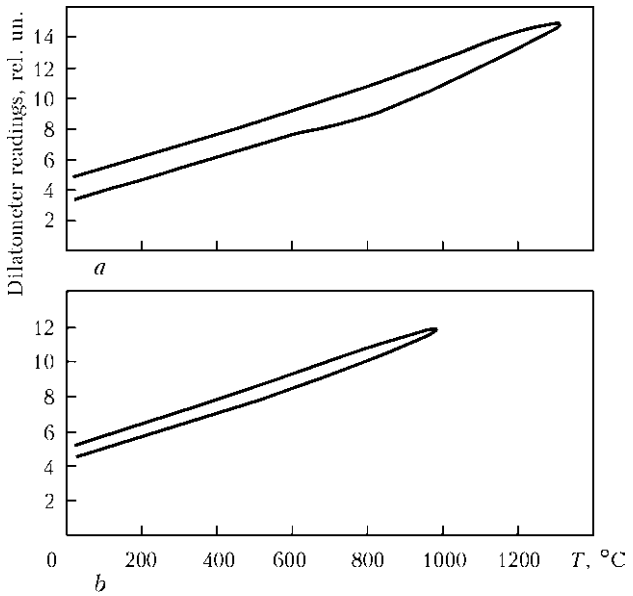


**Figure 2.** Dilatometry curves of heating and cooling of T3SGM deposited metal (*a*) and core iron (*b*)

tures and thermal expansion coefficients are close.

Therefore, the investigations performed show that even at a carbon content of the deposited metal equal to 0.5 %, due to alloying with titanium this metal solidifies as the ferritic one and undergoes no transformations in the solid state.

Investigation of mechanical properties of metal deposited with wire PP-Np-T3SGM proves that they are sufficiently high: $\sigma_y$ = 393 MPa, $\sigma_t$ = 638 MPa, $\delta$ = 18.5 %, and $\psi$ = 24.5 %.

The developed flux-cored wire with a carbon content of up to 0.8 % was subjected to experimental-industrial verification in surfacing of tram rails made from steel M76.

As shown by measurements of hardness of the HAZ metal, the maximal hardness value near the fusion line under the first deposited bead is approximately *HV* 400 (Figure 3). Microstructure in this zone consists of tempered martensite + bainite (see Figure 1, *a*). It should be noted that there is almost no carbide ridge at the fusion line. The rest of the HAZ regions have a ferritic-pearlitic structure with hardness *HV* 280–350, and are not dangerous in terms of cold cracking.

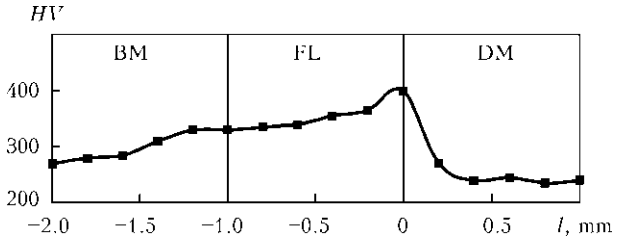


**Figure 3.** Hardness of fusion zone under the first deposited bead

Results of the experimental-industrial verification show that the developed flux-cored wire PP-Np-T3SGM provides the absence of all types of cracks, including spalls, in the deposited and HAZ metals over a wide range of surfacing parameters. Another advantage of flux-cored wire PP-Np-T3SGM is that it contains no scarce and expensive alloying elements. Hence, its price is not high.

## Conclusions

1. Flux-cored wire PP-Np-T3SGM was developed. It provides the ductile ferritic structure of the deposited metal and, as a result, the absence of cold cracks in surfacing of parts made from high-carbon steels without preheating.

2. The investigations and experimental-industrial verification performed allow flux-cored wire PP-Np-T3SGM to be recommended for surfacing of parts made from high-carbon steels without preliminary and concurrent heating.

1. Frumin, I.I. (1961) *Automatic electric arc surfacing*. Kharkov: Metallurgizdat.
2. Chernyak, Ya.P., Bursky, G.V., Kalensky, V.K. (2002) Resistance of the HAZ metal of steel M76 to cold cracking after surfacing using ferritic grade wires. *The Paton Welding J.*, **11**, 39–40.
3. Vasiliev, V.G., Malevsky, Yu.B. (1981) Dilatometer for examination of phase transformations in welding thermal cycle. In: *Physical methods of examination of metals*. Kiev: Naukova Dumka.
4. Vasiliev, V.G., Malevsky, Yu.B. (1965) Dilatometer for measuring of elongation in cross section of specimen. In: *Machines and devices for testing of metals and plastics materials*. Moscow: Mashgiz.

Received 11.07.2012

# ALGORITHM OF TECHNOLOGICAL ADAPTATION FOR AUTOMATED MULTIPASS MIG/MAG WELDING OF ITEMS WITH A VARIABLE WIDTH OF EDGE PREPARATION

**T.G. SKUBA, V.V. DOLINENKO, V.A. KOLYADA** and **E.V. SHAPOVALOV**
E.O. Paton Electric Welding Institute, NASU
11 Bozhenko Str., 03680, Kiev, Ukraine. E-mail: office@paton.kiev.ua

Area of research is automation of the processes of multipass MIG/MAG welding of thick-walled items in the downhand position. Objective of research is producing a weld with specified width and reinforcement, not having any lacks-of-penetration or undercuts in the presence of external disturbing influences in the form of a change of geometrical parameters of butt edge preparation (cut-out area). Research task is development of technological adaptation algorithm, which ensures the specified height of welded layer. Research procedure is synthesis of mathematical model based on equations containing both phenomenological descriptions of the processes and regression dependencies. An algorithm is proposed for technological adaptation of butt edge preparation based on machine vision means for multipass MIG/MAG welding. The algorithm ensures calculation of automatic welding mode (voltage, current and speed of welding) in real-time, based on current geometrical parameters of edge preparation. The algorithm uses the developed mathematical of model «power source–arc of steady-state MIG/MAG welding process». In order to verify the algorithm, welding experiments were performed, in which a metal layer of constant thickness of 0.2 cm with varying width of 2.0–3.3 cm was deposited on a steel plate. Range of variation of welding heat input is 4.0–8.5 J/cm with short-circuiting frequency of 5–54 Hz. No arc interruptions were observed, and defects of deposited layer macrostructure were absent. The proposed technological adaptation algorithm can be recommended for application in automatic control systems of multipass welding. 21 Ref., 8 Figures.

***Keywords:*** *multipass MIG/MAG welding, technological adaptation, layer of constant height, mathematical model, welding mode*

Multipass MIG/MAG welding is applied in fabrication and repair of structures of critical items, in order to ensure a high quality of welded joints [1–5]. Application of robotic welding using machine vision means [6] allows ensuring stability and repeatability of the quality of welded joint formation, as it eliminates the subjective factor — welder's qualification. One of the tasks of technological adaptation of multilayer robotic welding is producing a sound weld with the required reinforcement at maximum possible efficiency. The defined task is solved by development of a technological adaptation algorithm, which, proceeding from the current geometrical parameters of the groove, would allow forming the vector of parameters of optimum automatic welding mode: voltage, current and welding speed. Known are the procedures of solving this task based on full-factor active experiments. For instance in [7, 8] the regression models are synthesized, which are used to form optimum control of the welding process.

Development of systems of adaptive control of MIG/MAG welding is now given a lot of attention abroad [9–12]. However, the task of ensuring an optimum mode of multipass welding has not yet been solved completely.

This paper deals with development of technological adaptation algorithm for robotic multipass MIG/MAG welding of massive items in the downhand position.

Let us consider multipass arc welding, in which V-shaped groove (Figure 1, *a*) or cut-out area in the item (Figure 1, *b*) is filled with layers of the same height.

The first step of technological adaptation is scanning of the groove by a laser triangular sensor (LTS). Scanning results are used to draw a conclusion as to whether the geometrical parameters of the groove remain constant or change over its entire length.

In the first case, at constant geometry of the groove (cut-out area) technological adaptation for multipass MIG/MAG welding is associated with bead deposition in different $n$-th layers (see Figure 1, *a*) and consists in calculation of deposition mode for each $k$-th bead. Deposition mode

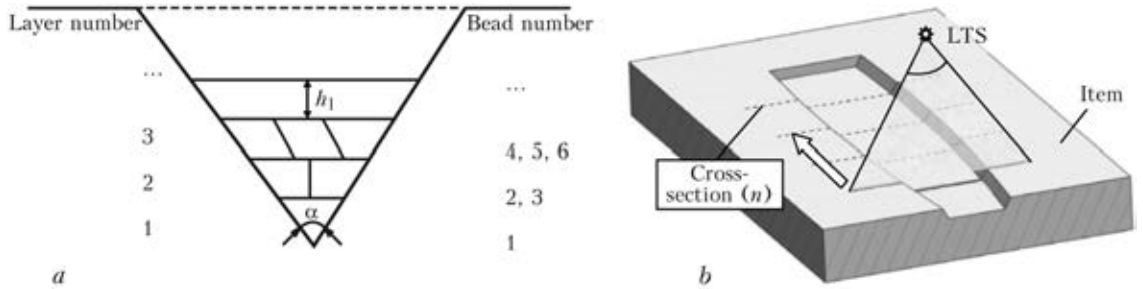


**Figure 1.** Schematics of multipass welding: *a* — filling of V-shaped groove of constant height layer (α — groove angle; $h_l$ — layer height, cm); *b* — filling the cut-out area in the item (longitudinal welds)

parameters remain constant along the entire length of the deposited bead.

In the second case at variable groove geometry technological adaptation can be associated, for instance, with variation of groove angle along the butt line (see Figure 1, *a*) or with varying shape of cut-out area (see Figure 1, *b*). To compensate for the above-mentioned disturbances, it is necessary to control the welding mode during deposition of each *k*-th bead. Thus, at deposition of a layer of a constant height into a groove of varying width it is necessary to constantly control the cross-section of each bead in the layer in real time.

**Formulation of technological adaptation concept for multilayer multipass welding.** Let us consider *n*-th cross-section of the deposited layer (Figure 1, *b*), which has the shape of a trapezoid (in the general case, the trapezoid is not isosceles) of area $S_d[n]$ (Figure 2).

We will calculate cross-sectional area $S_d[n]$ by the following formula:

$$S_d[n] = l_{low}[n]h_l + \frac{h_l^2}{2}(\text{tg}\,\theta_{left}[n] + \text{tg}\,\theta_{right}[n]), \quad (1)$$

where $l_{low}[n]$ is the width of layer lower surface, cm; $\theta_{left}[n]$, $\theta_{right}[n]$ is the angle of inclination of the surface of the left and right edge, deg.

Deposited layer consists of a whole number of beads $N$, cross-sectional areas of which $F_d[k]$ for each $S_d[n]$ have the same values:

$$F_d[k] = \frac{S_d[n]}{N}, \quad (2)$$

where $k$ is the bead number.

We will calculate bead width $E[k]$ by the following formula:

$$E[k] = \frac{l_{low}[k]}{(N - 2K_{s.ed} - (N-1)K_{adj.b})}, \quad (3)$$

where $K_{s.ed}$ is the coefficient determining the value of overlapping of extreme beads in each layer with side edges of the item; $K_{adj.b}$ is the coefficient determining the value of overlapping between the adjacent beads in the layer. Here $K_{s.ed} = 0.135$ and $K_{adj.b} = 0.27$.

The objective of this research is development of such an algorithm of adaptive control of welding, which for each $E[k]$ and $F_d[k]$ allows calculation of the following parameters of MIG/MAG welding mode: voltage $U$, current $I$ and welding speed $v_w$.

In the first part of technological adaptation algorithm, required heat input values are determined for calculated values of bead width $E[k]$. Let us consider the case of bead deposition on the surface, of a massive body. Width of the zone on item surface limited by isotherms of melting temperature $T_m$, can be found from the following equation [13]:

$$E[k] = \sqrt{\frac{8q_h[k]}{\pi e c\gamma \Delta T}}, \quad (4)$$

where $q_h[k]$ is the welding heat input, J/cm; $c\gamma$ is the volumetric heat capacity, J/(cm$^3$·°C); $\Delta T = (T_m - T_0)$ is the steel melting temperature, °C; $T_0$ is the initial item temperature, °C; $\pi$ = 3.14159265, $\varepsilon$ = 2.71828183 are the constants.

Calculations by formula (4) yield heat input values with more than 8 % error [14] that is unacceptable for the defined problem. With the known approach, the calculation accuracy can be increased by introducing an additional coefficient [15]. Correction factor $K_q$, which reduces the calculation error to 5 %, was determined experimentally for the range of heat input variation from 4200 up to 8400 J/cm. Then, equation (4) is written as follows:

$$q_h[k] = K_q \frac{\pi e}{8} E[k]^2 c\gamma \Delta T, \quad (5)$$

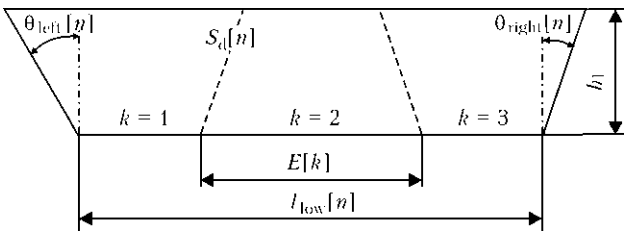


**Figure 2.** Schematic of *n*-th cross-section of the deposited layer

where $q_h[k]$ are the experimental data of welding heat input, J/cm; $K_q = (1.05–0.6.10^{-4})q_h$. After their substitution equation (5) becomes

$$q_h[k] \cong \frac{1.121E[k]^2c\gamma\Delta T}{1 + 6.405\cdot10^{-5}E[k]^2c\gamma\Delta T}. \quad (6)$$

Second part of technological adaptation algorithm is solution of a system of phenomenological and regression equations, describing MIG/MAG welding in the steady state. Input data are bead width $E[k]$, cross-sectional area of deposited bead $F_d[k]$ and welding heat input $q_h[k]$:

$$q_h[k] = \frac{I[k]U[k]\eta_{eff}}{v_w[k]}, \quad (7)$$

$$I[k] = (86.58 + 18.94v_{w.f}[k] - 4.2U[k] + \\ + 0.17Uv_{w.f}[k] - 0.46v_{w.f}[k]^2 + 0.09U[k]^2), \quad (8)$$

$$F_d[k] = \frac{\pi d_{el}^2 v_m[k](1-\psi)}{4v_w[k]}, \quad (9)$$

$$v_m[k] = \frac{K[k]U[k]j_{el}[k] + 10^4\rho_{el}j_{el}[k]^2L_{el}[k]}{M}, \quad (10)$$

$$K[k] = (0.285 - 0.0052U[k]), \quad (11)$$

$$j_{el}[k] = \frac{4I[k]}{\pi d_{el}^2}, \quad (12)$$

$$v_m[k] = v_{w.f}[k], \quad (13)$$

where $L_{el}$ is the length of electrode extension, cm; $v_{w.f}$ is the wire feed rate, cm/s; $v_m$ is the average integral value of electrode wire melting rate, cm/s; $K$ is the coefficient, determining the heat consumption for wire heating and melting, 1/cm$^2$; $M$ is the thermophysical constant of electrode wire, J/cm$^3$; $d_{el}$ = 0.12 cm is the electrode diameter; $j_{el}$ is the electrode wire current density, A/cm$^2$; $\rho_{el}$ is the average value of specific electrical resistance of electrode metal, Ohm/cm; $\eta_{eff}$ is the effective efficiency of the process of item heating by the arc; $\psi$ is the coefficient allowing for filler metal losses for spattering and evaporation.

Value $q_h[k]$ is found from formula (7) [16]. Equation (8) is a regression equation and allows calculation of electrode wire feed rate. It is synthesized by the authors for MIG/MAG welding mode with the following values: arc power source Fronius TransPuls Synergic-5000 at reverse polarity in shielding gas atmosphere of Ar + + 18 % $CO_2$, electrode diameter of 0.12 cm, welding current range of 200–300 A and welding voltage of 22–30 V. Value of cross-sectional area of the deposited bead is calculated from equation (7) [1]. Wire melting rate is calculated from equations (10), (11) for the steady-state mode of MIG/MAG welding at variation of welding voltage in the range of 15–35 V [17]. Current density in a round conductor is calculated from equation (12). Equation (13) describes the stability of the process of drop transfer in power source–arc system in MIG/MAG welding.

Solution of a system of equations (7)–(13) yields the required values of wire feed rate $v_{w.f}[k]$, welding voltage $U[k]$ and welding speed $v_w[k]$ for $k$-th section of the current bead of a multipass weld.

Investigation of the system of equations (6)–(13) shows that in many cases a unique solution cannot be obtained. Therefore, it is rational to apply a method of searching for a numerical solution by the criterion of minimum mean-root-square error. With this purpose additional conditions were defined, which, first of all, ensure a steady-state mode of MIG/MAG welding [18]; secondly minimize the mean-root-square error of the solution; and thirdly provide maximum efficiency of the welding process. As a result, the following system of inequalities was derived, which specifies the constraints for an algorithm of searching for a solution of the system of equations (6)–(13):

$$I_{min} < I[k] < I_{max}, \quad (14)$$

$$A_3I[k] < U[k] < A_4I[k], \quad (15)$$

$$\delta_{F_d[k]} = \\ = \sqrt{\left(\frac{\left(\frac{F_d[k] - \pi(d_{el})^2v_m[k](1-\psi)}{4v_w[k]}\right)}{F_d[k]}\right)^2} < \delta_{F_{d\,max}}, \quad (16)$$

$$\delta_{v_{w.f}[k]} = \sqrt{\left(\frac{v_{w.f}[k] - v_m[k]}{v_{w.f}[k]}\right)^2} < \delta_{v_{w.f\,max}}, \quad (17)$$

$$v_w[k] > v_{w\,min} \quad (18)$$

where $I_{min}$, $I_{max}$ are the values of the upper and lower limit for welding current; $A_3$, $A_4$ are the coefficients assigning the constraints for welding voltage, which ensure a steady-state mode of MIG/MAG welding in the selected range of welding currents [18, 19]; $\delta_{F_d}$, $\delta_{v_{w.f}}$ are the relative actual and maximum admissible error between the calculated and specified value of deposit cross-section; $\delta_{v_{w.f}}$, $\delta_{v_{w.f\,max}}$ are the relative

actual and maximum admissible deviation of the calculated value of wire feed rate relative to its melting rate; $v_{w\ min}$ is the minimum value of welding speed, at which the required level of cost-effectiveness at application of automatic multipass welding is achieved.

A simultaneous solution of a system of equations (6)–(13) and constraints (14)–(18) was derived using non-linear hill climbing techniques such as Levenberg–Marquardt algorithm, conjugate gradient or quasi-Newton methods [20]. Mathematical model and its solution algorithms were constructed in Mathcad mathematical package using «Minerr» operator [21] that allows assigning one of the three solution methods: Levenberg–Marquardt, Conjugate Gradient or Quasi-Newton, respectively.

As an example, the problem of deposition of a layer of 0.2 cm height with varying width from 2.0 up to 3.3 cm on a carbon steel plate of 1.2 cm thickness was solved. Electrode wire material is Sv-08G2S-0. Geometrical parameters $S_d[n]$ are calculated with 3 cm step by formula (1), based on geometrical characteristics of the projections of laser plane on the groove of the item being welded, obtained using LTS. As a result, the geometrical model of variation of the layer cross-section is a curve consisting of line segments, connecting the adjacent points of calculated values of $S_d[n]$, where $n$ = 1–8, depending on longitudinal coordinate $x$ (Figure 3).

Note that two points with numbers 2 and 7 were added on purpose in order to ensure correct performance of technological operations of «arc ignition» and «crater welding up».

Proceeding from the general geometrical model of a multipass weld, trajectories of torch displacement for welding three filling beads and two auxiliary (extreme) beads, which simulate the edges of cut-out area (Figure 4), were formed. Consideration of the problem of calculation of torch trajectories for automatic multipass welding is beyond the scope of this paper.

Proceeding from the results of analysis of the minimum and maximum values of layer cross-sections (see Figure 3) and allowing for the range of heat input values of 4200–8400 J/cm admissible for the developed mathematical model, we will calculate the required number of beads in the layer as 3. We assume that the cross-sectional areas of all the filling beads $F_d[k]$ are the same in the same layer section. Therefore, the file of initial values of bead cross-sections is as follows:

$$F_d[k] = (0.128;\ 0.136;\ 0.168;\ 0.194;\ 0.205;\ 0.201;\ 0.185;\ 0.181),\ \text{cm}^2. \quad (19)$$

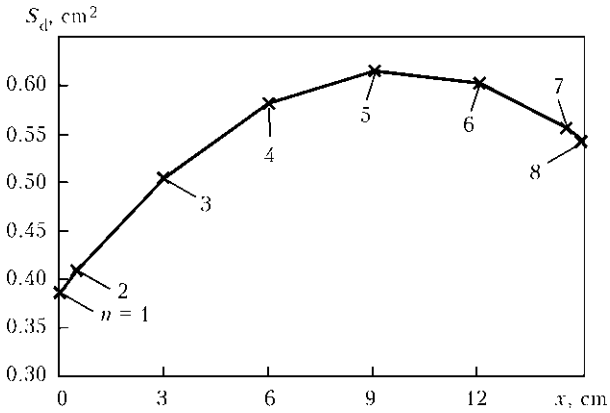


**Figure 3.** Curve of variation of deposited layer cross-section (linear interpolation between the calculated points was used)

We find the file of bead width values from formula (3) as follows:

$$E[k] = (0.83;\ 0.88;\ 1.10;\ 1.27;\ 1.35;\ 1.32;\ 1.22;\ 1.18),\ \text{cm}. \quad (20)$$

We obtain the data file for welding heat input by formula (6):

$$q_h[k] = (4244,\ 4651,\ 6344,\ 7592,\ 8091,\ 7902,\ 7177,\ 6964),\ \text{J/cm}. \quad (21)$$

Calculation of welding modes is performed at the following values of thermophysical and technological constants: $\eta_{eff} = 0.8$; $c\gamma = 4.9$ J/(cm$^3$·°C); $\psi = 0.1$; $\rho_{el} = 0.777 \cdot 10^{-6}$ Ohm/cm; $M = 9.75 \cdot 10^3$ J/cm$^3$; $T_m = 1520$ °C; $T_0 = 200$ °C; $I_{min} = 195$ A; $I_{max} = 300$ A; $A_3 = 0.1$; $A_4 = 0.116$; $v_{w\ min} = 0.75$ cm/s; $\delta_{F_{d\ max}} = 0.05$; $\delta_{v_{w.f\ max}} = 0.1$.

Mathcad package was used to search for a solution. Application of Levenberg–Marquardt technique to system of equations (7)–(13) with constrains (14)–(18) allowed deriving the following values of parameters of multipass welding mode:

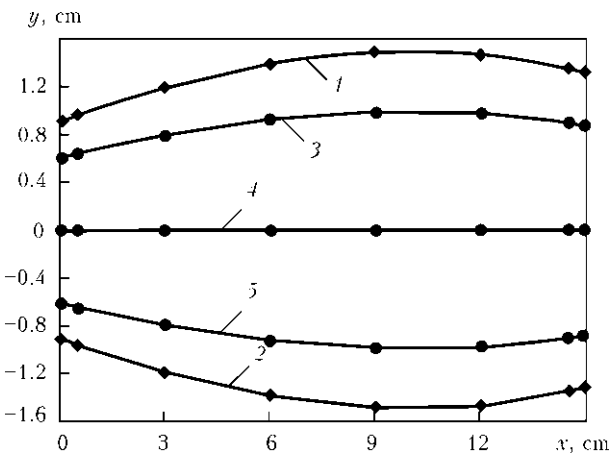


**Figure 4.** Trajectories of torch displacement at layer deposition: $x$, $y$ — coordinates of longitudinal and transverse displacement of the torch; *1*, *2* — auxiliary extreme beads; *3*–*5* — main filling beads

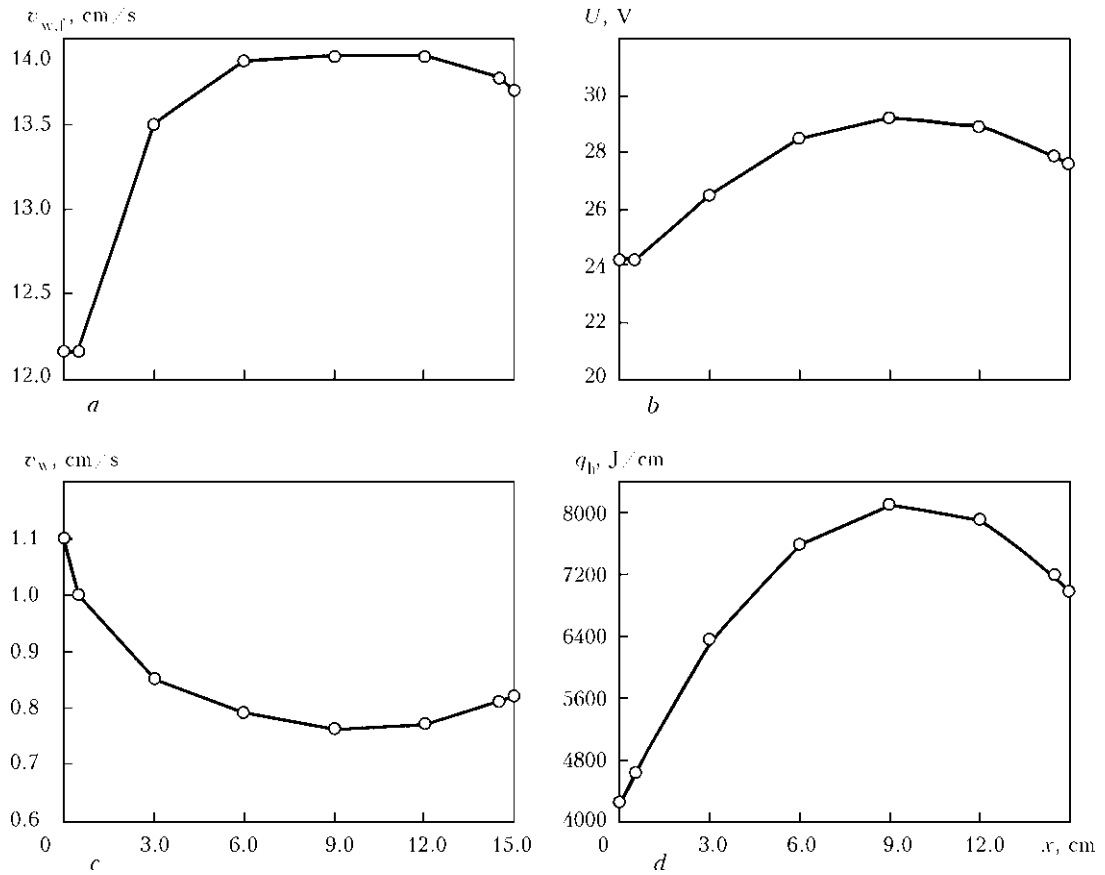


**Figure 5.** Curves of variation of mode parameters of bead welding at deposition of multipass layer of varying width

$$v_{w.f}[k] = (12.16;\ 12.16;\ 13.50;\ 13.87;\ 13.90;\ 13.90;\ 13.77;\ 13.70),\ \text{cm/s}, \quad (22)$$

$$U[k] = (24.2;\ 24.2;\ 26.5;\ 28.5;\ 29.2;\ 28.9;\ 27.9;\ 27.6),\ \text{V}, \quad (23)$$

$$v_w[k] = (1.1;\ 1.0;\ 0.85;\ 0.79;\ 0.76;\ 0.77;\ 0.81;\ 0.82),\ \text{cm/s}, \quad (24)$$

$$\delta_{F_d}[k]\cdot 100 = (4.6;\ 3.4;\ -1.1;\ 2.1;\ 3.3;\ 2.8;\ 1.1;\ 0.6),\ \%, \quad (25)$$

$$\delta_{v_{w.f}}[k]\cdot 100 = (8.0;\ 8.0;\ 11.5;\ 16.1;\ 17.5;\ 17.0;\ 14.8;\ 14.1),\ \%. \quad (26)$$

When assigning the current welding mode, intermediate values for mode parameters were calculated by the method of linear interpolation. Graphs of the resulting functions are shown in Figure 5 (graph of $q_h$ variation is given to verify the calculations).

Note that calculation of welding modes using Mathcad «Minerr» operator in PC with Intel Core(TM)2 Quad CPU 2.50GHz processor and RAM volume of 2 GB takes less than 1 s. Therefore, such an approach can be used in adaptive control system in real time.

Analysis of derived solutions for multipass welding modes shows that anticipated errors of bead formation by such parameters as deposit section and bead width do not exceed 5 % that guarantees uniform deposition of the layer. Mismatch of melting rates and electrode wire feed rates does not exceed 20 %. Calculated modes of multipass MIG/MAG welding provide a high efficiency of technological operation of deposition of 0.2 cm layer: welding speed varies from 0.76 up to 1.1 cm/s, and welding current — from 241 up to 262 A.

**Experimental verification of technological adaptation algorithm.** To verify the calculated modes of multipass welding, experiments were conducted on deposition of 0.2 cm thick layer on a low-carbon steel plate. Deposited layer consisted of five beads: two auxiliary, which simulate the cut-out area edges, and three filling beads. Welding was performed in a mixture of gases of Ar + 18 % $CO_2$ (25 l/min), $d_{el}$ = 0.12 cm, $L_{el}$ = = 1.4 cm. Item temperature was measured by chromel-alumel thermocouples that allowed controlling preheating temperature $T_0$, using technological pauses between bead deposition. As is seen from the deposited layer appearance (Figure 6), values of overlapping between the beads correspond to specified values, while losses for evaporation and spatter are satisfactory.

Analysis of welding process stability was performed on the basis of recorded and averaged values (trends) of $U$, $I$, $v_{w.f}$ and frequency of

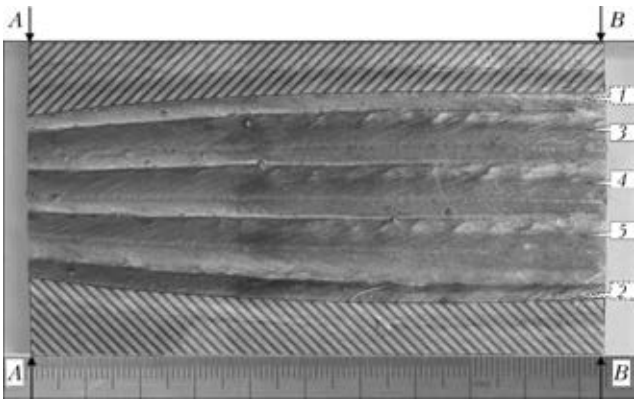


**Figure 6.** Macrosection of deposited layer (hatched regions simulate sectional view of the cut-out area): *1*, *2* — auxiliary extreme beads; *3*–*5* — main filling beads

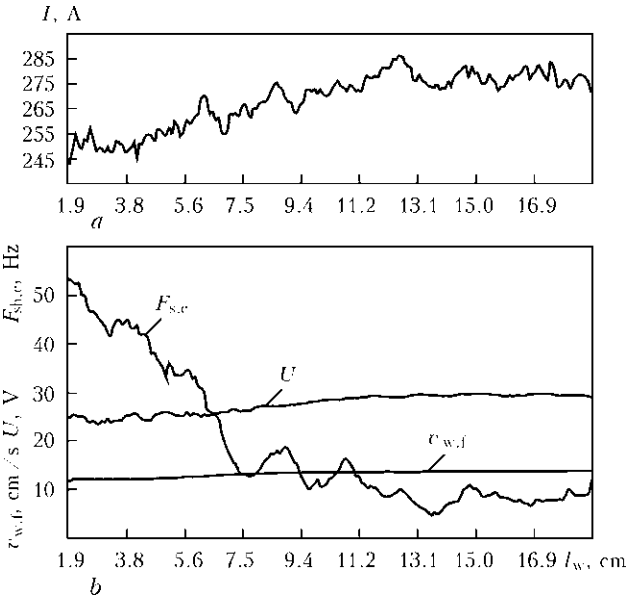


**Figure 7.** Trends of variation of MIG/MAG welding parameters at realization of technological adaptation algorithm (bead 3): *a* — welding current; *b* — frequency of arc gap short-circuiting, welding voltage and wire feed rate

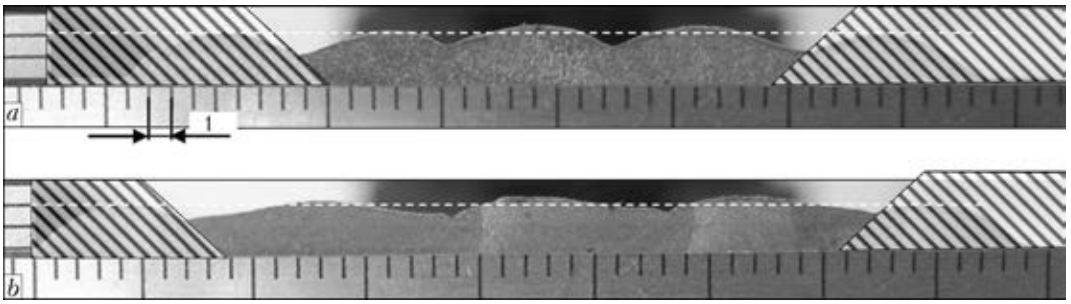


**Figure 8.** Macrosections of deposited layer using multipass MIG/MAG welding (hatched regions simulate section view of cut-out area): *a* — layer initial section (*A*–*A* section in Figure 6); *b* — layer end section (*B*–*B* section in Figure 6)

arc gap short-circuiting $F_{sh.c}$. Figure 7 shows the trends of technological parameters of welding bead 3 along the entire weld length $l_w$ (except for «arc ignition» and «crater welding-up» intervals). Analysis of derived trends shows that the actual changes of welding mode parameters corresponded to calculated curves of setting variations (see Figure 5). Process of MIG/MAG welding was of a steady nature. Parameter $F_{sh.c}$ varied in the range from 54 to 5 Hz that corresponds to admissible in MIG/MAG welding variation of drop transfer mode from fine- to coarse-drop transfer. No arc interruptions were observed.

Analysis of deposited layer macrosection was performed (Figure 8), which demonstrated the good quality of the deposited layer, in which slag inclusions or pores were absent. Errors by width and height of the deposited layer do not exceed 5 %. Layer height (hatched line in Figure 8) remains constant along its entire length.

Results of experimental verification of the developed algorithm of technological adaptation show that the proposed algorithm of welding mode control by $I$, $U$ and $v_w$ allows producing a layer of specified width and height without defects. High speed of welding mode calculation allows application of the developed algorithm in systems of technological adaptation for robotic multipass MIG/MAG welding of thick items with variable width of edge preparation.

1. Berezovsky, B.M. (2003) *Mathematical models of arc welding*. Vol. 2: Mathematical modeling and optimization of formation of different weld types. Chelyabinsk: YuUrGU.
2. Kiji, N., Kobayashi, K., Ishii, J. et al. (2003) Development of high efficiency arc welding methods. *The Paton Welding J.*, **10**/**11**, 56–60.
3. Poznyakov, V.D., Kiriakov, V.M., Gajvoronsky, O.A. et al. (2009) Investigation and development of the technology of arc welding of rail ends of frogs. In: *Problems of resource and safe service of structures, constructions and machines*. Kyiv: PWI, 579–584.
4. Tsaryuk, A.K., Ivanenko, V.D., Volkov, V.V. et al. (2009) Repair welding of turbine hull parts of heat-

resistant steels without postweld heat treatment. *Ibid*., 519–524
5. Memhard, D., Pfeiffer, W., Siegele, D. (2005) Determination of residual stress in multipass weldments of high strength steels with experimental and numerical techniques. In: *Proc. of Int. Conf. WELDS-2005* (Hamburg, Germany, 8–9 Sept. 2005), 1–14.
6. Gladkov, E.A. (2006) *Control of processes and equipment in welding*: Manual. Moscow: Akademia.
7. Srimath, N., Murugan, N. (2011) Prediction and optimization of weld bead geometry of plasma transferred arc hardfaced valve seat rings. *Europ. J. Sci. Res*., 51(**2**), 285–298.
8. Choteborsky, R., Navratilova, M., Hrabe, P. (2011) Effects of MIG process parameters on the geometry and dilution of the bead in the automatic surfacing. *Res. Agr. Eng*., 57(**4**), 56–62.
9. Muligan, S.J. (2007) *Development of laser vision-based adaptive control of robotic multipass MAG welding*: TWI Ind. Mem. Peport Summary 872. Cambridge: TWI.
10. Moon, H.S., Beattie, R.J. (2002) A fully automated adaptive pressure vessel welding system. In: *Proc. of AWS Conf*. (Orlando, Florida, 17–18 Sept. 2002), 1–6.
11. Moon, H.S., Beattie, R.J. (2002) Development of adaptive fill control for multitorch multipass submerged arc welding. *Int. J. Adv. Manuf. Technol*., 19(**12**), 867–872.
12. Lipnevicius, G. (2009) Robotic shop. *Modern Steel Construction*, May, 1–3.
13. Belchuk, G.A., Gatovsky, K.M., Kokh, B.A. (1980) *Welding of ship structures*: Manual. Leningrad: Sudostroenie.
14. Volchenko, V.N., Yampolsky, V.M., Vinokurov, V.A. et al. (1988) *Theory of welding processes*: Manual on equipment and technology of welding production. Ed. by V.V. Frolov. Moscow: Vysshaya Shkola.
15. (1991) *Welding and materials being welded*. Vol.1: Weldability of materials: Refer. Book. Ed. by E.L. Makarov. Moscow: Metallurgiya.
16. Rykalin, N.N. (1951) *Calculations of thermal processes in welding*. Moscow: Mashgiz.
17. Marishkin, A.K., Popkov, A.M., Postaushkin, V.F. (1970) Melting of electrode wire in automatic welding with systematic arc gap short-circuiting. *Avtomatich. Svarka*, **4**, 9–11.
18. Nikolaev, G.A. (1978) *Welding in machine-building*. Vol. 1. Moscow: Mashinostroenie.
19. Potapievsky, A.G. (2007) *Consumable-electrode gas-shielded welding*. Pt 1: Welding in active gases. 2nd ed. Kiev: Ekotekhnologiya.
20. Gill, F.E., Murray, W., Wright, M.T. (1985) *Practical optimization*. Moscow: Mir.
21. Ochkov, V.F. (2009) *Mathcad 14 for students and engineering*. St.-Petersburg: BHV.

Received 26.07.2012

## *NEWS*

### *High-Speed Electroslag Welding of Thick-Plate Metal without Normalization of Welded Joints*

When the traditional ESW is used, the separate regions with a reduced resistance to brittle fracture as compared to that of parent metal are observed in the welded joint. As a rule, the heterogeneity of structure and mechanical properties in these regions is eliminated by the application of postweld high-temperature treatment, for example, normalization. However, it leads to an abrupt increase in cost of the product manufacture.

The new method of a high-speed ESW with an automatic commutation of current connectors to a group of electrodes and edges of welded joints and equipment for its realization have been developed, allowing producing quality welded joints without postweld high-temperature treatment.

To realize the new technological process of ESW, the automatic two- and three-channel commutators of alternating (combined) current (current of up to 6 kA, 1–17 Hz frequency, 2–6 on–off time ratio) and two-channel direct current (1.5 kA current, 10 Hz frequency, 2–6 on–off time ratio) have been designed, which are compatible with existing serial power sources. Controllers and sensors of metal pool molten metal level, voltage stabilizers at the slag pool, digital meters of electrode wire feed speed, have been designed, having no analogues in the national and foreign engineering.

The new technological process makes it possible to weld steels of 40–150 mm thickness at high efficiency (3–6 m/h welding speed) and lower specific energy input (4–6 times reduced as compared with that of conventional conditions) at 3–4 times decrease of power consumption as compared with conventional ESW for the above-mentioned thicknesses.

*Field of application*. Welding of thick-plate steels in shipbuilding, reactor construction, boiler and converter production, hydro-engineering works, cryogenic engineering, cement machine building (steels of 25KhN3MFA, 16GNMA, 20K, 22K, 16GS, 09G2S, 03Kh20N16AG6, 10KhSND, 25L, 25GSL, 35L and other types), as well as control of structure of welds in ESW of copper, titanium alloys.

Completion of repair of blast furnace (inside view) at «Krivorozhstal» Works. As-welded part of wall is shown

Pollutions of toxic elements are 3–4 times reduced as compared with conventional ESW.

Equipment has been implemented at the number of metallurgical and machine-building plants of CIS, including «Ukrtsemremont» (Zdolbunov city) for welding of kiln furnace bands, «Sibenergomash» (Barnaul city) for welding of boiler fragments of 90, 110 and 150 mm thickness, made of steels 16GS, 22K and 16GNMA, as well as in repair of body of blast furnace DP-9 and assembly of converter body at «Krivorozhstal» Metallurgical Works (Krivoj Rog city).

*NON-DESTRUCTIVE TESTING OF WELDED JOINTS*

# PECULIARITIES OF ACOUSTIC EMISSION SIGNALS IN EVALUATION OF FRACTURE MECHANISM IN WELDED JOINTS ON ALUMINIUM ALLOYS

**V.R. SKALSKY, I.N. LYASOTA** and **E.M. STANKEVICH**
H.V. Karpenko Physico-Mechanical Institute, NASU
5b Aivazovskogo Str., 79053, Lvov, Ukraine. E-mail: skal@ipm.lviv.ua

High-strength aluminium alloys are widely applied in modern science and technology owing to a combination of their physical-mechanical and corrosion properties. Electron beam welding is used to join structural members, in particular in aircraft engineering. Micro- and macrofractures often occur in operation of such members under the effect of various factors. Crack propagation can be very effectively determined by the acoustic emission method. The purpose of this study was to investigate peculiarities of generation of the acoustic emission signals under static loading of specimens, and identify the character of fracture in different regions of the welded joints on aluminium alloy 1201-T. Crack resistance of the specimens measuring 10 × 20 × 160 mm made from the through electron beam welded joints on 20 mm thick 1201-T alloy plates was investigated by the three-point bending tests. The acoustic emission signals were fixed by using system SKOP-8M. The parallel measuring channel method was employed to select useful signals from noise. As established on the basis of analysis of wave reflections and continuous wavelet-transforms of the fixed acoustic emission signals, the method allows identifying sources of their generation in static fracture of aluminium alloys and their welded joints. Tough (weld and HAZ metals) and brittle-tough (base metal) fractures of a solid solution of copper in aluminium generate signals of low and medium amplitudes ($A$ = = 0.2–0.5 mV), for which the criterial index varies from 0.15 to 0.30. Detachment of melted grains is accompanied by generation of the acoustic emission signals with an amplitude range of $A$ = 0.4–0.5 mV and index $\kappa$ = 0.3–0.4, whereas cracking of brittle intermetallics is accompanied by generation of high-power signals ($A$ = 0.5–4.0 mV) with index $\kappa$ = 0.5–0.9. 15 Ref., 5 Figures.

***Keywords:*** *aluminium alloy, welded joints, acoustic emission, microstructure, microfractography pattern, wavelet-transform, fracture mechanism*

Current development of the industry of Ukraine stimulates growth of output of aluminium and its high-strength alloys owing to a combination of their physical-mechanical, corrosion and operational properties, which allows their successful application practically in all areas of science and technology. Electron beam welding (EBW) is used to join critical structural members (aerospace engineering, construction industry, etc.), as this welding method provides high quality of the weld metal when joining heavy sections in one pass.

Micro- and macrofractures may initiate and propagate in structural members made from aluminium alloys during their operation under the effect of various factors. Crack propagation can be very effectively determined by the acoustic emission (AE) method [1]. However, the AE method was little used for evaluation of fracture of the welded joints on aluminium alloys [2]. Therefore, to effectively diagnose the state of the structural members made from aluminium alloys it is important to investigate the AE activity and peculiarities of the AE signals in initiation and development of the processes of fracture in different zones of the welded joints.

Reported are some results of such investigations. In particular, the authors of study [3] employed the AE method for investigation of development of artificially simulated defects in the form of cracks under internal pressure loading of welded vessels made from alloy AMg6M. Based on analysis of the AE signals fixed during an experiment, the authors determined the critical crack size at which the vessel can still remain in operation.

The effect of microstructure of smooth specimens made from commercial aluminium and alloy AMg6M on generation of the AE signals during tension was investigated in study [4]. The AE activity in this alloy is more than an order of magnitude higher than in aluminium, this being

caused by behaviour of grain boundaries and presence of particles of intermetallics. Investigations of behaviour of AE signals in fracture of the welded joints on alloy AMg6M and dependence of the AE signal character on the types of defects are described in study [5]. High activity of the AE signals (6–8 pulse/s), which are characterised by low amplitude, can be observed even at low stresses within the elastic deformation limits (80–90 MPa). It was established that loading of a specimen to stresses that result in formation of plastic deformation (300–320 MPa) causes no pronounced AE. Further growth of deformation is characterised by appearance of isolated AE signals with a low energy and activity. In the deep plastic deformation zone, AE is of a pulse character, i.e. it shows up in the form of «emission of the explosive type». Increasing the load up to fracture is accompanied by generation of the low-amplitude AE signals.

Studies [6, 7] established the character of generation of the AE signals in tension of smooth specimens cut out from different regions of a welded joint. Deformation of the specimens to 13 % resulted in the total quantity of the AE signals equal to 500–800 pulses, and in the fusion zone under the same conditions — equal to $85 \cdot 10^3$ pulses. This character of generation of the AE signals is caused by the presence of a considerable amount of structural defects in the transition zone and accumulation of different non-metallic inclusions along the grain boundaries. Similar experiments were carried out by the authors of study [8], during which the effect of heat input in argon arc welding on the character of generation of the AE signals was investigated by subjecting smooth specimens with a welded joint to static tension. It was shown that increase in heat input is accompanied by growth of ductility of the weld metal, while this leads to decrease in the AE activity.

The purpose of this study was to investigate peculiarities of generation of the AE signals under static loading of specimens, and identify the character of fracture of different regions of the welded joint on alloy 1201-T.

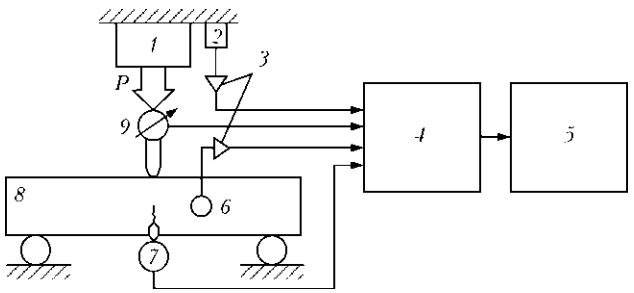


**Figure 1.** Flow diagram of experimental study of static crack resistance of specimens (*1–9* see in the text)

**AE test materials and procedure.** Static crack resistance was investigated by testing specimens cut from the welded joints on 20 mm thick plates made by through EBW without filler metal to three-point bending. Welding heat input was equal to 337.3 kJ/cm. Heat-hardened aluminium alloy of the 1201-T grade was the material of the welded plates. The tests were conducted on four types of the prismatic specimens measuring 10 × × 20 × 160 mm with the induced crack: I — in base metal, II — in HAZ, III — in fusion zone, and IV — in weld metal.

The specimens were made following the rules and characteristic proportions of geometric dimensions specified in GOST [9]. Length of the fatigue crack together with a stress raiser was 10 mm. Flow diagram of the experimental studies of static crack resistance of the specimens is shown in Figure 1.

The specimens were loaded by using machine SVR-5 *1*, where force *P* via dynamometer *9* was imparted to test specimen *8*. Displacement of the crack lips was fixed by crack lip displacement strain-gauge transducer *7*. The AE signals generated as a result of fracture were sensed by primary AE converter *6*, which was placed on the side surface of the specimen. Parallel AE channel *2* was used to select useful signals from noise [1]. Electric AE signals were amplified by preamplifiers *3*, after which they were registered by multichannel measuring AE system SKOP-8M *4* [1] and processed by personal computer *5*. Anti-frictional gaskets were used to decrease the effect of spurious AE signals induced by friction in locations of contact of surfaces of the beam specimen with supports of the machine. Loading and displacement of crack lips were fixed by parametric channels of the above system. Diagrams «load *P*–displacement of crack lips *v*», as well as acoustic patterns of the AE activity accompanying fracture of the specimens were plotted in the post-processing mode. The test results are given in study [10].

The primary AE converter with working frequency band of 0.2–0.6 MHz was used to sample signals. Measuring channels were calibrated prior to each experiment [4]. The following settings were used for AE system SKOP-8M: quantity of the measuring channels — 4 (two for registration of AE signals), amplification of each channel — 40 dB, sampling duration — 0.5 ms, period of analogue signal digitisation — 0.25 μs, cutoff frequency of low-frequency filter — 700 kHz, cutoff frequency of high-frequency filter —

40 kHz, discriminating threshold — 28 %, level of self-noise reduced to the preamplifier input — 7 μV, and gain factor of the preamplifiers — 34 dB.

**Examination of microstructure and fractography of alloy 1201-T.** To identify fracture sources by the AE method it is necessary to conduct microstructural and fractographic examinations of fractures in the characteristic regions of welded joints. Aluminium alloy 1201-T of the Al–Cu–Mn alloying system is susceptible to substantial decomposition of solid solution of the weld metal and HAZ, in which structural transformations decreasing strength of the welded joints to a level characteristic of metal in the annealed state take place at a temperature of 673 K and higher [11]. Therefore, each zone of the welded joint has its own peculiarities of fracture under quasi-static loading (Figure 2).

At room temperature, microstructure of alloy 1201-T consists of grains. The bulk of the grains is composed of α-solid solution of copper and manganese in aluminium and the secondary $Al_2Cu$ phase uniformly distributed within a grain in the form of fine acicular inclusions, as well as along their boundaries in the form of coarse flakes (Figure 2, *a*). It can be seen from the fractography pattern of the base metal (Figure 2, *e*) that fracture is energy-intensive and corresponds to a brittle-tough fracture type. There are many quasi-cleavage facets. The fracture consists mainly of big protrusions and valleys, the surfaces of which are studded with small facets. Comparison of microstructure and microfractography pattern of the base metal of alloy 1201-T shows that grains precisely coincide with the protrusions and valleys in shape and size, and that the grain size is approximately 120–150 μm. Geometry of inclusions of the secondary $Al_2Cu$ phase in the microstructure is comparable with sizes of brittle cleavages in the microfractography pattern (25–35 μm).

Therefore, the crack in the base metal of alloy 1201-T under its static loading propagates primarily along the grain boundaries, and fracture is of a brittle-tough character, where the tough

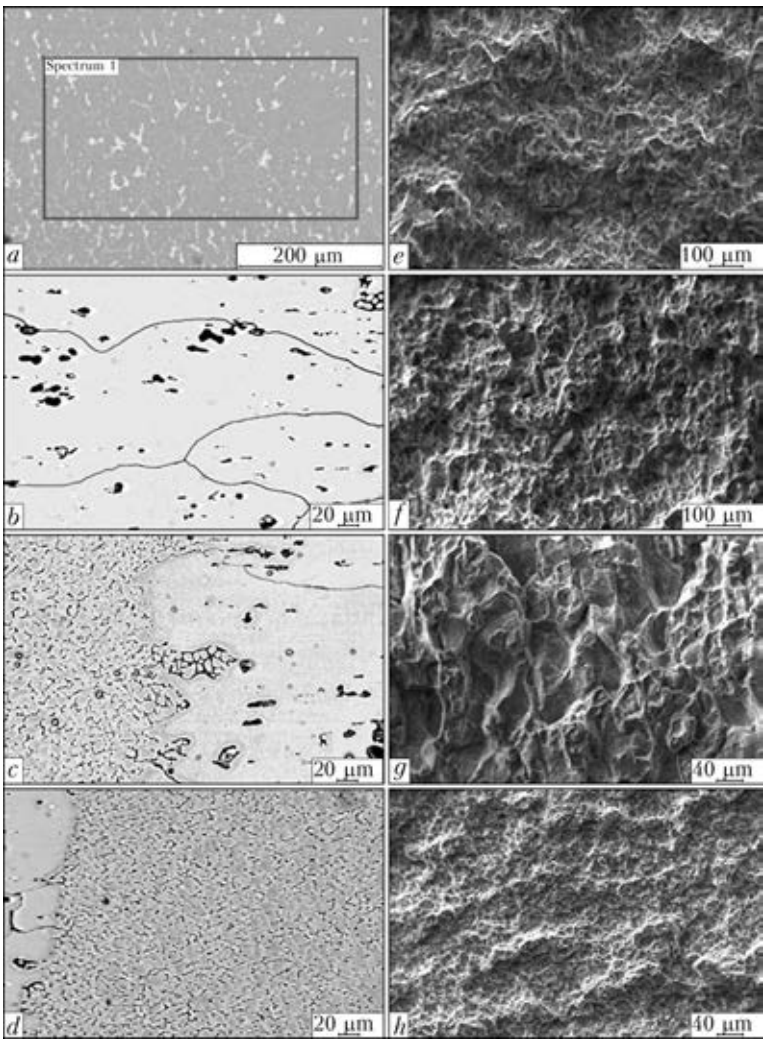


**Figure 2.** Microstructures (*a–d*) and microfractography patterns (*e–h*) of base metal (*a*, *e*), HAZ metal (*b*, *f*), fusion line (*c*, *g*) and weld (*d*, *h*)

component corresponds to fracture of the α-solid solution, and the brittle component — to cracking of the strengthening phase inclusions.

Microstructure of the HAZ metal consists of recrystallised grains depleted in copper (Figure 2, *b*), which precipitated in the form of the secondary $Al_2Co$ phase along their boundaries and coagulated in the form of local clusters during repeated decomposition of the solid solution. Metal of this region is a bit more ductile compared to the base metal. Hence, the microfractography pattern (Figure 2, *f*) shows predominance of the tough fracture with a rare occurrence of brittle inclusion cracking facets.

Dramatic structural changes can be seen at the weld and HAZ metal interface. Melted coarse recrystallised grains of the base metal merge here with the finely dispersed weld metal (Figure 2, *c*). During solidification of the weld pool the secondary phase precipitates and joins into local inclusions, first of all at protrusions of the melted HAZ grains. Therefore, as a rule, the fusion boundary is characterised by a big cluster of intermetallic phases, which causes decrease in its ductility. Fracture of the specimens is of a macrobrittle character (Figure 2, *g*) with quasicleavage facets of cracking of coarse eutectic inclusions.

The high rate of cooling of the weld metal leads to formation of a fine-grained structure (Figure 2, *d*), the strength of which is almost twice as low compared to the base metal. Fracture is of a tough character (Figure 2, *h*) with a bumpy — cup-shaped relief and cells of an evident plastic flow of metal.

As shown by fractography, structural and mechanical heterogeneity of the electron beam welded joints on alloy 1201-T causes a different character of fracture in each zone of the welded joint. In tests of the HAZ metal to static crack resistance, the crack in the majority of cases changed its propagation direction and moved along the fusion line of the welded joint, as much less energy is consumed for the brittle fracture than for the tough fracture. This is indicative of the fact that the given region is dangerous in terms of strength of the welded joint.

**Investigation of peculiarities of AE signals generated in fracture of aluminium alloys.** Important information on peculiarities of the dynamics of fracture processes in solids can be obtained by using the wavelet-transform method [12].

Studies [13, 14] put forward the criterion for quantitative evaluation of fracture of structural materials from parameters of continuous wavelet-transforms of the AE signals. Software AGU-Vallen Wavelet [15] was used to investigate peculiarities of the AE signals. The Gabor wavelet was chosen as the mother one, as it allows distinguishing local peculiarities of the AE signals and provides their frequency-time presentation.

Considering properties of the wavelet-coefficients of the continuous wavelet-transform of the AE signals and results of theoretical investigations of changes in the amplitude-frequency characteristics of the elastic AE waves in various fracture processes occurring in solids, the following criterial index was proposed for quantitative characterisation of the AE signals and their identification [14]:

$$\kappa = \frac{WT_{\max}\Delta f_0}{\Delta f},$$

where $WT_{\max}$ is the maximal value of the wavelet-coefficient of an AE event at a certain time moment; $\Delta f$ is the range of the band of the frequency spectrum corresponding to $WT_{\max}$ in the AE event on the wavelet-coefficient $WT$–frequency $f$ coordinate; $\Delta f_0$ is the width of the working band of the AE path determined by the working frequency band of the AE converter (here it is equal to 0.2–0.6 MHz).

Macrofractures of structural materials are subdivided into the tough ($\kappa \le 0.2$), tough-brittle ($0.2 \le \kappa \le 0.3$) and brittle ($\kappa \ge 0.3$) types, depending on the value of the experimentally determined criterial parameter. Further increase in this value is accompanied by growth of the sensitivity of a test object material to brittle fracture [14].

The sequence of processing of the AE signals fixed in fracture of different regions of the welded joint was as follows:

1) continuous wavelet-transform was plotted for each signal, and maximal value of the wavelet-coefficient in an AE event was determined;

2) projection of the continuous wavelet-transform was plotted in plane $WT$–$f$ upon reaching $WT_{\max}$;

3) width of frequency band $\Delta f$ (MHz) corresponding to $WT_{\max}$ was determined;

4) value of criterial index κ relative to the above one was calculated.

Two types of the AE signals were registered in AE tests of the base metal of alloy 1201-T: AE signals with low amplitudes ($A$ = 0.4–0.5 mV) and κ = 0.2–0.3; and high-power AE signals with $A$ = 1.5–2.0 mV and κ = 0.5–0.6.

Like in the case of the base metal, fracture was accompanied by generation of the two types of the AE signals. Characteristic feature of all the signals is their considerable duration ($t$ = = 20–30 μs), compared to the AE signals fixed

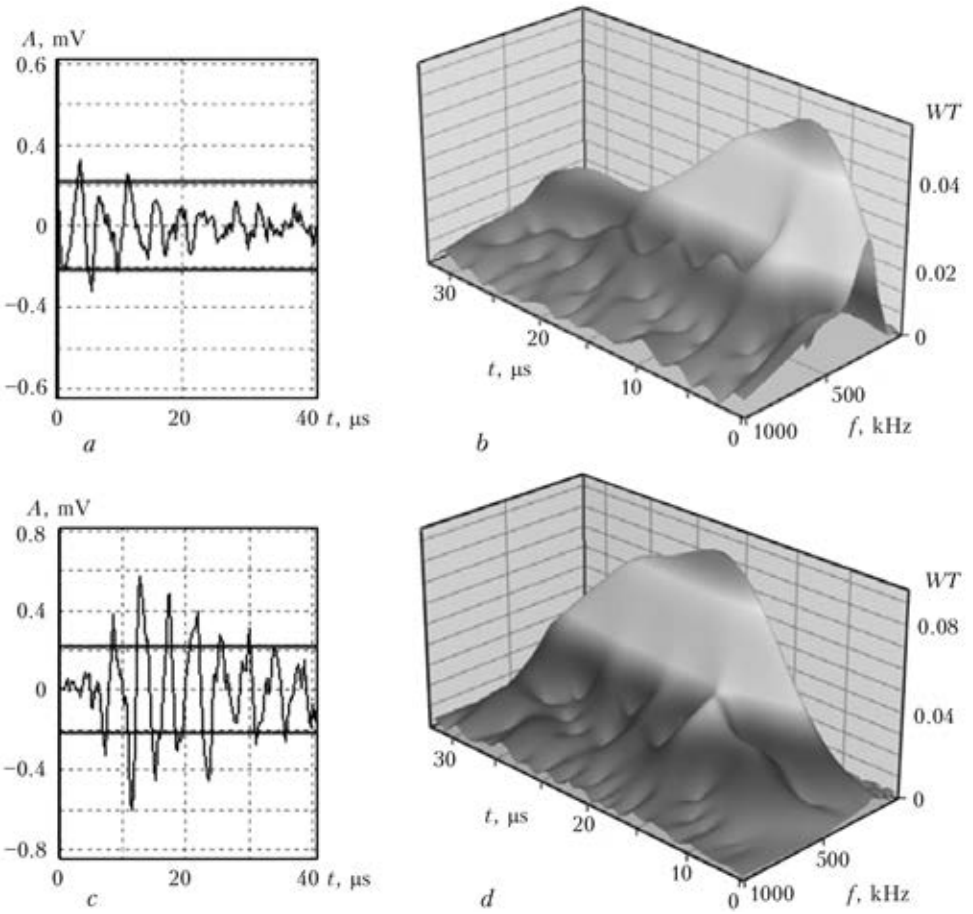


**Figure 3.** Wave reflections (*a*, *c*) and continuous wavelet-transforms (*b*, *d*) of characteristic AE signals (fracture of HAZ metal on alloy 1201-T)

in fracture of other materials [13, 14], this resulting in the characteristic shape of the wavelet-spectra (see Figure 3, *b*, *d*).

The first group of the signals included weak signals (see Figure 3, *a*) with amplitudes $A$ = = 0.2–0.3 mV, which are characterised by low values of maximal wavelet-coefficients $WT_{max}$ = = 0.04–0.05 (see Figure 3, *b*), wide frequency bands $\Delta f$ = 125–130 kHz and $\kappa$ = 0.15–0.20. These EA signals are generated in tough fracture of the solid solution, which makes up the bulk of the recrystallised ductile HAZ grains.

The second group of the AE signals features high values of maximal wavelet-coefficients $WT_{max}$ = 0.08–0.10 (see Figure 3, *d*) and narrow frequency bands $\Delta f$ = 95–105 kHz. These signals are generated in quasi-brittle cracking of local clusters and thin layers of intermetallic $Al_2Cu$ located at the grain boundaries.

Peculiarity of fracture of the welded joint fusion line is that it is accompanied both by cracking of the coarse clusters of eutectic inclusions and by detachment of the melted HAZ grains. In the latter case the AE signals with amplitudes $A$ = 0.4–0.5 mV and $\kappa$ = 0.3–0.4 are generated (Figure 4, *a*, *b*).

Brittle spalling of intermetallics at the fusion line generates strong signals of high amplitudes $A$ = 4–5 mV (Figure 4, *c*), the values of the maximal wavelet-coefficients of which are $WT_{max}$ = 0.15–0.16 (Figure 4, *d*), and frequency bands are $\Delta f$ = 80–90 kHz. Here criterial index $\kappa$ = 0.7–0.9 has the highest value.

The weld in the joint on alloy 1201-T, compared to the base metal, has a finely dispersed structure and is weakened. Fracture in this case occurs by the tough mechanism and is accompanied by weak AE signals (Figure 5, *a*) at $\kappa$ = = 0.10–0.15. Their distinctive feature is considerable duration ($t$ = 40–60 μs) and presence of several peaks on the wavelet-spectra (Figure 5, *b*), which indicates to simultaneous fracture of matrix and delamination of inclusions.

Therefore, cracking of the intermetallic inclusions occurs by the brittle mechanism ($\kappa \geq 0.3$) with maximal values of $\kappa$ at the fusion line, as there the biggest cluster of coarse intermetallics is found, and the solid solution of copper in aluminium is characterised by a fracture occurring mostly by the tough mechanism ($\kappa \leq 0.2$). The character changes into the brittle one only outside the welded joint, because hardness of the

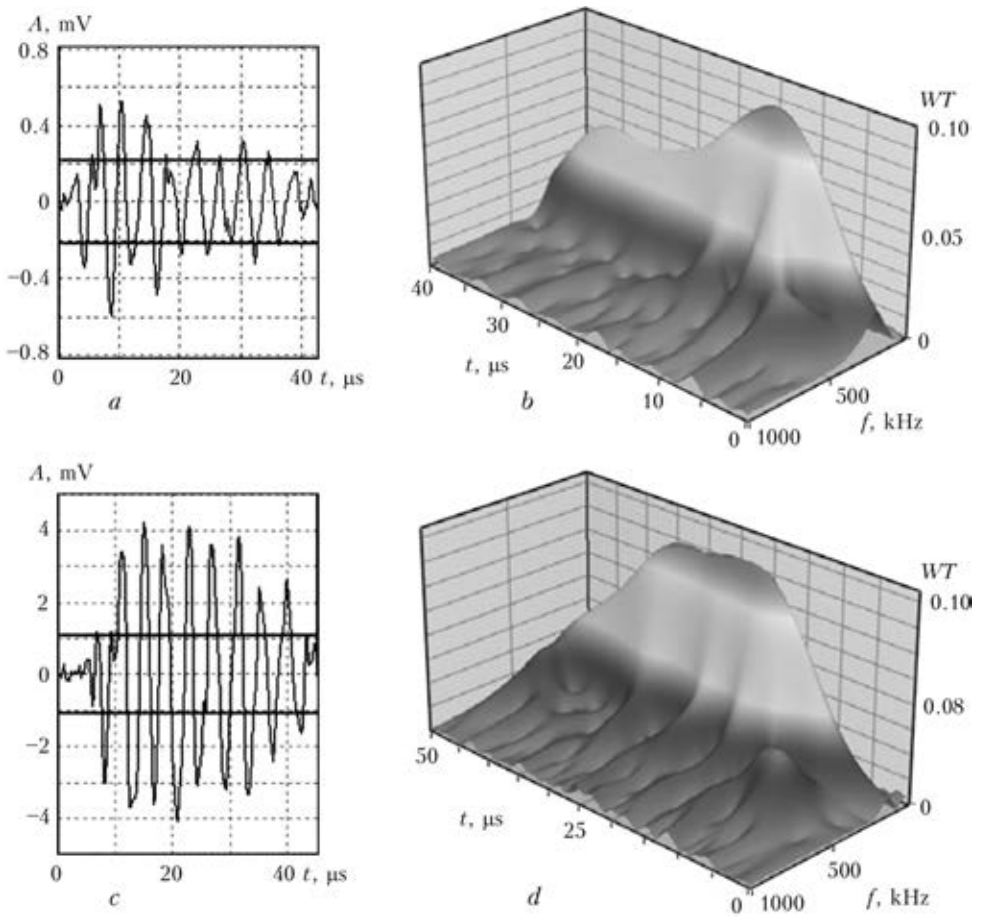


**Figure 4.** Wave reflections (*a*, *c*) and continuous wavelet-transforms (*b*, *d*) of characteristic AE signals (fracture of fusion line of welded joint on alloy 1201-T)

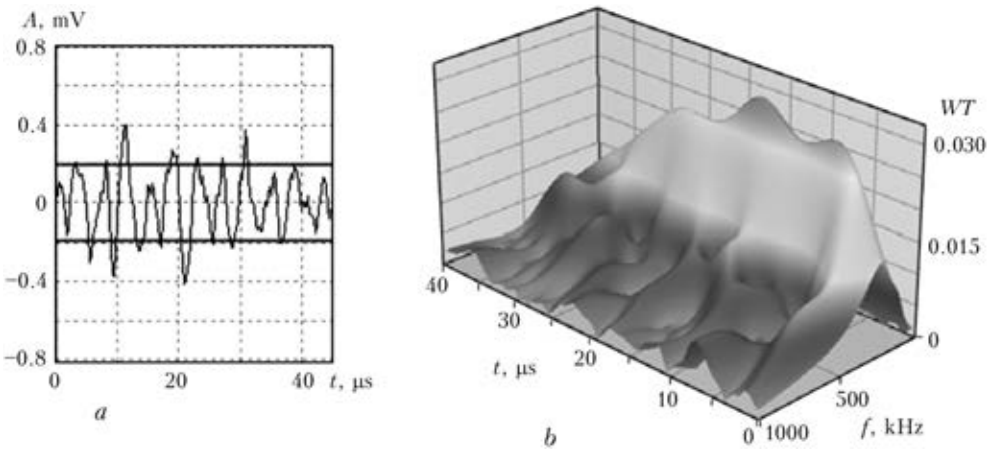


**Figure 5.** Wave reflection (*a*) and continuous wavelet-transform (*b*) of characteristic AE signals (fracture of weld metal in welded joint on alloy 1201-T)

base metal is much higher than that of the weld and HAZ.

## Conclusions

As established from analysis of fixed wave reflections of the AE signals and continuous wavelet-transforms, the AE method allows identification of sources of the AE signals under static loading of aluminium alloys and their welded joints. Tough (weld and HAZ metals) and brittle-tough (base metal) fractures of the solid solution of copper in aluminium generate the AE signals of low and medium amplitudes ($A$ = 0.2–0.5 mV), for which the criterial index varies within 0.15–0.30. Detachment of the melted grains is accompanied by generation of the AE signals with an amplitude range of $A$ = 0.5–4.0 mV and $\kappa$ = 0.3–0.4, whereas cracking of coarse intermetallics is accompanied by generation of the high-power signals ($A$ = 0.5–4.0 mV) with index $\kappa$ = 0.5–0.9.

It was found from the experimental test results that the most dangerous region (in terms of

strength of structures) is the fusion line between the weld metal and HAZ, which is characterised by a dramatic change in size of structural components and mechanical characteristics. In this case the fracture occurs by the quasi-brittle mechanism. As a result, under static loading of the welded joint the crack propagates into this region, moving along the clusters of secondary phases and melted planes of the HAZ grains, thus decreasing the consumption of energy for fracture. In this case, the AE signal parameters change according to the mechanisms of fracture in different zones of the welded joints.


1. Nazarchuk, Z.T., Skalsky, V.R. (2009) *Acoustic emission diagnostics of structural members*. Kyiv: Naukova Dumka.
2. Skalsky, V.R., Lyasota, I.M. (2009) Application of acoustic emission phenomenon for diagnostics of fracture of welded aluminium alloy joints (Review). *Mashynoznavstvo*, **9**, 42–47.
3. Mezintsev, E.D., Tikhy, V.G., Karasyov, L.P. (1982) Application of simulated defects in testing of the technical diagnostics acoustic emission system. *Avtomatich. Svarka*, **9**, 28–30.
4. Tikhonov, L.V., Prokopenko, G.I. (1991) Detonation mechanisms of deformation, fracture and acoustic emission in aluminium and its alloys. *Tekhn. Diagnostika i Nerazrush. Kontrol*, **1**, 73–76.
5. Tikhy, V.G., Sanin, F.P., Borshchevskaya, D.G. (1982) Study of dependence of the acoustic emission signals on the character of welding defects in alloy AMg6. *Avtomatich. Svarka*, **9**, 36–38.
6. Skalsky, V.R., Sergienko, O.M., Golaski, L. (1999) Generation of acoustic emission from cracks propagating in welded joints. *Tekhn. Diagnostika i Nerazrush. Kontrol*, **4**, 23–31.
7. Skalsky, V.R., Koval, P.M. (2005) *Acoustic emission in fracture of materials, products and structures*. Lviv: SPOLOM.
8. Venkitakrishnan, P.V., Sinha, P.P., Krishnamurthy, R. (2006) Study and analysis of effect of various thermal processes in AA2219 annealed sheet using acoustic emissions. *Mater. and Design*, **27**, 770–775.
9. *GOST 25506–85*: Methods of mechanical tests of metals. Determination of crack resistance (fracture toughness) characteristic in static loading. Moscow: Standart.
10. Skalsky, V.R., Lyasota, I.M. (2012) Application of the acoustic emission method for determination of moment of initiation of macrofracture in aluminium alloy welded joint. *Tekhn. Diagnostika i Nerazrush. Kontrol*, **3**, 7–12.
11. Lozovskaya, A.V., Chaika, A.A., Bondarev, A.A. et al. (2001) Softening of high-strength aluminium alloys in different fusion welding processes. *The Paton Welding J.*, **3**, 13–17.
12. Astafieva, N.M. (1996) Wavelet-analysis: theoretical principles and application examples. *Uspekhi Fizich. Nauk*, 166(**11**), 1145–1170.
13. Skalsky, V.R., Bujlo, S.I., Stankevich, E.M. (2012) Criterion for evaluation of brittle fracture of glass from acoustic emission signals. *Defektoskopiya*, **5**, 26–34.
14. Skalsky, V.P., Botvina, L.R., Stankevich, O.M. (2011) Diagnostics of fracture mechanisms in steel 38KhN3MFA by using wavelet-transforms of acoustic emission signals. *Tekhn. Diagnostika i Nerazrush. Kontrol*, **3**, 12–17.
15. Vallen system: The Acoustic Emission Company. *www*.vallen.de


Received 09.07.2012

## *NEWS*

## *Technology and Equipment for Manufacture of Rectilinear Welded Pipes of 20–76 mm Diameter Using the Method of Electric Welding with High-Frequency Currents*

Strip is formed into a tubular billet from a coiled metal by multi-stand successive forming, the edges of this billet are brought together under an acute angle, heated, approaching the site of their abutting by high-frequency currents and upset up to obtaining the welded joint. The process of welding is continuous. Cutting of ready pipes is performed by a fly cutting device automatically.

**Technical characteristics of the equipment:**

| | |
|---|---|
| Welding speed, m/h | 30 ÷ 50 |
| Capacity of HF power source, kW | 100 ÷ 250 |
| Capacity of electric drives, kW | 90 |
| Thickness of pipe wall, mm | 1.2 ÷ 3.5 |
| Length of pipes, m | up to 8 and more |
| Material being welded | cold-rolled or hot-rolled coiled steel, aluminium |

*Field of application*. Machine building, construction, furniture industry, consumer's goods.

*Efficiency*. 3–4 km per shift.

*Payback*. The term of payback depends on annual program and at a full loading of pipe-welding mill it can be 1 ÷ 1.5 years.

# EFFECT OF FRICTION WELDING PARAMETERS ON STRUCTURE AND MECHANICAL PROPERTIES OF JOINTS ON TITANIUM ALLOY VT3-1

**A.G. SELIVERSTOV**[1], **Yu.M. TKACHENKO**[2], **R.A. KULIKOVSKY**[2], **V.I. BRAGINETS**[3] and **I.V. ZYAKHOR**[4]
[1]OJSC «Motor Sich», 15 Motorostroitelej Av., 69068, Zaporozhie, Ukraine
[2]Zaporozhie National University of the Ministry of Education and Science of Ukraine
64 Zhukovskogo Str., 69063, Zaporozhie, Ukraine
[3]Zaporozhie Research-Engineering Centre for Plasma Technologies
of the E.O.Paton Electric Welding Institute, NASU, 3 Uralskaya Str., 69068, Zaporozhie, Ukraine
[4]E.O. Paton Electric Welding Institute, NASU
11 Bozhenko Str., 03680, Kiev, Ukraine. E-mail: office@paton.kiev.ua

The study presents investigation results on formation of joints in friction welding (FW) of titanium alloy VT3-1, which is used in structure of axial-flow compressors of aircraft gas turbine engines (GTE). The purpose of the study was to optimise parameters of FW of alloy VT3-1, based on the possibility of its implementation by using modern equipment for linear friction welding (LFW) in order to manufacture and repair GTE monowheels, i.e. the so-called blisks. Optimal values of the FW parameters were determined on the basis of results of mechanical tensile tests, metallographic examinations and measurements of microhardness of the welded joints produced by FW in air and in shielding gas atmosphere (argon). It was established that in FW of alloy VT3-1 the sound (defect-free) joints can be produced over a wide range of variations in the process parameters, providing that the specified value of the total length loss in welding in ensured. Strength values of the joints exceed those of the base metal of alloy VT3-1. As a result of intensive thermomechanical deformation at temperatures above the β-transus temperature of alloy VT3-1 and rapid cooling after FW, the joining zone metal has a dynamically recrystallised fine-grained structure and increased hardness. Based on the results obtained, the FW parameters were optimised for alloy VT3-1 at a comparatively low linear velocity of relative motion of the billets, which is feasible in LFW of titanium alloys by using the existing equipment. 22 Ref., 1 Table, 6 Figures.

***Keywords:*** *friction welding, titanium alloys, mechanical properties, full strength, welding parameters*

Titanium alloys are widely applied in aircraft engine construction, in particular for manufacture of components of axial-flow compressors of gas turbine engines (GTE). Modern machining methods allow manufacturing complex components, having a relatively high cost. However, the more complicated the machining process, the higher the probability of formation of defects.

Repair operations are most often performed by welding and cladding. However, it is extremely difficult to produce the full-strength joints in repair of parts made from multi-component alloys, and from titanium alloys in particular, while this is especially important for repair of actuated parts, e.g. blades of GTE blisks. Because of high reactivity of titanium with respect to atmospheric gases (oxygen, nitrogen, hydrogen), in fusion welding (FW) of titanium the welded joint metal becomes saturated with these gases. This leads to decrease in mechanical properties and embrittlement of the welded joints, thus negatively affecting the level of reliability of a repaired part. Shielding of the welding zone with oxygen-free fluxes, pure argon, helium or their mixtures provides the welded joints with a strength factor of no more than 0.9 [1].

Also, during the welding process it is necessary to provide the minimal distortions of workpieces, as they will determine the values of allowances and, hence, the scope of subsequent machining. Postweld heat treatment of a weldment is undesirable either (in a number of cases it is unfeasible). The above reasons limit the application of the known FW methods for titanium and its alloys.

The said drawbacks can be minimised by using pressure welding methods, and FW in particular. Joining of metals by this method occurs in the viscous-plastic state without melting of the faying surfaces. Owing to this fact, properties of metal of the joining zone (JZ) and heat-affected

*The study was performed with participation of A.I. Petrik.

zone (HAZ) change but insignificantly, while welding stresses and strains are usually much lower than in FW [2].

The issues of the use of different technologies for FW of titanium alloys are covered in a number of domestic and foreign publications [3–18]. Study [3] shows that conventional FW allows producing the sound joints on titanium alloy OT4, the mechanical properties of which are at a level of the base metal (BM). The FW parameters were set at a level of those for low-alloy steels [2] (heating pressure $P_h$ and forge pressure $P_f$ = 60 and 100 MPa, respectively; total length loss $\Delta_w$ = 6 mm).

Studies [4, 5] investigated the effect of ambient and shielding atmospheres (welding in air and in argon), as well as parameters of conventional FW on formation of structure and mechanical properties of the welded joints on titanium (99.7 %) and titanium alloys of the Ti–6Al–4V and Ti–6Al–2Sn–4Cr–2Mo systems. For all of the investigated alloys the presence of the shielding atmosphere was found to exert no effect on formation of structure of the JZ metal. Parameters of FW in [4] were characterised by comparatively low values of heating pressure $P_h$, forge pressure $P_f$ (25.5 and 31.1 MPa, respectively) and relative motion linear velocity $v$ = = 2.2 m/s.

Study [6] investigated peculiarities of formation of structure and mechanical properties of the welded joints on different titanium alloys in inertia FW of aircraft GTE compressor rotor disks. Weldability of different titanium alloys, such as Ti–6Al–4V, Ti–6Al–4V–2Sn, Ti–8Al–1V–1Mo, Ti–6Al–2Sn–4Cr–2Mo and Ti–6Al–2Sn–4Cr–6Mo, were investigated. As established on the basis of comprehensive mechanical tests and metallographic examinations, inertia FW provides the welded joints that meet specification requirements. The values of strength of the welded joints are higher, and the values of ductility and fatigue are lower than those of BM. Of notice is a very high value of the initial linear velocity of a relative motion in inertia FW of titanium alloys: $v_{init}$ = 35 m/s (rotation frequency of 1130 $min^{-1}$, outside diameter of cylindrical billets of 584 mm).

Study [7] gives results of investigation of structural changes and associated welding stresses in inertia FW of two-phase ($\alpha$ + $\beta$)-alloy Ti–6Al–2Sn–4Cr–6Mo. It was found that structural changes of metal in FW cause a substantial increase in hardness values of the JZ metal. At the same time, the maximal level of residual welding stresses is fixed at the HAZ–BM interface, and this leads to the necessity to subject the welded joints to heat treatment.

Study [8] gives an example of commercial application of inertia FW in manufacture of helicopter rotor components made from alloy of the Ti–6Al–4V system. It is noted that the JZ metal is of a high quality and free from defects, this providing correspondence of mechanical properties to specification requirements.

Therefore, FW by rotation of titanium alloys can produce sound welded joints over a wide range of process parameters: $P_h$ = 25.5–350 MPa, $\Delta_w$ = 2–18 mm, and $v$ = 2.2–35 m/s, provided that the specified upsetting is ensured. Other modifications of FW are also employed to join parts of titanium and its alloys. For instance, it is proposed to use friction stir welding (FSW) to manufacture complex-configuration tubular parts [9].

Linear friction welding (LFW) holds promise for manufacture and repair of GTE blisks [10]. A number of foreign publications considered the prospects of using LFW for manufacture of blisks [11, 12], studied structures and mechanical properties of LF welded titanium alloys [13, 14], described models of thermomechanical processes occurring in LFW [15, 16], and presented designs and specifications of the welding equipment [10, 17].

Analysis of the available publications shows that it is possible to produce the sound welded joints on titanium alloys by using LFW, provided that the sufficient thermal power is generated during the heating process for rapid softening and certain deformation of the JZ metal. The value of the thermal power in LFW is determined to a greater degree by the frequency and amplitude of a relative oscillatory motion, and to a lesser degree — by the heating pressure [15, 16].

Designing of a prototype of the machine for LFW of GTE blisks manufactured by OJSC «Motor Sich» involved a problem associated with optimisation of its technical characteristics. This was related to selection of optimal parameters for LFW of domestic high-strength titanium alloys. It is difficult to identify the optimal parameters of LFW for specific dimension types of billets for the GTE blisks by using the available data on rotational (conventional, inertia) FW. These data can be used only partially, as weldability was investigated mostly on foreign titanium alloys, and the majority of studies recommended using comparatively high values of the linear velocity of a relative motion of billets ($v$ = = 2.2–35 m/s).

The fundamental difference of LFW of metals consists in complexity of technical implementa-

**Figure 1.** Standard (*a*) and special (*b*) specimens of welded joints on alloy VT3-1 after tensile tests

tion of the required process parameters. Modern welding machines for LFW are capable of working over wide ranges of oscillation frequencies (10–250 Hz) and amplitudes (1–7 mm) [10]. This allows setting, e.g. in joining of thermoplastics, the required combination of the oscillation frequency and amplitude, and applying LFW under industrial conditions. However, at comparatively high values of the axial thrust (LFW of high-strength alloys) it is hard to technically realise a combination of the high values of oscillation frequency and amplitude. Therefore, usually $v \le 1$ m/s in LFW [10], and it is this value that predetermines peculiarities of formation of the welded joints, compared to conventional FW.

For this reason, when optimising parameters of LFW of domestic titanium alloys it is important to define permissible limits of variations in process parameters, heating pressure $P_h$ and heating time $t_h$ at comparatively low values of the linear velocity determined by a specific character of the process and technical characteristics of the LFW equipment. To study technical feasibility of formation of the sound (defect-free) joints on high-strength titanium alloy VT3-1 in manufacture of GTE blisks, and to evaluate their mechanical properties, the experiments were carried out on rotational FW, as the thermal deformation cycle of this modification of FW is identical to that of LFW [2].

The purpose of the present study was to optimise parameters of FW of high-strength titanium alloy VT3-1 at a comparatively low specified value of the linear velocity of a relative motion, which is technically feasible with LFW by using the existing equipment.

Preliminary experiments on investigation of formation of structure of the welded joints in FW of VT3-1 alloy specimens with a diameter of 10–30 mm were carried out by using machine ST120, which allows adjusting the values of rotation frequency, axial thrust and time of deceleration of rotation over wide ranges [18]. Welding of the 10 mm diameter billets of alloy VT3-1 to conduct mechanical tests and metallographic examinations was performed by using upgraded machine MST-2 providing the FW cycle at a constant rotation frequency of 1430 $min^{-1}$ and at $P_f = P_h$. FW of the specimens was carried out both in air and in argon atmosphere. Alloy VT3-1 has the following chemical composition, wt.%: 0.2–0.7 Fe, up to 0.1 C, 0.15–0.4 Si, 0.8–2.3 Cr, 2–3 Mo, up to 0.05 N, 5.5–7 Al, up to 0.5 Zr, up to 0.18 O, up to 0.015 H, up to 0.3 — impurities, and titanium is the base [19].

Mechanical properties of alloy VT3-1 are as follows: $\sigma_t$ = 1000–1250 MPa, $\delta$ = 12 %, $\psi$ = 32–35 %, *KCU* = 300 kJ/$m^2$, and hardness (after quenching + tempering) *HRC* = 38–42 [20].

Tensile strength of the resulting welded joints was investigated by using tensile testing machine IR-100. Both standard specimens and special specimens with a notch in the JZ (Figure 1) were tested, which made it possible to determine the strength values of metal in this zone. Microhardness of the JZ metal was measured by using microhardness meter PMT-3. The main criterion of formation of a sound welded joint was reaching the maximal strength values of the joints at the minimal value of upsetting. To optimise the FW parameters the technological process parameters were varied within the following ranges: $P_h$ = = $P_f$ = 10–30 MPa, and $t_h$ = 1.8–8.0 s. At a ro-

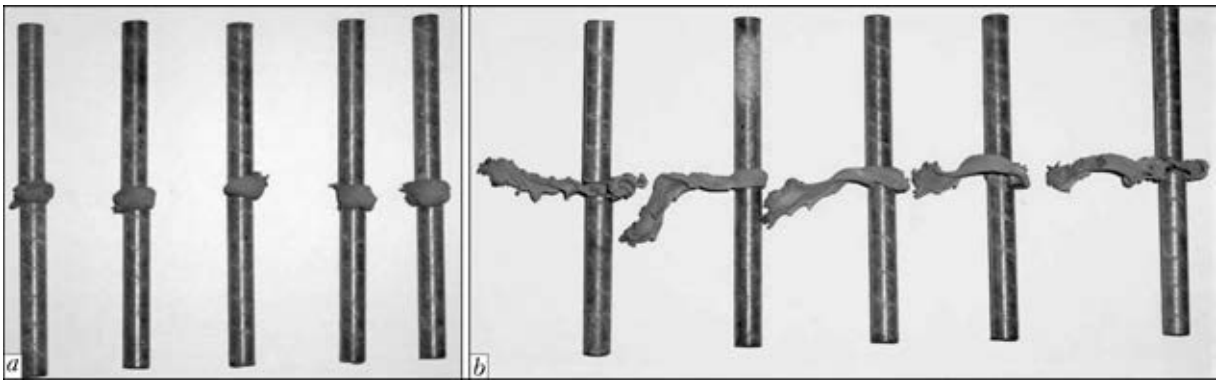

**Figure 2.** Welded joints made by FW at $P_h = P_f$ = 15 MPa, and $t_h$ = 2.2 (*a*) and 4.5 (*b*) s

tation frequency of 1430 $min^{-1}$ and billet diameter of 10 mm, $v = 0.75$ m/s, this corresponding to the values achievable in LFW of high-strength alloys by using the existing welding equipment [10].

As seen from Figure 2, the shape of reinforcement (flash) at $v = 0.75$ m/s approximately corresponds to the shape of flash in LFW of titanium alloy of the Ti–6Al–4V system (Figure 3). The shape of the flash changes with increase in $t_h$ from 2.2 to 4.5 s, this proving advantages of the FW parameters with minimal $t_h$ (see Figure 2).

Characteristics of strength of the FW joints are shown in Figure 4.

As shown by analysis of the results, in FW of alloy VT3-1 the strength values of the welded joints are not lower than those of the BM at all of the above values of $P_h$: 10, 15 and 27 MPa. However, $t_h$ differs substantially for different values of $P_h$. For example, at $P_h = 10$ MPa, $t_h$ should be not lower than 5.3 s, at $P_h = 15$ MPa it should be not lower than 2.2 s, and at $P_h = 27$ MPa the sound joints were produced at $t_h = 2$ s.

Increasing the heating time leads to growth of the total length loss of specimens at an insignificant increase in strength of a welded joint. For instance, at $P_h = 10$ MPa the strength of the joints exceeds that of the BM at $t_h \geq 5.3$ s. However, in this case the total length loss of the specimens considerably grows to 24 mm, compared to $\Delta_w = 7$ mm at $P_h = 15$ MPa and $t_h = 2.2$ s. The results obtained evidence that under industrial conditions $P_h$ should be set within 15–27 MPa to minimise allowances for upsetting and machining.

Similar results obtained in investigation of the effect of the total length loss in FW of alloy of the Ti–6Al–4V system on the quality of the welded joints are given in study [4]. It was established that at $v = 2.2$ m/s, $P_h = 25.5$ MPa and $P_f = 31.1$ MPa the total length loss in welding can be decreased from 12.7 to 3.2 mm without prejudice to the quality of the joints. Similar results were obtained also in study [5], however at much higher values of $v$, $P_h$ and $P_f$.

As noted above, titanium is characterised by a high reactivity with respect to gases contained in the atmosphere at a temperature higher than 350 °C. The effect of probable saturation of the weld metal with gases was checked on the specimens made by FW in air and in the atmosphere of a gas inert with respect to titanium and its alloys. Argon was used to shield the JZ in FW. As established, increase in metal hardness on the specimen surfaces in the HAZ metal to a depth of 0.5 mm was observed in FW performed in air. Moreover, the weld reinforcement forming during upsetting has a high hardness resulting from interaction of the softened metal pressed out from the joint by oxygen and nitrogen present in air.

Results of mechanical tests of the joints on standard VT3-1 alloy specimens with a diameter of 10 mm welded in the argon atmosphere are given in the Table. Fracture of the standard specimens was found to occur in the BM outside JZ and HAZ (see Figure 1, *a*). No substantial effect of the ambient atmosphere on strength values of the joints at the optimal values of heating pressure and time was revealed.

Results of mechanical tests of welded joints on VT3-1 alloy specimens to tensile strength ($t_h = 2.2$ s, $P_h = 15$ MPa)

| Specimen No. | $\Delta_w$, mm | $\sigma_t$, MPa |
|---|---|---|
| 1 | 6 | 1321 |
| 2 | 7 | 1446 |
| 3 | 6 | 1326 |
| 4 | 8 | 1258 |

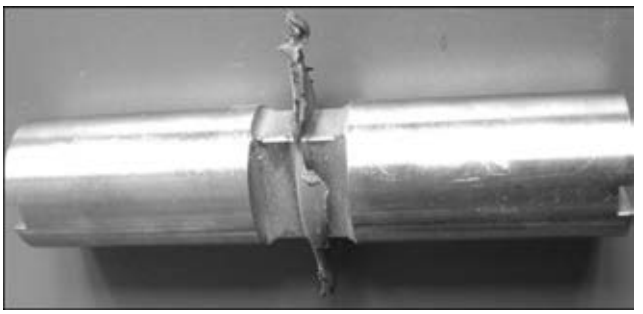

**Figure 3.** LF welded joint on titanium alloy (specimen is supplied by The Welding Institute, Great Britain)

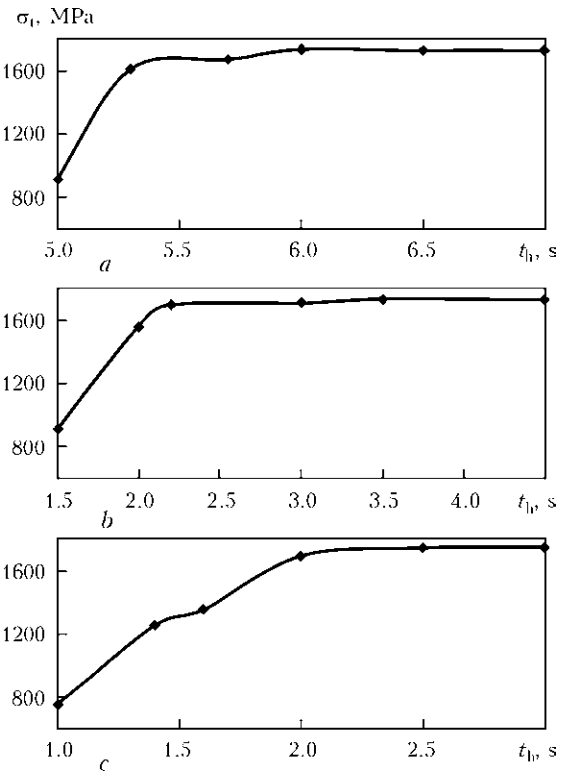


**Figure 4.** Tensile strength of the JZ metal on alloy VT3-1 versus heating time at $P_h = 10$ (*a*), 15 (*b*) and 27 (*c*) MPa

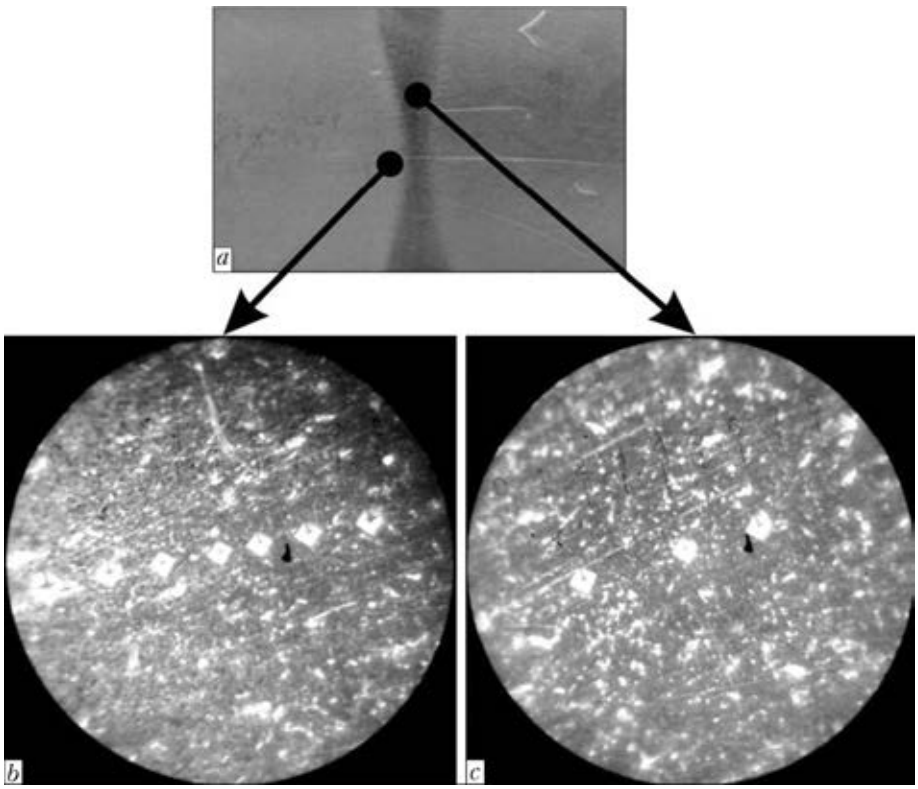

**Figure 5.** Macrostructure (*a*) and zones of measurement of microhardness (*b*, *c* — ×100) of FW joint on alloy VT3-1

The results obtained allowed establishing that the strength values of the welded joints exceed those of the BM. Examination of microstructure of the welded joints made in air and in argon revealed the difference in etchability of the JZ, near-weld and base metals (Figure 5, *a*), the values of microhardness changing from 4.6 GPa in BM to 4.8 GPa in the JZ metal.

In our opinion, increase in strength and hardness values of the weld metal is related to intensive thermomechanical deformation of metal at the temperature above the β-transus temperature. Refining and stirring of structural components of alloy VT3-1 in FW and during rapid cooling after welding result in considerable structural changes occurring in JZ: formation of fine-grained, dynamically recrystallised structure of β-grains with dispersed precipitates of the α-phase (Figure 6).

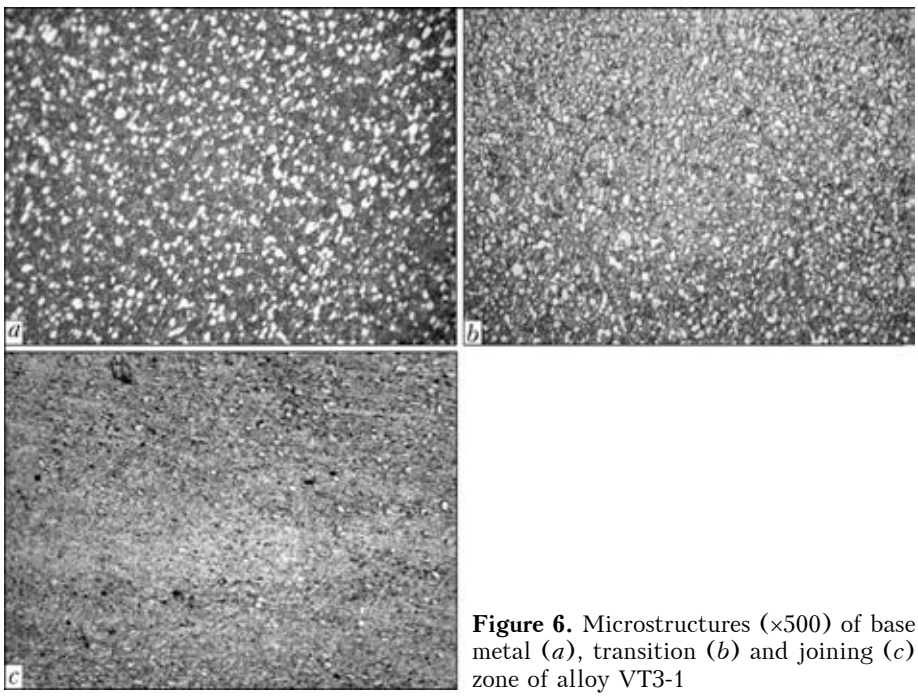

**Figure 6.** Microstructures (×500) of base metal (*a*), transition (*b*) and joining (*c*) zone of alloy VT3-1

In addition, increase in hardness of the joints made by FW in air can be caused by short-time oxidation of the faying surfaces at the initial stages of the process (prior to pressing out of the softened metal from the joint) and redistribution of the formed oxide phases of titanium in JZ. Formation of JZ with increased hardness results from peculiarities of decomposition of β-titanium under conditions of rapid cooling and presence of small amounts of oxygen in the weld, as well as from a partial presence of the β-phase in the meta-stable state [3]. The higher the content of the residual β-phase after high-temperature thermomechanical treatment, the higher the strengthening of (α + β)-titanium alloys during this treatment [21].

Therefore, during the FW process the JZ metal is subjected to high-temperature thermomechanical treatment, which provides refining of structure, increase in dislocation density and increase in the content of the β-phase, which, according to the data of [22] for alloy VT3-1, provides increase in strength by 280–480 MPa, compared to conventional heat treatment.

**Conclusions**

1. It was experimentally proved that the FW parameters affect formation of structure and mechanical properties of the welded joints on titanium alloy VT3-1. Strength values of the joints at $P_h$ = 15–27 MPa and $t_h$ of more than 2.2 s exceed those of BM.

2. Increase in strength of the welded joints on alloy VT3-1 compared to that of BM is related to high-temperature thermomechanical deformation of metal in FW. Refining and stirring of structural components of alloy VT3-1 during heating and deformation, as well as rapid cooling after welding result in considerable structural changes occurring in JZ: formation of fine-grained, dynamically recrystallised structure of β-grains with dispersed precipitates of the α-phase.

3. Based on the results obtained, optimisation of parameters of FW of alloy VT3-1 was achieved at a comparatively low linear velocity of a relative motion, which is technically feasible with LFW of titanium alloys by using existing welding equipment.


1. Tretiakov, V.E. (1968) *Fusion welding of titanium and its alloys*. Moscow: Mashinostroenie.
2. Lebedev, V.K., Chernenko, I.A., Vill, V.I. et al. (1987) *Friction welding*: Refer. Book. Leningrad: Mashinostroenie.
3. Bolshakov, M.V., Chernitsyn, A.I. (1974) Structure and properties of OT4 titanium alloy joints made by friction welding. *Svarochn. Proizvodstvo*, **7**, 40–42.
4. Eichhorn, F., Kes, P., Maser, D. (1990) Gefuegeausbildung und Eigenschaften artgleicher Reibschweissverbindungen aus Titanwerkstoffen. *Schweissen und Schneiden*, 42(**4**), 189–191.
5. Bohm, K.-H., Ventzke, V., Kocak, M. et al. (2003) Parameter study into the friction welding of the intermetallic TiAl and the alloy Ti6Al4V. *Welding and Cutting*, **2**, 90–96.
6. Nessler, C.G., Rutz, D.A., Eng, R.D. et al. (1971) Friction welding of titanium alloys. *Welding J.*, 50(**9**), 379–385.
7. Attallah, M.M., Preuss, M., Booncharoen, C. et al. (2012) Microstructural and residual stress development due to inertia friction welding in Ti–6246. *Metallurg. and Mat. Transact. A*, 43(**9**), 3149–3161.
8. Schwartz, M.M. (1985) Inertia friction welding of helicopter components. In: *DVS Lectures of 2nd Int. Conf. on Welding and Brazing in Aircraft and Spacecraft Construction* (Essen, Sept. 16–17, 1985), 36–43.
9. Threadgill, P.L., Russell, M.J. (2007) Friction welding of near shape performs in Ti–6Al–4V. In: *Proc. of 11th World Conf. on Titanium Science and Technology* (Kyoto, Japan, June 3–7, 2007), 1283–1286.
10. Shtrikman, M.M. (2008) Linear friction welding. *Svarochn. Proizvodstvo*, **12**, 35–40.
11. Vairis, A., Frost, M. (1998) High frequency linear friction welding of a titanium alloy. *Wear*, 217(**4**), 117–131.
12. Wilhelm, H., Furian, R., Moloney, K.C. (1996) Linear friction bonding of titanium alloys for aeroengine application. In: *Proc. of 8th World Conf. on Titanium Science and Technology* (Birmingham, UK, 22–26 Oct. 1995).
13. Tie-jun, S., Dong-gang, S., Yong, Z. et al. (2009) Mechanical properties and microstructure of linear friction welded TC4 + TC17 joint. *J. Aeronaut. Materials*, 29(**4**), 33–37.
14. Wanjara, P., Jahazi, M. (2005) Linear friction welding of Ti–6Al–4V: Process, microstructure and mechanical property interrelationships. *Metallurg and Mat. Transact. A*, 36(**8**), 2149–2164.
15. Vairis, A., Frost, M. (2000) Modeling the linear friction welding of titanium blocks. *Material Sci. and Eng. A*, **292**, 8–17.
16. Vairis, A., Frost, M. (1999) On the extrusion stage of linear friction welding of Ti6Al4V. *Ibid.*, **271**, 477–484.
17. Vairis, A., Frost, M. (2006) Design and commissioning of a friction welding machine. *Materials and Manufact. Proc.*, **21**, 766–773.
18. Zyakhor, I.V. (2001) Modern equipment for friction welding. *The Paton Welding J.*, **7**, 48–52.
19. *GOST 19807–91*: Titanium and wrought titanium alloys. Grades. Instead of GOST 19807–74. Introd. 17.07.91. Moscow: Standart.
20. Akimova, A.Yu., Arzamasov, B.N., Arutyunova, I.A. et al. (1976) *Reference book of metalist*. Vol. 2. Moscow: Mashinostroenie.
21. Brun, M.Ya. (1971) Influence of phase composition on thermomechanical strengthening of (α + β)-titanium alloys. *Tsvet. Metally*, **12**, 53–56.
22. Gurevich, S.M., Zamkov, V.N., Blashchuk, V.E. et al. (1986) *Metallurgy and technology of welding of titanium and its alloys*. Kiev: Naukova Dumka.


Received 14.06.2012

# TECHNOLOGICAL PECULIARITIES OF ELECTROSLAG NARROW-GAP WELDING OF TITANIUM

**I.V. PROTOKOVILOV, V.B. POROKHONKO** and **D.A. PETROV**
E.O. Paton Electric Welding Institute, NASU
11 Bozhenko Str., 03680, Kiev, Ukraine. E-mail: office@paton.kiev.ua

The aim of the work consisted in development of technology for electroslag narrow-gap welding of titanium billets of 120 mm thickness using consumable nozzle, investigation of technological and metallurgy peculiarities of the process and formation of welded joint. The billets of commercial titanium VT1 of the size 120 × 120 × 270 mm were subjected to welding. The consumable nozzles of commercial titanium with two channels for electrode wires of 5 mm diameter were applied. As a slag, the flux AN-T4 was applied. The experiments were realized with the standard size of a gap between the edges of 30 mm and 22 mm into a narrow gap. The modes of welding processes, thermal cycles, macrosections of welded joints and parameters of molten metal pool were analyzed. The results of experiments showed that decrease of welding gap results in increase of welding speed by 13 %, decrease of specific energy input of the process by 23 % and reduction in area of heat-affected zone. The penetration of the edges being welded is decreased on average from 12 to 5.5 mm (by 54 %). The investigation of parameters of molten metal pool showed that width of a pool in electroslag narrow-gap welding decreased from 54 to 33 mm, at decrease of depth of a pool from 22 to 19 mm. According to the results of investigations the technology was developed and the modes of electroslag narrow gap welding of titanium were recommended providing the stable running of the process with a good formation of welded joint, without lacks of penetration, pores, cracks and other defects. 10 Ref., 1 Table, 9 Figures.

***Keywords:*** *electroslag welding, narrow gap, titanium, thermal cycle of welding, weld metal, macrostructure, weld pool*

The electroslag welding (ESW) is the efficient method for joining of structures of titanium and titanium alloys of large thicknesses [1–4]. One of its main advantages is high productivity and possibility of joining the metal of 30–400 mm thickness in one pass without edge preparation. The weld metal is characterized by high density, lack of defects in the form of micro- and macropores, lacks of fusion, etc. The technological advantages of ESW of titanium can also be relative simplicity and reliability of the equipment being in use, easy technology of welds making, additional protective and refining action on the liquid slag metal [1–3].

The disadvantages of ESW of titanium alloys limiting its practical application are undesired structural transformations in near-weld zone under the action of thermal cycle of welding and formation of a rough, coarse-grain structure of weld metal which negatively influences the operational properties of welded joints.

In work [5] the rationality of application of complex methods of influence on ESW process is shown based on thermal and hydrodynamic mechanisms of control of formation of welded joints. The thermal methods can be based on decrease of energy input of welding and redistribution of heat evolution in the volume of a pool which allows decreasing the overheat and non-uniformity of penetration of the base metal and meantime exclude the non-desirable structural transformations in it. The hydrodynamic methods consist in contact-free power influence on weld pool using external magnetic fields to control the processes of heat mass transfer and crystallization of weld metal.

It is very difficult to control the thermal cycle of welding in ESW as far as this process is characterized by large energy inputs and volumes of molten slag and metal. One of the methods allowing decrease of energy input of welding and reduce the width of HAZ is narrow-gap welding. Such investigations were conducted in the 1970s in USSR, England, Japan, USA, Canada and other countries [6–8]. It was shown that narrow-gap welding is characterized by the decrease of volume of slag pool, filler material and increase of welding speed.

According to the standards accepted for ESW of steels, the gap between the edges in the place of welding for metal of 81–160 mm thickness should be 30 mm in the lower part of the edges and 33–49 mm in the upper one [9]. Such sizes are accepted judging from the conditions of guaranteed penetration of the edges being welded and exclusion of the possibility of short-circuiting of

the electrodes (consumable nozzle) to the base metal. The similar gaps of 30–32 mm are recommended also in welding of titanium alloys [1].

The possibility of decrease of welding gap in ESW of steels down to 19 ± 1 mm as applied to the tasks of bridge construction is given in work [8]. It is noted that new technology of narrow-gap ESW provides improved fatigue characteristics and impact toughness of weld metal and HAZ. The mentioned effects are achieved due to decrease of heat input, optimization of a shape of metal pool, application of welding wire which improves the structure of metal.

The aim of present work consisted in development of narrow-gap ESW technology of titanium billets of 120 mm thickness using consumable nozzle, investigation of technological and metallurgy peculiarities of the process and formation of welded joint. The obtained results are planned to be used in carrying out the further investigations in ESW with external electromagnetic effects.

The billets of commercial titanium VT1 of the sizes 120 × 120 × 270 mm were subjected to welding. The experiments were carried out using installation A-1494 with transformer TShP-10000/1 (Figure 1). The consumable nozzles of commercial titanium with two channels for electrode wires of 5 mm diameter were applied. As a slag the flux AN-T4 was applied. The welding was performed with the standard gap between the edges of 30 mm and in narrow gap — 22 mm. In the first case the welded-on titanium cover plates were used as run-in and run-out pockets, in the second case the copper water-cooled forming straps were used. To investigate the thermal cycle of welding the thermocouples of the chromel-alumel type were used which were arranged in welding specimens at the distance of 30, 40, 50, 60 mm from the edges. The hot junctions of thermocouples were fixed in the holes of the base metal at the depth of 20 mm with application of capacitor-type welding. For registration and processing of the process parameters the program packages LabView and PowerGraph were used. From the produced welded joints the longitudinal and transversal templates for the analysis of metal structure, parameters of welds and HAZ were manufactured.

As it was stated above, the technology of narrow-gap welding requires application of additional measures directed to prevention of short-circuiting of the electrodes to the edges being welded and guaranteed penetration of the base metal. For this purpose the consumable nozzle was used, the design of which was selected coming from the conditions of the uniform penetration of edges being welded (Figure 2, *b*). The thickness of nozzle was reduced to 12 mm, and channels for electrode wires were shifted to the edges of the nozzle to increase the heat evolution in the region of water-cooled forming straps. To prevent the short-circuiting of a nozzle to the edges being welded, especially in welding with longitudinal welds, it is rationally to apply insulators manufactured of material similar to the used flux (Figure 3). On fusion of nozzle the insulators are melted compensating the consumption of a slag on formation of skull crust on the weld surface. The insulators can be fixed on the nozzle using welded-on titanium rings (Figure 3,

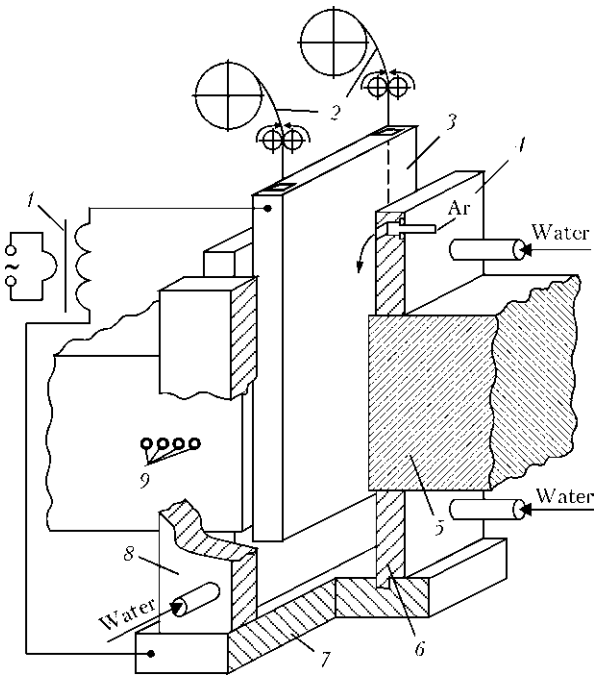


**Figure 1.** Scheme of assembly of specimens for ESW: *1* — power source; *2* — welding wire; *3* — consumable nozzle; *4* — run-out water-cooled forming strap; *5* — specimen being welded; *6* — run-in water-cooled forming strap; *7* — bottom plate; *8* — side forming device; *9* — holes for thermocouples

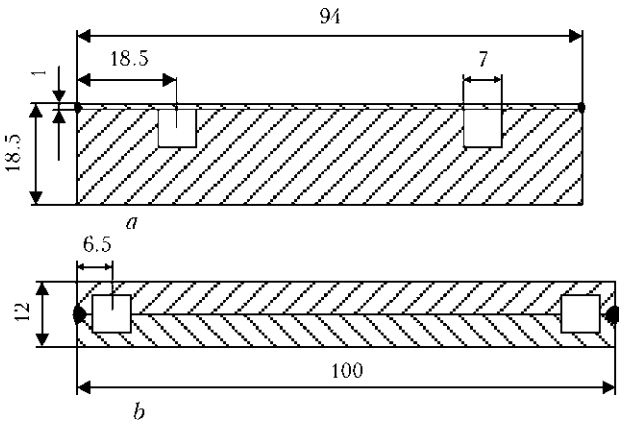


**Figure 2.** Design and geometry of consumable nozzles used during standard method of ESW (*a*) and in narrow-gap ESW (*b*)

Parameters of ESW of titanium billet ($\delta_{b.m}$ = 120 mm)

| Process | Gap size, mm | Welding current, A | Voltage, V | Welding speed, m/h | Specific energy input of welding, kJ/cm$^2$ | Value of penetration of edges, mm | Depth of molten metal pool, mm | Width of molten metal pool, mm | Coefficient of pool shape | Angle of intersection of crystallites of a weld (see Figure 9), deg |
|---|---|---|---|---|---|---|---|---|---|---|
| Traditional ESW | 30 | 3000–4000 / 3500 | 23–25 / 24 | 2.2 | 93–135 / 114 | 10–14 / 12 | 22 | 54 | 2.5 | 120 |
| Narrow-gap ESW | 22 | 2500–3500 / 3000 | 24–26 / 25 | 2.5 | 70–106 / 88 | 4–7 / 5.5 | 19 | 33 | 1.7 | 160 |

*a*) or pressed-in (cast) into special holes in it (Figure 3, *b*, *c*).

The welding parameters and basic results of investigations are given in the Table and in Figures 4–9.

In both cases (standard ESW and narrow-gap ESW) the electroslag process was stable, without splashes of a slag pool, short circuits and arc discharges. The welds had gliterring, smooth side surface (Figure 4). The macrostructure of weld metal was dense, without slag inclusions, pores, cracks and other defects (Figures 5 and 6). Hardness *HB* in the height of a weld was distributed uniformly. Across the width of a weld the increase of hardness in the fusion zone was observed on average by 10 %.

The penetration of edges of the base metal in the cross section in narrow-gap welding was relatively uniform (see Figure 6). The negligible decrease of penetration in the central part of a weld (4 mm) was observed as compared to periphery areas (7 mm) which was connected with heat evolution in the pool, in the place of fusion of electrode wires.

The results of experiments show that decrease of welding gap from 30 to 22 mm results in increase of welding speed (productivity of the process) by 13 % and decrease of specific energy input of the process on average by 23 %. The value of penetration of the edges being welded is decreased on average from 12 to 5.5 mm (by 54 %). The mentioned effects are first of all achieved due to decrease of volume of the deposited metal and optimization of heat mass transfer in the pool.

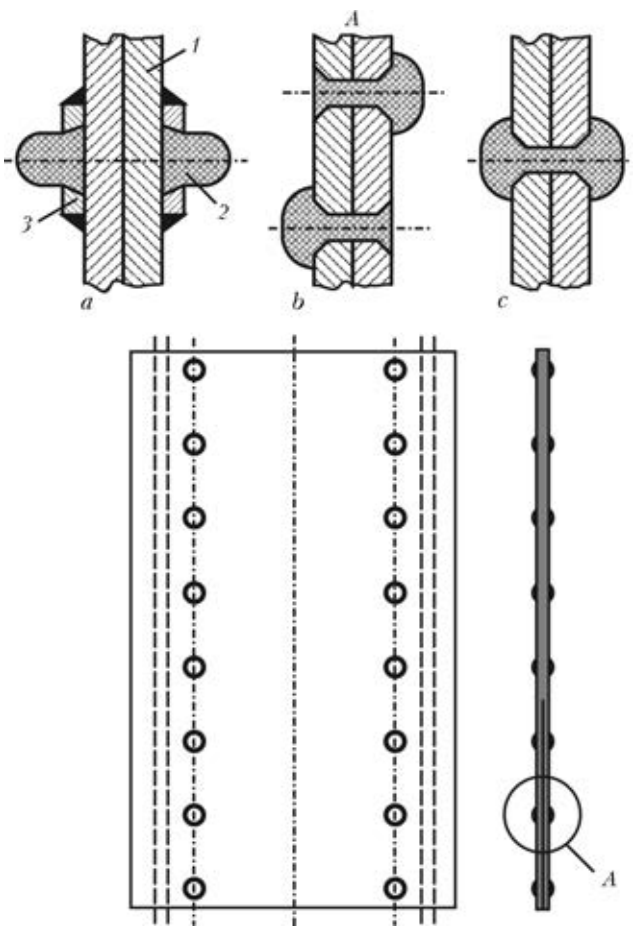


**Figure 3.** Design of electric insulators of consumable nozzle for ESW of titanium: *a* — fixed insulator; *b*, *c* — pressed-in (cast) insulators; *1* — consumable nozzle; *2* — electric insulator; *3* — titanium washer

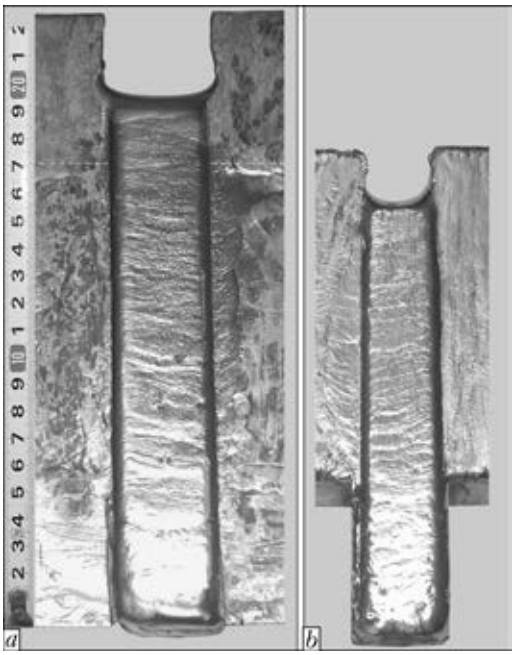


**Figure 4.** Side surfaces of welded joints produced using standard (*a*) and narrow-gap ESW (*b*)

**Figure 5.** Macrostructures of welded joints (longitudinal section) produced using standard (*a*) and narrow-gap ESW (*b*)

**Figure 6.** Macrostructure of welded joint (cross section) produced using narrow-gap ESW

The analysis of thermal cycles of welding (Figures 7 and 8) shows that during decrease of welding gap the maximal temperature of preheating the base metal at the distance of 30 mm from the edge being welded is decreased from 1250 to 640 °C. The width of a heating zone of the metal is higher than the temperature, for example, 840 °C (minimal temperature of start of polymorphous transformations for (α + β)-titanium alloys [10]) in narrow-gap ESW decreased more than twice (from 32 to 14.5 mm). The effect of reduction in area of HAZ is achieved due to a number of factors, first of all decrease in specific energy input of welding and decrease in the volumes of slag and molten metal pools, and also increase in welding speed. The given circumstance decreases the probability of running of the processes of undesirable structural transformations in the base metal.

The investigations of the parameters of molten metal pool show that width of a pool in narrow-gap ESW decreased from 54 to 33 mm at decrease of a pool depth from 22 to 19 mm. Respectively, the coefficient of shape of a pool decreased from 2.5 to 1.7, and angle of crossing the crystallites along the axis of a weld increased from 120 to 160° (Figure 9). Such changes of coefficient of shape of the weld and directions of growth of crystallites can negatively influence the mechanical properties of welded joints, especially along the axis of a weld. Therefore, to reorient the direction of growth of crystallites it is necessary to decrease the depth of metal pool, which can be achieved, for example, by decrease of welding voltage to 19–22 V.

It should be noted that only by change of welding conditions it is impossible to control the solidification of deposited metal to achieve the formation of a weld with homogeneous fine-grain structure. Besides, excessive reduction of a gap and energy input of welding can result in nonstable penetration of base metal and the welding process itself. This requires application of additional mechanisms of influence on heat mass transfer in weld pool and solidification of weld metal, in particular, using external magnetic fields [2, 5]. Such investigations applying pulse electromagnetic effects are planned to be carried out in future.

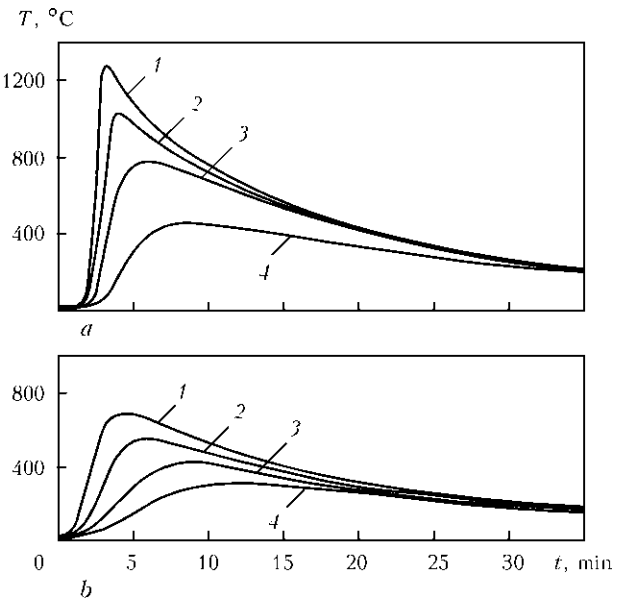


**Figure 7.** Thermal cycles of standard (*a*) and narrow-gap ESW (*b*) for different distances from edge welded: *1* — *l* = = 30; *2* — 40; *3* — 50; *4* — 60 mm

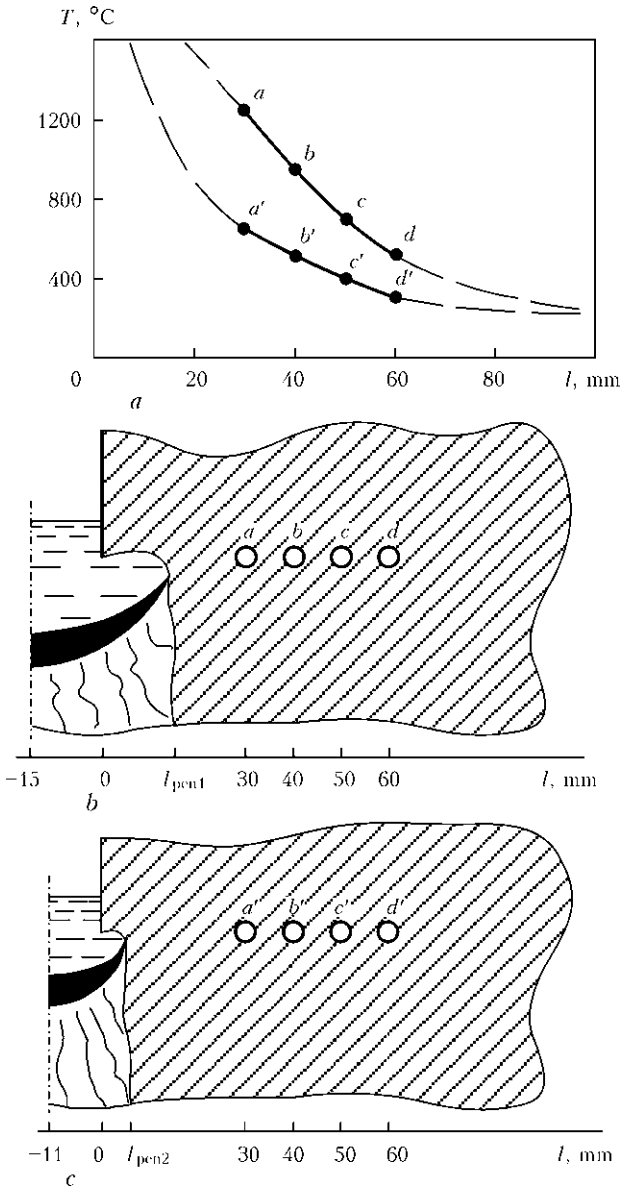


**Figure 8.** Maximal temperatures in welding specimen (*a*) depending on the distance to edge being welded in standard (*b*) and narrow-gap ESW (*c*): *a*–*d* (*a*′–*d*′) — spots where thermal couples are located

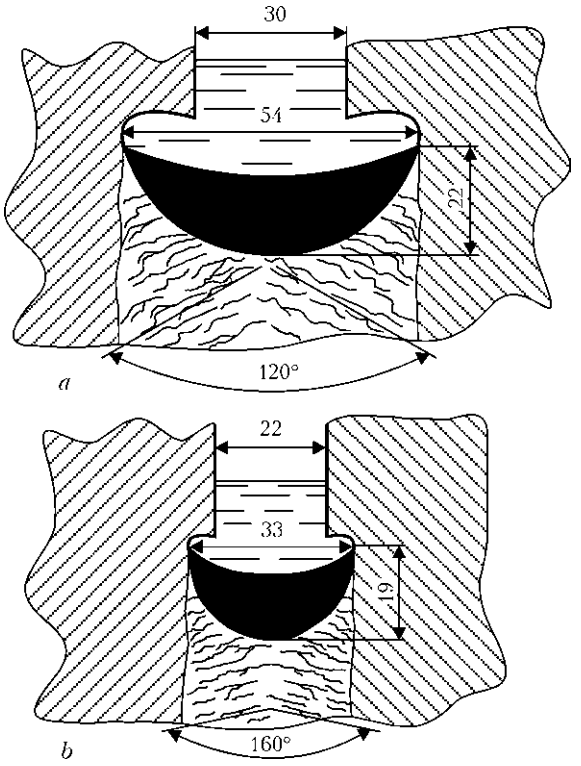


**Figure 9.** Scheme of molten metal pool in standard (*a*) and narrow-gap ESW (*b*)

## Conclusions

1. It was shown that it is possible to decrease the welding gap to 22 mm in consumable nozzle ESW of titanium billets of 120 mm thickness.

2. The technique and conditions of narrow-gap ESW of titanium were developed providing stable running of electroslag process with good formation of welded joint, without lacks of penetration, pores, cracks and other defects.

3. It was established that decrease of welding gap from 30 to 22 mm results in increase of welding speed (process efficiency) by 13 % and decrease of specific energy input of welding on average by 23 %. The thickness of molten metal pool is decreased from 54 to 33 mm, and depth — from 22 to 19 mm.

4. The decrease of energy input in narrow-gap ESW results in decrease of width of HAZ and decreases the probability of proceeding of undesired structural transformations in base metal.

5. The formation in ESW of rough, coarse-grain structure of weld metal, decreasing mechanical properties of welded joint, requires application of additional mechanisms of effect on solidification of metal which can be based on application of external magnetic fields.


1. Kompan, Ya.Yu., Grabin, V.F., Abralov, M.A. et al. (1975) *Electroslag welding of titanium alloys*. Tashkent: Fan.
2. Kompan, Ya.Yu., Shcherbinin, E.V. (1989) *Electroslag welding and melting with controlled MHD-processes*. Moscow: Mashinostroenie.
3. Gurevich, S.M. (1990) *Reference book on welding of non-ferrous metals*. 2nd ed. Kiev: Naukova Dumka.
4. Zamkov, V.N., Lychko, I.I., Topolsky, V.F. (1999) ESW of plates of grade 5 titanium alloy. *Avtomatich. Svarka*, **9**, 73–75.
5. Protokovilov, I.V., Porokhonko, V.B. (2012) Control of formation of welded joints in ESW (Review). *The Paton Welding J.*, **10**, 49–54.
6. Medovar, B.I., Tsykulenko, A.K., Bogachenko, A.G. et al. (1982) *Electroslag technology abroad*. Kiev: Naukova Dumka.
7. Berkovich, I. (1971) Going up faster with narrow-gap electroslag welding. *Weld. Eng.*, **11**, 44–45.
8. Krishna, K. (1996) Narrow-gap improved electroslag welding for bridges. *Welding in the World*, 38(**11**), 325–335.
9. *GOST 30482–97*: Electroslag welding of steels. Requirements to technological processes. Moscow: Standart.
10. Iliin, A.A., Kolachyov, B.A., Polkin, I.S. (2009) *Titanium alloys. Composition, structure, properties*: Refer. Book. Moscow: VILS–MATI.


Received 15.10.2012

# TRANSVERSE MAGNETIC FIELD INPUT DEVICES FOR ARC WELDING AND SURFACING PROCESSES (Review)

**A.D. RAZMYSHLYAEV, M.V. MIRONOVA** and **S.V. YARMONOV**
Priazovsky State Technical University of the Ministry of Education and Science of Ukraine
7 Respubliki Str., 87500, Mariupol, Ukraine. E-mail: gefest@pstu.edu

Application of controlling longitudinal and transverse magnetic fields is promising in arc welding and surfacing, allowing improvement of efficiency of electrode wire melting, refining of the structure of weld metal (deposited bead) and reducing the depth of base metal penetration. In arc welding and surfacing the influence of transverse magnetic fields on geometrical dimensions of welds (beads) and electrode melting efficiency was mainly determined. These works either do not give the input device designs, or they are presented without discussion of the subject of optimality of the used designs, or dimensions of each element of these devices. The objective of this work was analysis of known designs of input devices to assess the effectiveness of their application in arc welding and surfacing. It is shown that the devices described in publications consist of an electric magnet with Π-shaped ferrite core with an air gap and windings. In some works just the transverse component of magnetic field $B_x$ was measured, and longitudinal component of induction $B_z$ induced by the applied input device, was not measured. However, the shape and dimensions of the cross-section of welds and deposited beads in this case could be influenced not only by transverse $B_x$, but also by longitudinal component of magnetic field $B_z$. Design features, as well as distribution of induction components $B_x$, $B_z$ generated by known circuits of devices for application of transverse magnetic fields in the zone of welding arc and pool, were analyzed, and their disadvantages were noted. Urgency of development of new circuits is shown, as well as rationality of optimization of structural dimensions of known circuits of the devices to improve the effectiveness of arc welding and surfacing with application of transverse magnetic fields. 15 Ref., 5 Figures.

***Keywords:*** *arc welding and surfacing, longitudinal and transverse magnetic field, magnetic field induction, input device for transverse magnetic field application*

Application of longitudinal (LMF) and transverse magnetic fields (TMF) in arc welding and surfacing mainly allows improving the efficiency of electrode wire melting, refinement of the structure of weld metal (deposited bead) and reducing base metal penetration depth. It should be noted that in all the works, where LMF or TMF are used at arc welding or surfacing, it is assumed that longitudinal component of induction $B_z$ is directed along electrode axis, and transverse component of induction $B_x$ (or $B_y$) is normal to electrode axis, i.e. is located in the plane of deposited item (plate).

Works [1, 2] deal with LMF input devices (ID) which consist of a solenoid with ferromagnetic core, presence of which considerably increases the longitudinal component of induction in the zone of the welding arc and liquid metal of the pool. In [3] optimum dimensions of solenoid with a round ferromagnetic core with an opening for welding wire passage are calculated for the case of modes of arc welding and surfacing with LMF impact.

Data on TMF ID designs for arc welding and surfacing are sparse. In some papers devoted mainly to consideration of TMF influence on the geometry of welds (beads) in arc welding (surfacing) no data on the design of applied TMF ID are given. Subject of their optimum application is not discussed in most of the publications. Let us consider in greater detail the currently available designs of TMF ID for the case of consumable electrode arc welding and surfacing.

Note that in [4–9] various aspects of the processes of arc welding and surfacing with TMF impact are studied, but they do not give any data on applied TMF ID designs. Studies [10–15] deal with TMF ID constructed by one and the same schematic — an electric magnet with Π-shaped ferromagnetic core with air gap and windings.

In one of the first works, devoted to investigation of the influence of an alternating TMF on butt weld geometry in submerged-arc welding of St.3 steel with Sv-08A wire and AN-348A flux, it is shown that a special electric magnet attached to ADS-1000 automatic welding machine is used

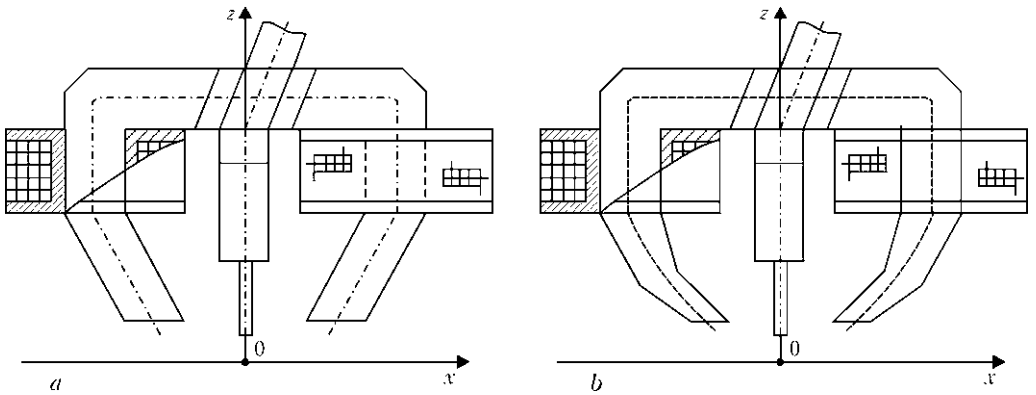


**Figure 1.** Schematic of electric magnets with constant (*a*) and variable (*b*) pole section [11]

for generating TMF [10]. It is established that at transition from a square-edge plate to a grooved plate magnetic induction decreased 4–7 times. TMF application in submerged-arc surfacing promoted lowering of penetration depth by 10–50 % and increase of weld width by 20–25 %. However, this paper does not give the design of the applied TMF ID.

Work [11] deals with TMF ID in the form of a П-shaped electric magnet with two coils, placed on rods with constant (Figure 1, *a*) and variable (Figure 1, *b*) pole cross-section, for the case of DC submerged-arc welding with Sv-08GA wire and AN-348A flux of circumferential roll butt joints of steel pipes (11–12 mm wall thickness).

It is established that sound formation was ensured at ampere-turn number of 3000–7500 and magnet core section of 25 × 25 mm with 20–30 mm air gap between the poles. This device with electric magnets of a constant cross-section, at other conditions being equal, ensured a higher magnetic field induction than the device with variable cross-section rods, tapering towards the poles. Note that in this work just the transverse component of magnetic field $B_x$ was measured in the butt zone. However, in the same zone the magnitude of longitudinal component of induction $B_z$, which was not measured, is considerable. Weld shape in this case could be influenced not only by transverse, but also by longitudinal component of magnetic field induction.

Study [12] presents TMF ID for surfacing cylindrical samples of 76 mm diameter from steel 45, which consists of electric magnet with П-shaped core (Figure 2), which was used in submerged-arc surfacing with Np-30KhSGA wire. It is shown that TMF impact leads to a change of the coefficient of electrode wire melting. This device, however, is applied only at surfacing of

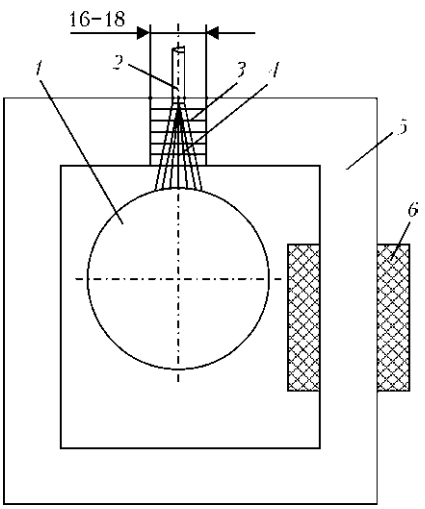


**Figure 2.** Schematic of ID for TMF application to arcing zone in welding [12]: *1* — surfaced sample; *2* — electrode wire; *3* — magnetic lines of force; *4* — welding arc column; *5* — electric magnet core; *6* — coil

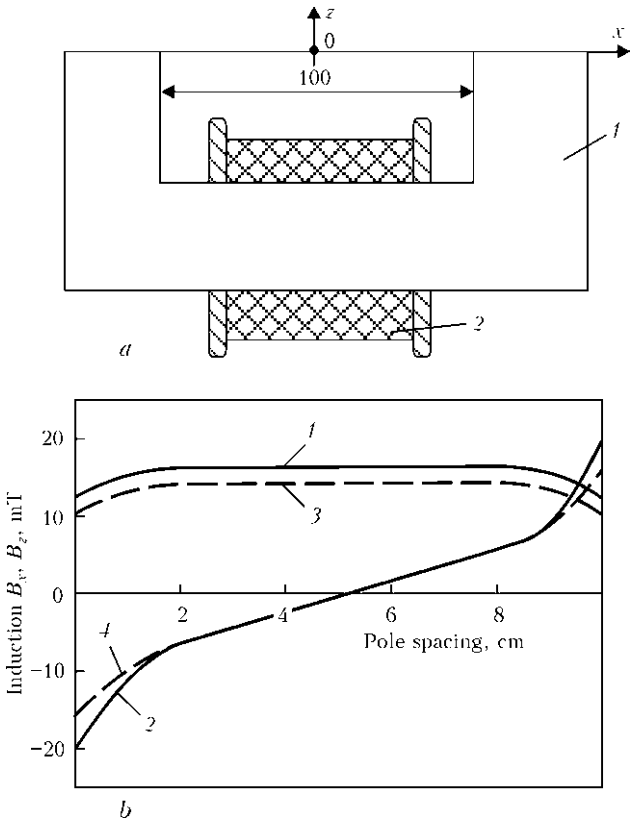


**Figure 3.** Schematic of electromagnetic input device (*a*) and induction distribution between its poles (*b*): *1*, *3* — $B_x$; *2*, *4* — $B_z$; *1*, *2* — $y$ = 0; *3*, *4* — 10 mm

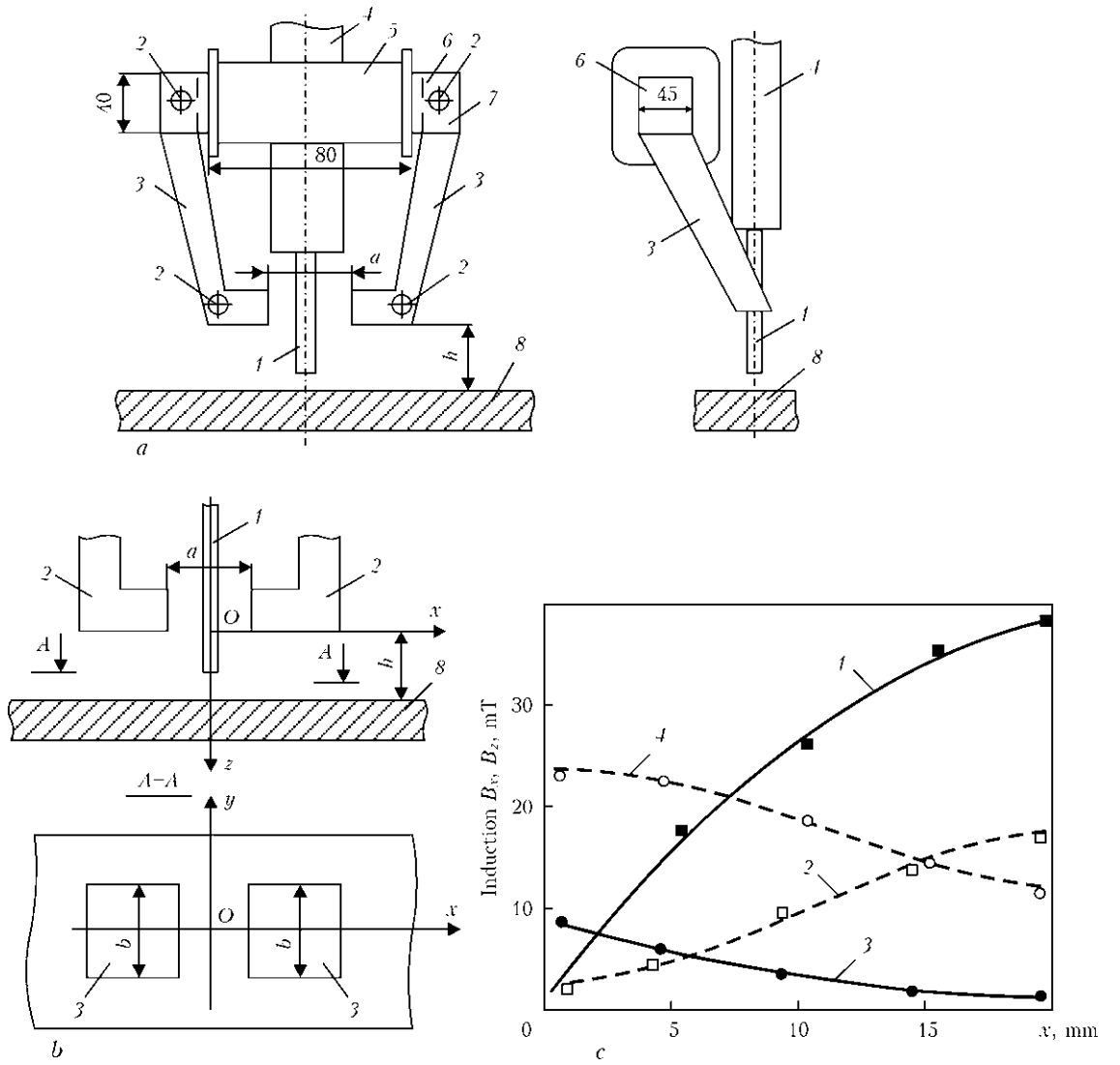


**Figure 4.** Schematic of device for inducing TMF (*a*), coordinate system at measurement of magnetic field induction (*b*) (for designations see the text) and distribution of TMF induction components $B_z$, $B_x$ in the direction of axis $Ox$ (*c*) [14]: *1*, *2* — induction $B_z$; *3*, *4* — induction $B_x$; *1*, *3* — ferromagnetic item; *2*, *4* — item from nonmagnetic material ($y$ = 0, $h$ = 20 mm, $I_w$ = 1920 A)

components of a cylindrical shape and is not applied for surfacing of flat items. Another advantage of such a device is a limited diameter of items which can be reconditioned by surfacing.

In [13] the impact of TMF on the arc in submerged-arc surfacing with wire was made at application of a device consisting of П-shaped magnet core *1* (steel 45) and coil from insulated copper wire *2* (turn number $w$ = 120) (Figure 3, *a*). Surfaced plates from nonmagnetic 12Kh18N10T steel 15–20 mm thick were placed on poles of this П-shaped magnet core. With such a design of the input device, the transverse component of magnetic field induction $B_x$ along the central part between the poles (at the surfaced plate surface) was uniformly distributed, and was higher than the normal component of induction $B_z$ (Figure 3, *b*). It is shown that the impact of alternating TMF leads to widening of deposited beads. At TMF frequency of 50 Hz bead widening proceeds in proportion to induction $B_x$. However, such a design of TMF ID can be applied for research purposes and only for welding nonmagnetic materials and alloys.

Work [4] shows a device (Figure 4, *a*), consisting of magnet core *7*, assembled from sheets of electric steel and frame of coil *5* with turn number $w$ = 480, placed on magnet core *6*. Rods of magnet core *3* (25 × 25 mm section) had a gap of width $a$, through which electrode wire *1* passed. Magnet core rods were connected by bolts *2*. Device was attached to nozzle *4* of automatic welding machine by yokes (not shown in Figure 4, *a*).

It is established that tangential component of induction $B_x$ at the surface of ferromagnetic plate is maximum in the system center and decreases in the direction from electrode axis to electric magnet poles (Figure 4, *c*). Presence of a ferromagnetic item significantly (approximately by

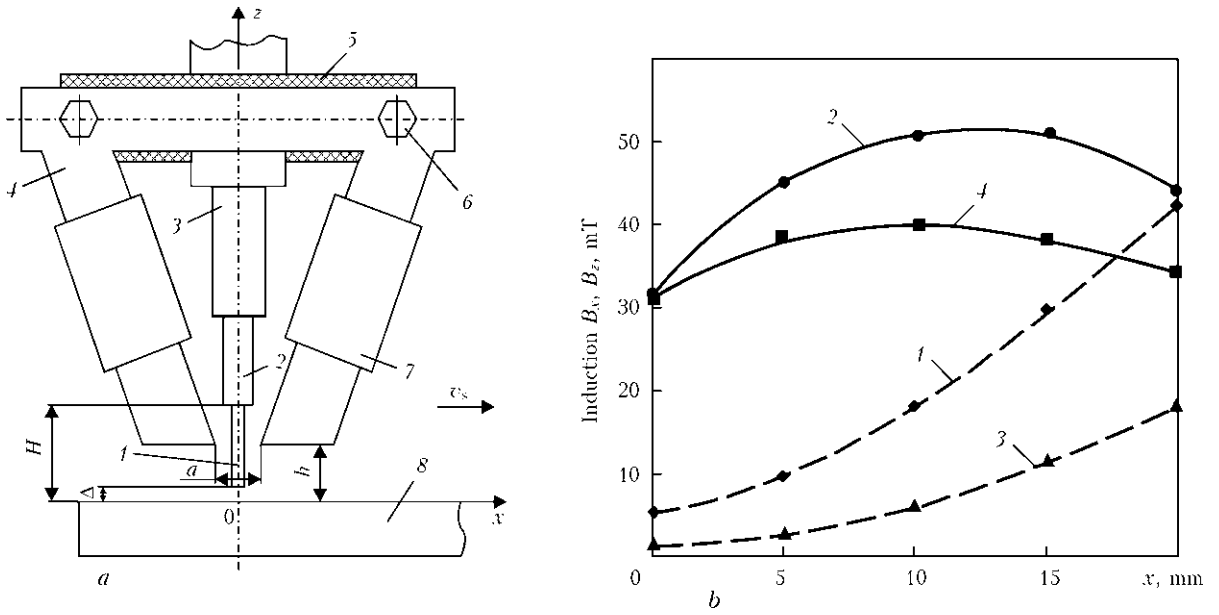


**Figure 5.** Schematic of the device for inducing TMF (*a*) (for designations see the text) and distribution of TMF induction components $B_z$, $B_x$ along axis $Ox$ ($z = 0$, $y = 0$, $I_c = 60$ A) [15]: *1*, *3* — induction $B_z$; *2*, *4* — induction $B_x$; *1*, *2* — constant TMF; *3*, *4* — variable TMF of 50 Hz frequency

4–6 times) lowers $B_x$ and increases the normal component of induction $B_z$ at ferromagnet surface (see Figure 4, *c*) that is associated with weakening action of ferromagnetics on the tangential (transverse) component of TMF induction.

In [15] a device, the schematic of which is given in Figure 5, *a*, was developed for inducing controlling TMF. The device is magnet core *4*, consisting of three sections: two inclined sections, on which coils *7* are located, as well as a horizontal section connected to inclined sections by bolted joints *6*. Magnet core is assembled from plates of electric steel 0.5 mm thick. Pack cross-section is 30 × 20 mm. Number of turns of one coil was $w = 70$. Device generating TMF was attached to automatic welding machine of ADS-1002 type using yokes. Magnet core *4* was insulated from automatic machine by insulator *5*. Automatic machine allows varying parameter $H$ (electrode extension), i.e. distance between current-conducting jaws *2* and plate *8*, as well as distance $h$ from end faces of magnet core *4* to surface of plate *8*. Device design allows measuring the distance between magnet core lower sections at electrode tip (parameter $a$). Electrode wire *1* passed through nozzle *3* (Figure 5, *a* gives the system of coordinates accepted for magnetic field investigation, with the origin of coordinates being located on plate surface under electrode axis).

At measurements of TMF induction the following values were kept constant: distance from electrode tip to plate surface $\Delta = 5$ mm, value of electrode extension $H = 25$ mm, parameter $h = 25$ mm, distance between lower end faces of magnet core along the horizontal $a = 35$ mm. When studying magnetic field induction, Sv-12Kh18N10T wire of 4 mm diameter was used, and base metal was 12Kh18N10T steel plates.

Distribution of inductance $B_z$ of constant and alternating TMF of 50 Hz frequency rises when moving away from axis $Oz$ towards device poles along axis $Ox$ (Figure 5, *b*, curves *1*, *3*). It is characteristic that induction component $B_z$ is much smaller than component $B_x$ in the zone under electrode tip (Figure 5, *b*, curves *2*, *4*). In addition, at running of direct current in TMF ID coils, induction component $B_x$ is greater than at running of alternating current of 50 Hz frequency. This is, apparently, due to the fact that at application of alternating current of 50 Hz frequency losses for eddy currents and hysteresis curve occur in the device magnet core.

It should be noted that data given in Figures 4, *c* and 5, *b* on the nature of distribution of induction $B_x$ along axis $Ox$ are different. This is associated, in our opinion, with the influence of the shape of TMF ID rods on distribution of induction $B_x$ along axis $Ox$. In the considered papers this question was not discussed and requires further study.

Considering the data of [14] showing that in the presence of an item from ferromagnetic steel longitudinal component of induction $B_z$ in the weld pool zone is practically by an order of magnitude higher than transverse component of induction $B_x$ of TMF (see curves *1*, *3* in Figure 4, *c*), it can be assumed that established in works [10–12] effects of TMF influence on geometrical dimensions of cross-sections of welds and depos-

ited beads are due to the impact of not just the transverse, but also the longitudinal component of TMF induction.

Thus, earlier published works on investigation of TMF influence on geometrical dimensions of welds in arc welding and surfacing did not allow for the features of TMF ID design. This task is believed to be urgent for arc welding and surfacing processes.


1. Chernysh, V.P., Kuznetsov, V.D., Briskman, A.N. et al. (1983) *Welding with electromagnetic stirring*. Kiev: Tekhnika.
2. Chernysh, V.P., Kukhar, S.N. (1984) *Equipment for welding with electromagnetic stirring*. Kiev: Vyshcha Shkola.
3. Razmyshlyaev, A.D., Maevsky, V.R., Sidorenko, S.M. (2001) Calculation of magnetic field induction of a solenoid with a ferromagnetic core for arc surfacing. *The Paton Welding J.*, **8**, 18-21.
4. Demiinsky, Yu.A., Dyatlov, V.I. (1963) Magnetic control in consumable electrode gas-arc welding. *Avtomatich. Svarka*, **4**, 82–83.
5. Akulov, A.I., Kopaev, B.V. (1972) Magnetic control of the arc in argon metal-arc welding. *Ibid.*, **7**, 39–42.
6. Boldyrev, A.M., Tkachenko, Yu.S., Tolokonnikov, N.P. et al. (1975) Refining of weld metal structure in welding with arc oscillating in transverse magnetic field. *Ibid.*, **7**, 70–71.
7. Gagen, Yu.G., Perun, I.V., Dobrovolsky, S.T. et al. (1975) Magnetic control of weld formation in automatic submerged-arc welding. *Ibid.*, **11**, 73–74.
8. Demyantsevich, V.P., Lebedev, G.A., Maksimets, N.A. (1975) Influence of external magnetic field and welding parameters on weld formation. *Svarochn. Proizvodstvo*, **11**, 7–9.
9. Razmyshlyaev, A.D. (1994) Control of weld geometry in arc welding and surfacing under the action of magnetic fields (Review). *Ibid.*, **9**, 28–31.
10. Shejnkin, M.Z., Shmeleva, I.A., Varyakhov, N.F. (1969) Application of magnetic oscillations in submerged-arc welding. *Ibid.*, **6**, 24–25.
11. Patskevich, I.R., Zernov, A.V., Ivantsov, V.Ya. (1970) Distribution of induction of induced magnetic field in the zone of welding arc running. *Ibid.*, **2**, 9–10.
12. Iofinov, P.A., Ibragimov, V.S., Dmitrienko, A.K. et al. (1991) Influence of external electromagnetic field on the rate of electrode wire melting in automatic submerged-arc surfacing. *Ibid.*, **1**, 34–35.
13. Razmyshlyaev, A.D., Maevsky, V.R. (1996) Effect of controlled magnetic field on weld geometry in automatic submerged-arc welding. *Ibid.*, **2**, 17–19.
14. Razmyshlyaev, A.D. (2000) *Magnetic control of weld formation in arc welding*. Mariupol: PGTU.
15. Razmyshlyaev, A.D., Mironova, M.V., Kuzmenko, K.G. et al. (2011) Efficiency of melting of electrode wire in submerged-arc surfacing with influence of transverse magnetic field. *The Paton Welding J.*, **5**, 39–42.


Received 24.10.2012

## *NEWS*

### *Laser Cutting of Metallic and Non-Metallic Materials*

The pattern cutting of sheet material according to any preset contour is realized using a program-controlled cutting by a laser radiation of up to 1 kW power. Here, the products of erosion are removed from the zone of radiation action by a jet of air-oxygen mixture. The installation for cutting includes a fast-flowing laser, a three-coordinate manipulator, mirror of optic track, cutter with a focusing lens. Dimensions of the sheet being cut depend on sizes of a manipulator and lie usually within 1–2 m. One of the operating installations is shown in the Figure.

*Field of application*

• cutting of «ferrous» and stainless steels of up to 6 mm thickness;

• cutting of wood, cardboard, plywood of up to 20–30 mm thickness;

• cutting of plastics and organic glass of up to 40 mm thickness;

• cutting of rubber, hard-alloy and other structural materials.

*Technical-economical advantages*

• as compared with a microplasma cutting the accuracy (up to ±0.01 mm) is much increased, there is no cut conicity;

• cut width does not exceed 0.7 mm, that reduces greatly the amount of wastes, making technology ecological;

Process of laser cutting

• labor conditions are improved, there are no such harmful factors, typical for plasma cutting, as noise, illumination of electric arc, exhaustion of harmful aerosols is much reduced;

• there appears a feasibility to cut non-electroconductive thick materials.

*Efficiency*

• up to 500 mm/min in cutting of 6 mm thick black steel;

• up to 2000 mm/min in cutting of 1 mm thick stainless steel.

# EFFECT OF MODE PARAMETERS OF PLASMA SPRAYING USING CURRENT-CARRYING WIRE ON FRACTIONAL COMPOSITION OF SPRAYED PARTICLES

**G.M. RUSEV**[1], **A.G. RUSEV**[1], **V.V. OVSYANNIKOV**[1], **O.G. BYKOVSKY**[2] and **A.N. PASKO**[2]
[1]SPE «Plazmatekh», 4 Gogol Str., 69000, Zaporozhie, Ukraine
[2]Zaporozhie State Technical University of the Ministry of Education and Science of Ukraine
64 Zhukovsky Str., 69063, Zaporozhie, Ukraine. E-mail: root@zstu.zaporizhe.ua

A connection was stated between the parameters of mode of plasma spraying using current-carrying wire and fractional composition of sprayed particles, process efficiency and strength characteristics of coating. Plasmatron «Ornitof-5M» was used for spraying of Np65G wire in a water-filled vessel. Collected drops were sifted. Formation of plasma coating mainly of 0.315–0.1 mm fraction size was determined at cathode deepening from 0 up to 1.5 mm, cathode–anode distance from 8 up to 14 mm, 120–220 A welding current, argon consumption of 15–37.5 l/min and 12–22.5 $m^3$/h air consumption. Movement of the sprayed particles in the center and on the periphery of plasma flow is different and main amount of them is transferred by periphery part of the flow. Distance of spraying was changed in the range from 40 up to 150 mm, content of the elements in the surface layer at optimum distance 100 mm made 0.4–0.43 % C, 0.7–0.77 % Mn, 0.17 % Si and the rest was Fe. Process efficiency makes 0.8–1.1 g/s, coating cohesive strength is 80 MPa at 90–100 mm distance of spraying, hardness makes *HB* 220–240 and porosity — 1–2 %. Layer-by-layer removal of smaller and dust-like fractions using high-speed wire brush provides 25–30 % increase of cohesive strength. Optimum mode parameters, i.e. $d_e$ = 1.2–1.6 mm, $I_w$ = 170 A, $U_a$ = 65 V, $Q_{Ar}$ = 30 l/min, $Q_{air}$ = = 16.5 $m^3$/h, distance of spraying 100 mm with Np65G, PP-100Kh15M2G2R grade wires are used for spraying of wear protection coatings over the parts of power and metallurgical equipment. 2 Ref., 1 Table, 2 Figures.

***Keywords:*** *plasma spraying, sprayed particles, current-carrying wire, fractional composition, mode parameters, cohesive strength, efficiency*

Plasma spraying using current-carrying wire can be performed in a wide range of technological parameters depending on plasmatron design. Change of the parameters provides effect on fractional composition of sprayed particles and their oxidation level, amount of transported heat, temperature of backing (part), thermal cycle of sprayed coating, its strength, density as well as efficiency of the process itself.

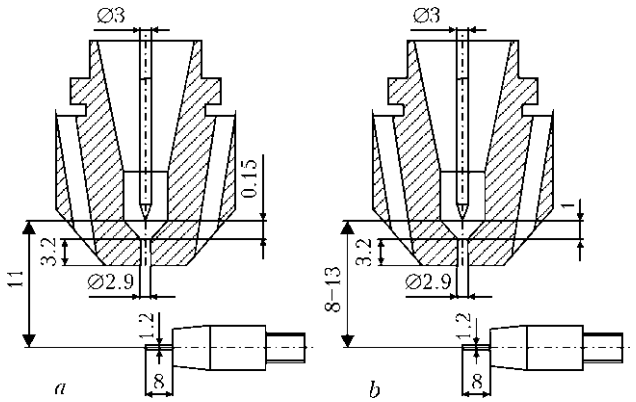


**Figure 1.** Scheme of variants of interelectrode spaces: *a* — cathode deepening (cathode unit); *b* — cathode–anode distance (anode unit)

Investigations were performed with the help of «Ornitof-5M» grade plasmatron [1] on scheme shown in [2]. Np65G wire of 1.2 mm diameter was sprayed in a water-filled vessel of 250 mm diameter from 320 mm distance. Formed drops (fractions) were gotten from the vessel, dried and sifted in sieves of 2.5; 1.6; 1.0; 0.63; 0.4; 0.315; 0.2; 0.16; 0.1; 0.063; 0.05 mm mesh.

Cathode deepening and cathode–anode distance, determining arc voltage, are the important parameters of the plasmatron having effect on mode of plasma spraying. Figure 1 provides the limits of their changing.

Spraying was performed using 160 and 170 A current, and the rest of parameters were as follows: argon consumption $Q_{Ar}$ = 30 l/min, air consumption $Q_{air}$ = 16.5 $m^3$/h, and time of spraying made 100 s. Increase of arc voltage from 60

Results of experimental evaluation of effect of spraying technological parameter on fractional composition of sprayed metal, %

| Parameter | Dimensions of fractions, mm | | | | | |
|---|---|---|---|---|---|---|
| | 2.5–0.4 | 0.315 | 0.2 | 0.16 | 0.1 | <0.1 and dust |
| Cathode deepening, mm | 4–8 | 8–10 | 26–28 | 15–16 | 20–24 | 12–13 |
| Cathode–anode distance, mm | 5 | 6–8 | 24–26 | 18–19 | 22–23 | 12–13 |
| Welding current, A | 5–8 | 34–23 | 18–13 | 18–22 | 10–15 | 7–9 |
| Air consumption, $m^3/h$ | 5–4 | 9–10 | 30–29 | 16–17 | 19–20 | 7–12 |
| Argon consumption, l/min | 4–3 | 12–8 | 25–28 | 16–17 | 23–24 | 14–10 |

up to 66 V at 170 A current and from 59 up to 63 V at 160 A current was determined at change of cathode deepening from 0 up to 1.5 mm. Spraying efficiency makes 1 g/s at 170 A and 0.80–0.84 g/s at 160 A, and burn-out loss is 18–22 and 15–20 %, respectively.

Fractional composition of the drops shows no dependence on current change and being in the specified limits as the parameters' change (Table).

Increase of arc voltage from 54 to 69 V at 170 A and from 52 to 67 V at 160 A was determined for anode unit of the plasmatron at change of cathode–anode distance from 8 up to 14 mm. Efficiency of spraying rises from 0.83 to 1 g/s at 170 A, and this index is somewhat lower and lies in the range from 0.74 to 0.94 g/s at 160 A. The burn-out loss of metal is higher at 170 A (16–22 %) and they achieves 15–16 % at 160 A. There is small change of the fractional composition. It lies in the same range as for cathode deepening (see the Table). The cathode deepening should make 0.5 mm for 160–170 A currents and recommended cathode–anode distance is to be in the range from 9 to 11 mm as was accepted by result of the experiments. At that high process stability is preserved.

These parameters were used for study of effect of welding current changing in the range of 120–220 A.

Increase of the burn-out loss from 0.60 to 1.15 g/s and efficiency from 8 up to 14 % was determined as the welding current rise. Hardness of the layer sprayed over a reference specimen reduces from *HB* 278 to *HB* 222, that can be related with increased burn-out of carbon and alloying elements. Fractional composition of the sprayed particle changes in that or another side (see the Table), at that tendency to reduction of 0.315 mm size fraction is observed, however the latter remains the most coarse constituent.

Different speed of movement of the particles in the center and on the periphery was noticed at visual investigation of plasma flow. This is, obviously, connected with their various mass. Four glass water-filled vessels were used in order to study this effect. Vessels of 40, 65, 90 and 250 mm diameter were inserted one into another. The distance from the plasmatron to water surface level made 320 mm and $I_w$ = 120–200 A. It was determined that the mass of fractions increases from 16 up to 24 g in the central part (40 mm diameter vessel) or somewhat reduces from 20 to 11 g (90 mm diameters vessel), and significant rise from 22 to 35 g is observed on the periphery part (250 mm diameter vessel) at current increase.

This indicates the preferred transfer of the sprayed material by the periphery part of plasma flow. Fractional composition of the particles also changes on plasma flow section. Thus, content of coarse particles of 0.2 mm in the center makes 33–37 %, and on the periphery it reduces up to 17–24 %. Fractions of 0.315, 0.16 and 0.1 mm size in the center of flow make 15–18 %, and on the periphery their presence reduces up to 11–14 %. Quantity of 0.1 mm fraction in presense of 0.16 fraction increases up to 18–25 %, and it reduces up to 8–10 %, in presence of 0.315 mm fraction with current rise. Coarse 0.4 mm fractions, fractions less than 0.1 mm and dust make 1–6 % in the flow center and 6–9 % on the periphery. Increase of welding current promotes somewhat reduction of content of coarse fractions and rise up to 20–23 % of fine ones.

Mass of transported particles significantly depends on consumption of transporting and plasma gases. Consumption of these gases also determines the oxidation level of sprayed particles, their speed, focusing and voltage.

Investigations were carried out using 160–170 A current, firstly changing consumption of air at constant consumption of argon and then — consumption of argon at stable air consumption.

Increase of voltage up to 60–64 V is observed at rise of air consumption, at that, maximum 0.9 g/ s efficiency is achieved.

Increase of $Q_{air}$ in 12.0–22.5 $m^3/h$ range provides smaller change of fractional content of particles (see the Table). Higher heating of nozzle,

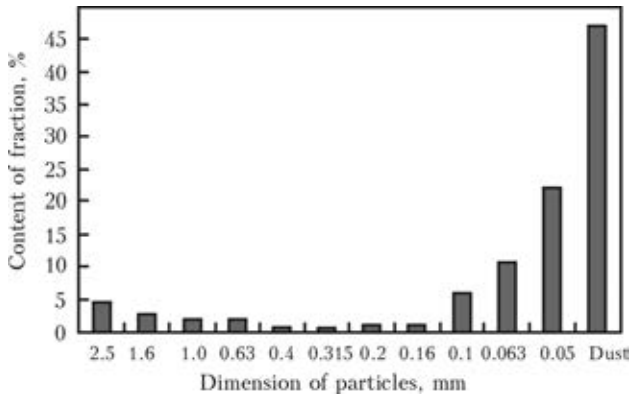


**Figure 2.** Fractional composition of sprayed particles removed layer-by-layer from the surface of part

that can result in its quick fail, takes place at $Q_{air}$ less than 12.5 $m^3/h$.

$Q_{air}$ = 15–17 $m^3/h$ was considered as an optimum one. Increase of $Q_{Ar}$ from 15.0 to 37.5 l/min promotes rise of process efficiency from 0.82 to 1.02 g/s, at that at $Q_{Ar}$ = = 30 l/min reduction up to 0.73 g/s is observed ($Q_{Ar}$ = 37.5 l/min at 160 A). Efficiency increases from 0.96 to 1.09 g/s at $Q_{Ar}$ = 20 l/min, whereupon it reduces up to 0.85 g/s at $Q_{Ar}$ = = 37.5 l/min.

It was noticed that less than 30 l/ min consumption of argon provides more intensive heating of the nozzle and rise of wear of tungsten electrode, that determined $Q_{Ar}$ = 30 l/min as an optimum value. Stability of plasma process appeared to be higher at 170 A welding current. There was virtually no change of fractional composition of the particles (see the Table). Efficiency at that makes 0.98–1 g/s.

The composition of initial material, sprayed on the backing, changes since in a process of air-plasma spraying the particles are heated up to temperature significantly exceeding the melting temperature, their movement takes place in argon-air atmosphere and they steadily interact with oxygen and nitrogen of air. The level of interaction of metal with gas atmosphere will depend to significant extent on spraying distance.

Spraying distance was changed in 40–150 mm range and rest of the parameters of mode of plasma spraying were constant ($d_e$ = 1.2 mm, $I_w$ = 170 A, $U_a$ = 65 V, $Q_{Ar}$ = 30 l/min, $Q_{air}$ = = 16.5 $m^3/h$).

It was determined that the highest coating strength, determined by pin probe method, was achieved at 90–100 mm spraying distance and made 80 MPa at coating thickness 0.5 mm. At that, content of elements in the surface layer was as follows, %: 0.4–0.43 C, 0.7–0.77 Mn, 0.17–Si, and the rest being Fe.

Hardness of coating made *HB* 220–240 and porosity of sprayed layer was in the range of 1–2 %.

Treatment of each sprayed layer of the surface using high-speed steel brush, which separates poorly-attached particles, is an important technological method. Figure 2 shows their fraction composition and based on it the main constituent (84 %) is a tiny and dust-like fraction, preventing valid cohesive adherence of the particles. Cohesive strength of coating adherence can be increased by 27 % as a result of layer-by-layer mechanical treatment.

## Conclusions

1. Increase of welding current and argon consumption results in arc voltage rise.

2. Parameters of mode of plasma spraying, considered in present work, provide no significant effect on fraction composition of the sprayed particles which are manly of 0.1–0.315 mm size.

3. Particles of less than 0.1 mm size and dust-like fractions have low cohesive capacity and their layer-by-layer removal using high-speed steel brush allows increasing cohesive strength of coating by 27%.

1. Rusev, G.M., Kyseliov, S.M., Ovsyannikov, V.V. et al. *Electric arc plasmatron*. Pat. 45253 Ukraine. Int. Cl. 7H05H1/100, 1/24, H05B7/18, B23K10/00. Fil. 10.07.2001. Publ. 15.10.2003.
2. Rusev, G.M., Ovsyannikov, V.V., Kiselyov, S.M. et al. (2000) Technology of restoration and strengthening of surfaces of bodies of rotation and flat surfaces using plasma spraying. *The Paton Welding J.*, **12**, 60–61.

Received 06.09.2012

# INCREASE OF FATIGUE LIFE OF WELDED T-JOINTS WITH LACK OF ROOT PENETRATION USING HIGH-FREQUENCY MECHANICAL PEENING

**S.A. SOLOVEJ**
E.O. Paton Electric Welding Institute, NASU
11 Bozhenko Str., 03680, Kiev, Ukraine. E-mail:office@paton.kiev.ua

Represented are the results of fatigue tests of welded T-joints from low-alloyed steels 09G2S, 10KhSND and 15KhSND. Manufacture of such joints embedded a structural lack of root penetration of 3 × 3 mm cross section along the whole length of the welded joint. The purpose of present study is an experimental evaluation of effect of extensive lacks-of-penetration on fatigue life of the welded joints on low-alloyed steels strengthened by high-frequency mechanical peening which used in manufacture of critical welded metal structures. Testing of welded specimens was carried out with zero-to-tension stress cycle at 5 Hz frequency. It is shown that the fatigue life of high-loaded T-joints from low-alloyed steels strengthened by given technology and containing extensive structural lacks of root penetration of 3 × 3 mm cross section, is in a range of spread of experimental data for strengthened welded joints made with full penetration. Failure of the specimens at that takes place from the lack of root penetration along the rib and their fatigue life rises up to 10 times in comparison with that of unstrengthened specimens with full penetration. As was stated, the presence of structural lack-of-penetration in the unstrengthened high-loaded T-joints, cross ribs of which do not transfer main load, provides no effect on the fatigue life since formation and propagation of cracks take place on zone of weld metal to base metal transfer. 13 Ref., 4 Figures.

***Keywords:*** *welded metal structures, low-alloyed steels, T-joint, fatigue life, high-frequency mechanical peening, fatigue*

Most of welded metal structures of engineer designation (bridges, overpasses, stationary offshore structures) are manufactured from low-alloyed steels. As a rule welded T-joints make up to 70 % in such structures. Lack of root penetration is one of the most possible defects in welding of elements of metal structures by fillet welds. It is well known fact that the lacks of penetration are the reason of appearance of significant stress concentrations and promote rapid decrease of fatigue limit of the welded joints, in particular butt ones [1–3]. Presence of lack of root penetration provides smaller effect on fatigue life of the welded T-joints, cross ribs of which do not transfer main load. The lacks-of-perpetration in such joints can show no signs of presence during the whole service life at small levels of alternating loads and fatigue failure will take place in a zone of weld transfer on base metal.

Problem of increase of bearing capacity of the welded metal structures under service with the help different repair operations applying strengthening post-weld technologies is relevant in present time. High-frequency mechanical peening (HFMP), also known in literature as an ultrasonic impact treatment [4–9], finds increasingly wide application for rise of fatigue strength of the welded joints. Using of specified method of treatment of the welded joint is widely studied as for application to the T-joints with full penetration in as-welded condition as well as after running of specific number of cycles of stress change [8, 10–12]. It was shown that strengthening using HFMP technology allows significantly increasing characteristics of the fatigue strength of such joints and levels of applied stresses, respectively. There are no data in investigations performed on fatigue strength of welded T-joints strengthened by HFMP with technological or structural lacks of root penetration, including at increased levels of applied stresses correspondent to strengthened welded joints.

The aim of the present work is evaluation of effect of lacks-of-penetration on fatigue life of the T-joints from low-alloyed steels strengthened by HFMP.

Fatigue tests were carried out on specimens of welded T-joint from low-alloyed steels 09G2S ($\sigma_y$ = 375 MPa; $\sigma_t$ = 510 MPa), 10KhSND ($\sigma_y$ = = 420 MPa; $\sigma_t$ = 610 MPa) and 15KhSND ($\sigma_y$ = = 400 MPa; $\sigma_t$ = 565 MPa). Billets for specimens from these steels were cut out from sheet products so that a long side was oriented along the rolled products. Cross ribs were welded from two sides by fillet welds performed by manual arc welding with UONI-13/55 grade electrodes. The lack of

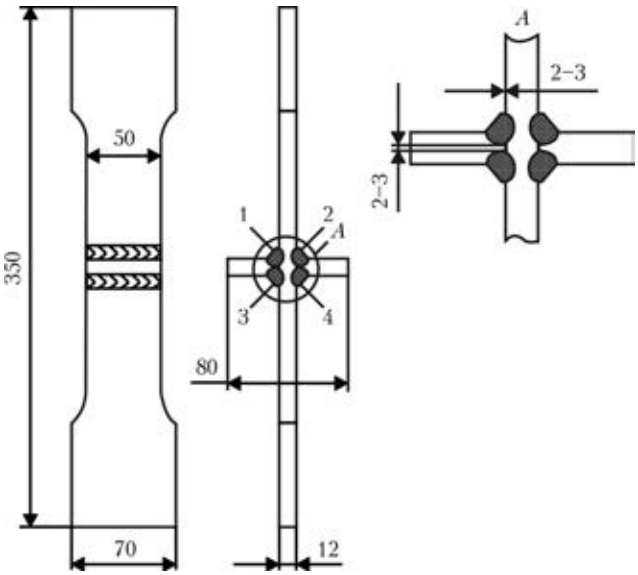


**Figure 1.** Shape and dimensions of specimens of T-joints from low-alloyed steels

root penetration of 3 × 3 mm cross section along the whole length of the specimen (length of weld) was formed by means of increase of gap between a plate and welded rib as well as rise of root face width. Figure 1 shows shape and geometry dimensions of the specimens with lack of root penetration. Thickness of the specimen made 12 mm that is caused by wide applicability of rolled products of this thickness in the welded structures, and width of working part of the specimen was taken based on capacity of testing equipment. Compact manual equipment US-TREAT-1.0 was used for strengthening of the welded joints. Fatigue tests of the specimen were performed on URS-20 machine at alternating zero-to-tension stress with 5 Hz frequency at regular and non-regular loadings (Figure 2). Each of the specimens was tested up to complete failure.

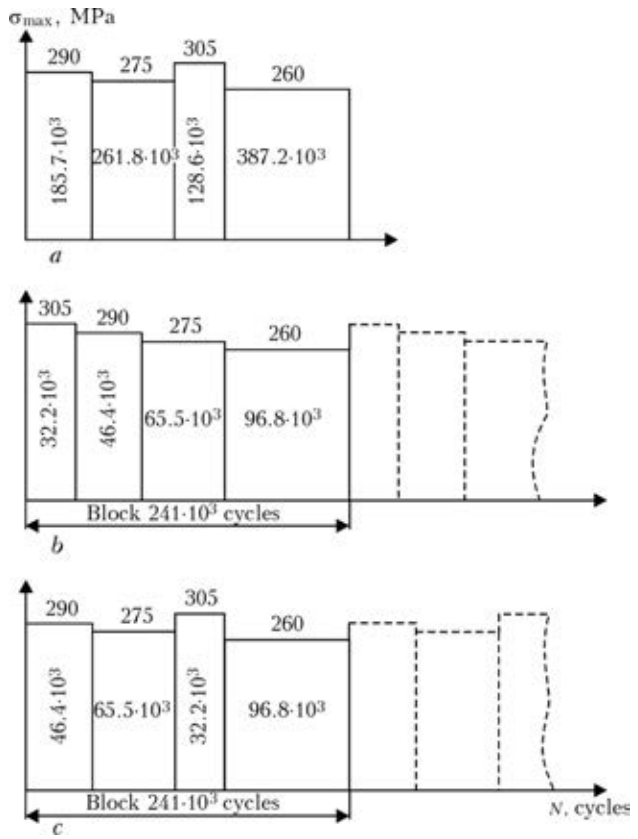


**Figure 2.** Schemes of loading of specimens of welded T-joints from 09G2S steel at multilevel (*a*) and block loading with descending (*b*) and quasirandom (*c*) sequences of loading application

Two specimens from 10KhSND steel were tested at increased levels of applied stresses for determination of place of crack nucleation (along a fusion line or starting from lack-of-penetration) in T-joints with lack of root penetration. Zones of weld transfer on base metal 1 and 2 (see Figure 1) were treated by HFMP in as-welded condition. Maximum applied stress 290 MPa was used for the tests. Fatigue cracks of up to 0.5 mm depth (up to 3 mm length) appeared after running of 102.3 and 119.0 thou cycles of stress change in the unstrengthened zones (zone 4 of specimen 1 and zone 3 of specimen 2, respectively). Zones damaged by fatigue cracks were treated using HFMP and the tests were continued with the same levels of loading. Similar cracks appeared in unstrengthened zone 3 of specimen 1 and zone 4 of specimen 2 after running of 232.5 and 152.8 thou cycles of stress change, respectively, in a course of further tests. The tests were continued after HFMP of the zones damaged by fatigue cracks. Specimen 1 failed after 858.9 thou cycles, and specimen 2 — after 1823.4 thou cycles of stress change. In both cases the fatigue cracks developed from the lacks-of-penetration and failure took place along the welded ribs which do not transfer main load. Figures 3 and 4 show failed specimens.

Obtained test results indicate that no signs of the lack-of-penetration in unstrengthened T-joints, cross ribs of which do not transfer main load, can appear during the whole service life since the failure will take place along the zone of weld transfer to base metal. The life of T-joints strengthened by HFMP and made with full penetration [10] will be in a range of 600–1100 thou cycles at the level of applied maximum stress 290 MPa based on stress–cycle diagram. The failure at that takes place along the zone of weld transfer to base metal. Thus, fatigue life of the joints after strengthening by HFMP increases 5–10 times in comparison with that of the unstrengthened specimens with full penetration [10] and failure takes place from the lack-of-penetration along the rib. Also, a high efficiency

of strengthening of the welded joints with fatigue cracks of insignificant depth (≈0.5 mm) using HFMP is confirmed by investigation performed.

Evaluation of effect of level of stresses applied to the place of crack nucleation (along the fusion line or from the lack-of-penetration) was carried out on specimens 3 and 4 of T-joints with lacks-of-penetration made from 09G2S and 15KhSND steels, respectively. Strengthening of all zones of welded joint using HFMP was carried out in the as-welded condition. Specimen from 09G2S steel was tested at the level of maximum applied stress 260 MPa. The failure from lack-of-penetration along the rib took place after 1127.2 thou cycles of stress change (Figure 4, *c*). The failure along the fusion line [11] in the range of 1150–1950 thou cycles of stress change occurred in the joints with full penetration which were strengthened using HFMP in the as-welded condition at loading by maximum stress cycle 260 MPa at similar tests. Specimen from 15KhSND steel was tested at level of maximum applied stress 300 MPa. The failure from lack-of-penetration along the rib took place after 830.7 thou cycles of stress change (Figure 4, *d*). The failure along the fusion line in a range of 600–900 thou cycles of stress change took place in the joints with full penetration, which were strengthened at loading by maximum stress 300 MPa at similar tests. Thus, the failure of studied specimens took place from the lack-of-penetration along the rib in the range of applied maximum stresses 260–300 MPa typical for high-cycle area of strengthened T-joints from low-alloyed steels. At that, fatigue life of the welded joints increases up to 10 times in comparison with that of the unstrengthened specimens with full penetration [11].

It is well known fact that the metal structures of engineer designation are, as a rule, exposed to complex irregular modes of loading [13] in the process of operation. Four specimens of welded T-joints with lack-of-penetration from 09G2S steel were manufactured for evaluation of effect of loading type (multilevel or block) on efficiency of strengthening using HFMP technology. Figure 2 shows the schemes of loading of specimens, indicating the levels of applied maximum stresses, their sequence and amount of cycles on each level. All the specimens were strengthened by HFMP in the as-welded condition. Similar tests of the specimens of T-joints with full penetration, which were strengthened using HFMP, were carried out earlier considering specified schemes of loading, and their results are shown in works [11, 12].

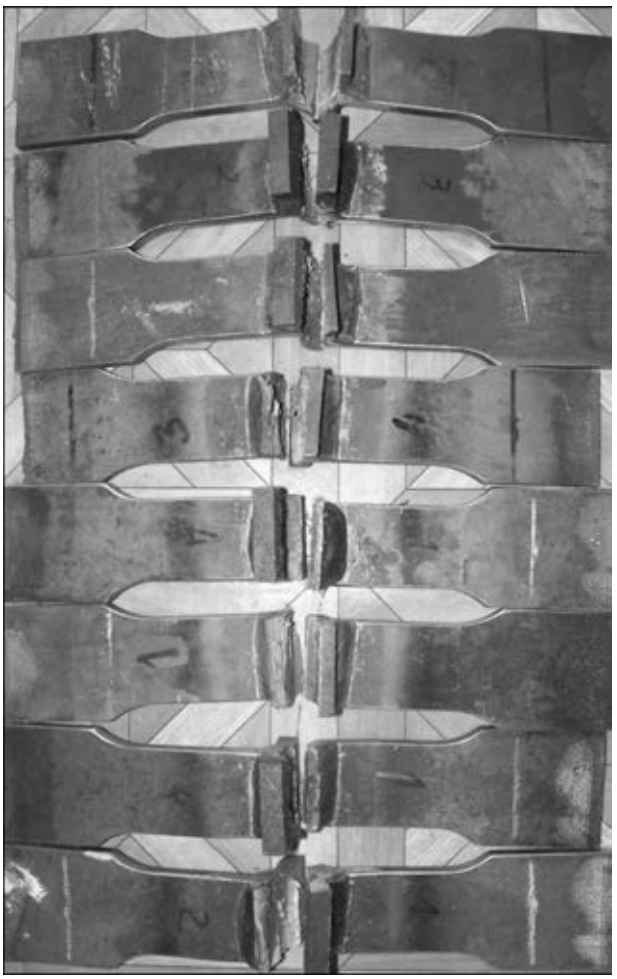

**Figure 3.** General view of welded T-joints with lack of root penetration which were strengthened by HFMP after fatigue tests

Specimen 5 which was tested under multilevel loading condition (see Figure 2, *a*) failed after running 119.4 thou cycles on the third level of loading (Figure 4, *e*). General running at three levels of loading made 566.9 thou cycles. Welded specimens with full penetration strengthened by HFMP failed along the fusion line [11] in the range of 565.8–1079.8 thou cycles at similar tests.

Specimens 6 and 7 were tested under block loading condition at descending order of load application in each block (see Figure 2, *b*). Failure of the specimens took place after 26.3 thou cycles on second step of the forth block of loading (total amount of cycles up to failure at all levels of loading is 781.2 thou cycles) and after 76.8 thou cycles on fourth step of the second block of loading (total amount of cycles up to failure at all levels of loading is 461.8 thou cycles), respectively. Photos of fatigue fractures are given in Figure 4, *f*, *g*, respectively. Strengthened joints with full penetration failed along the fusion line [12] in the range of 492.3–775.6 thou cycles of stress change at similar tests. High life of the specimen with lack-of-penetration is caused by

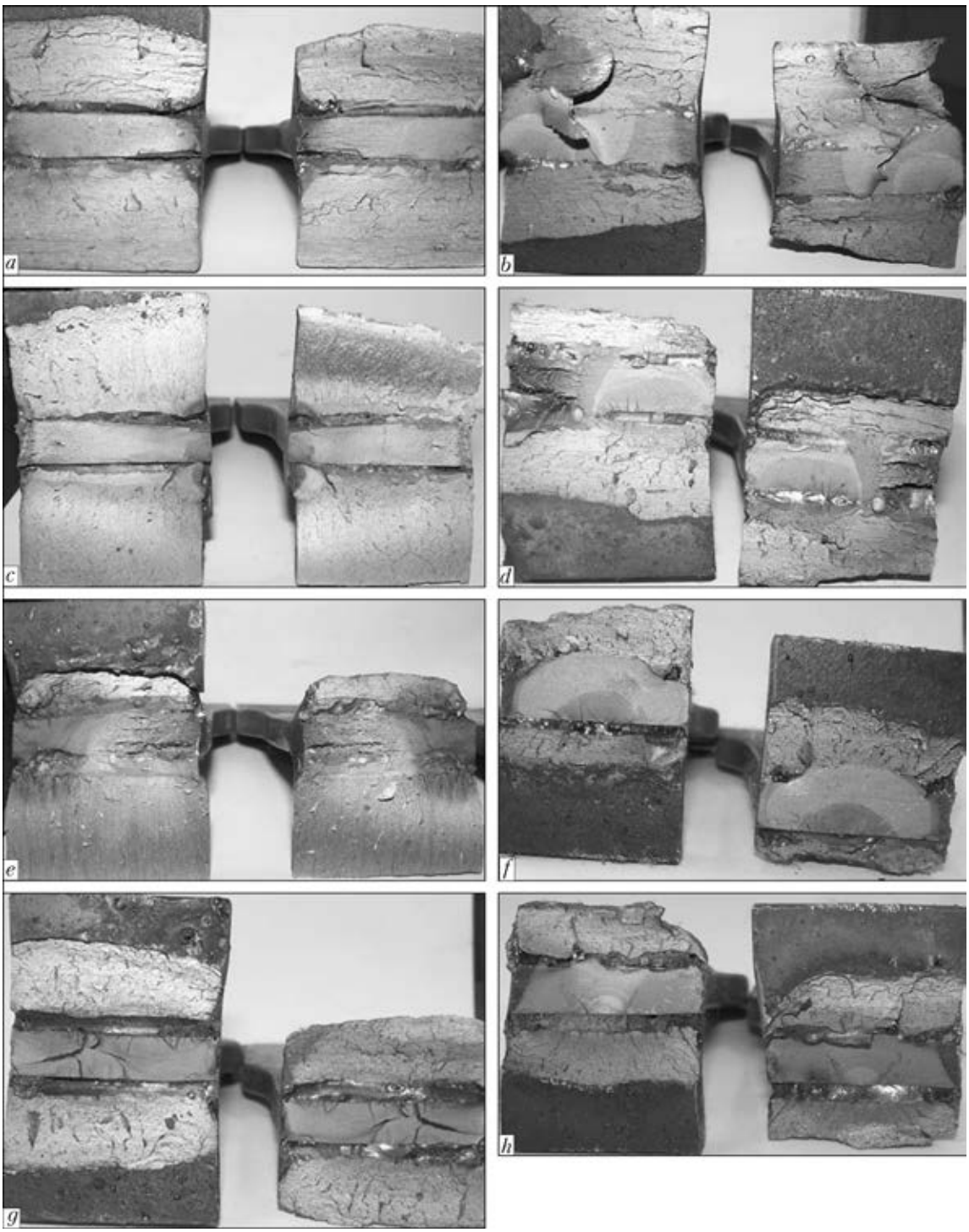

**Figure 4.** Fatigue fractures of welded T-joints with lack of root penetration: *a–h* — specimens 1–8, respectively

development of cracks in the rib and performance of welding of one rib virtually with full penetration as can be seen from Figure 4, *g*.

Specimen 8 was tested under conditions of block loading with quasirandom order of load application in each block (see Figure 2, *c*). The failure of the specimen took place after 54.4 thou cycles on second step of the third block of loading (total amount of cycles up to failure at all cycles of loading was 58.26 thou cycles). Welded specimens with full penetration strengthened by HFMP failed along the fusion line in a range of 578.2–737.8 thou cycles of stress change [12] at similar tests.

Visual analysis of the fatigue fractures of welded T-joints (see Figure 4) showed that the lacks-of-penetration were successfully embedded along the whole width (length of the weld) of the specimens from two sides immediately under the welded ribs in a course of their manufacture, except for specimen 7. Consistency of geometric dimensions of lacks-of-penetration is also hold in

a range of 2–3 mm (in height as well as in width) virtually along the whole length of the weld in all specimens.

Obtained results showed that the life of welded T-joints strengthened by HFMP with extensive lacks-of-penetration (cross section 3 × × 3 mm) is in a range of spread of experimental data of the specimens with full penetration. This can be explained in the following way.

Development of cracks in the specimens with lacks-of-penetration takes place in the base metal as well as in the rib metal (see Figure 4) while such a development happens only in the base metal along the fusion line in the specimens with full penetration as shown by the results of fractography analysis of the fatigue fractures of the tested specimens. Development of the fatigue crack takes place at lower stresses from external loading due to larger cross section of its development (considering height of the welded ribs) regardless that its nucleation from the lack-of-penetration can happen earlier than in zone of weld transfer to base metal. At that one of its tips develops in weakly loaded rib. Therefore, the failure in lack-of-penetration zone takes place less intensively, virtually, providing no reduction of the life of the joint in comparison with the life of defect-free joints up to complete failure. Significant part of determined fatigue life in the welded joint with lack-of-penetration falls at growth of fatigue crack in the base metal and in metal of welded rib (see Figure 4). Thus, critical crack depth in zone of weld transfer to base metal lies in the range of 4–8 mm in the welded joints with full penetration, while that achieves 12–20 mm in a moment of brittle fracture in strengthened joints with lack-of-penetration.

Such a peculiarity of kinetics of fatigue fracture of T-joints, ribs of which do not transfer main load, strengthened by HFMP and having lack-of-penetration allows significantly increasing their fatigue life using HFMP. At that, the indices of fatigue strength of the joints strengthened by HFMP with lack-of-penetration are at the level of that of strengthened welded joints made with full penetration.

**Conclusions**

1. It was stated that presence of extensive (along the whole length) lack of root penetration of 3 × × 3 mm cross section in the unstrengthened high-loaded welded T-joints, the cross ribs of which do not transfer main load, provides no effect on fatigue life since formation of cracks, and their development take place in the zone of weld transfer to base metal.

2. It was shown that the fatigue life of high-loaded HFMP-strengthened T-joints from low-alloyed steel containing structural and technological extensive lacks of root penetration of 3 × × 3 mm cross section lies in the range of spread of experimental data for strengthened joints made with full penetration. At that, fatigue life of strengthened joints with lacks of penetration increases up to 10 times in comparison with that of unstrengthened specimens with full penetration.


1. Trufyakov, V.I. (1973) *Fatigue of welded joints*. Kiev: Naukova Dumka.
2. (1990) *Strength of welded joints under alternating loadings*. Ed. by V.I. Trufyakov. Kiev: Naukova Dumka.
3. Trufyakov, V.I., Kyrian, V.I., Knysh, V.V. et al. (1988) *Carrying capacity of welded joints with technological defects*: Manual. Moscow: Mashinostroenie.
4. Xiaohui Zhao, Dongpo Wang, Lixing Huo (2011) Analysis of the *S–N* curves of welded joints enhanced by ultrasonic peening treatment. *Materials & Design*, 32(**1**), 88–96.
5. Abston, S. (2010) The technology and applications of ultrasonic impact technology. *Austral. Welding J.*, **55**, 20–21.
6. Danqing Yin, Dongpo Wand, Hongyang Jing et al. (2010) The effects of ultrasonic peening treatment on the ultra-long life fatigue behavior of welded joints. *Materials & Design*, 31(**7**), 3299–3307.
7. Marquis, G. (2010) Failure modes and fatigue strength of improved HSS welds. *Eng. Fract. Mech.*, **77**, 2051–2062.
8. Kudryavtsev, Y., Kleiman, J., Lugovskoy, A. et al. (2007) Rehabilitation and repair of welded elements and structures by ultrasonic peening. *Welding in the World*, 51(**7/8**), 47–53.
9. Kuhlmann, U., Durr, A., Gunther, P. et al. (2005) Verlaengerung der Lebensdauer von Schweisskonstruktion aus hoeherfesten Baustaehlen durch Anwendung der UIT-Technologie. *Schweissen und Schneiden*, 57(**8**), 384–391.
10. Knysh, V.V., Valteris, I.I., Kuzmenko, A.Z. et al. (2008) Corrosion fatigue resistance of welded joints strengthened by high-frequency mechanical peening. *The Paton Welding J.*, **4**, 2–4.
11. Knysh, V.V., Solovej, S.A., Kuzmenko, A.Z. (2008) Accumulation of fatigue damage in tee welded joints of 09G2S steel in the initial condition and after strengthening by high-frequency mechanical peening. *Ibid.*, **10**, 10–15.
12. Knysh, V.V., Kuzmenko, O.Z., Solovej, S.O. (2009) Accumulation of fatigue damage in tee welded joints in initial condition and after strengthening by high-frequency mechanical peening under block loading. *Mashynoznavstvo*, **9**, 27–31.
13. Troshchenko, V.T., Sosnovsky, L.A. (1987) *Fatigue resistance of metals and alloys*: Refer. Book. Pt 1. Kiev: Naukova Dumka.


Received 14.11.2012

# In Memory of Prof. Vladimir I. Makhnenko

In January 2, 2013 Makhnenko Vladimir Ivanovich, Doctor of Technical Sciences, Professor, Academician of the NAS of Ukraine, Honored worker of science and technology of Ukraine, laureate for the State Prize of Ukraine, has gone on the 82nd year of his life.

V.I. Makhnenko was born in Cherkassy city. After graduation from the Odessa Institute of Navy Engineers (now Odessa National Navy University) in 1955 he started his industrious activity at the ship-building plant in Arkhangelsk. He worked as a serviceman and then as a senior technologist of the hull-welding workshop of the plant «Krasnaya Kuznitsa».

In 1959 he entered the post-graduate courses of the Odessa Institute of Navy Engineers and successfully defended a thesis for the Candidate's degree in 1963. In 1964 he was invited to work at the E.O. Paton Electric Institute, where directly with his participation and on the initiative of B.E. Paton the Department of mathematical methods of study of physical and chemical processes in welding and special electrometallurgy was founded and headed by him till the last days of his life. The task of the Department was the wide application of computer engineering and numerical methods, actively developing in the world, for effective processing and analysis of the results of complicated experimental studies of the phenomena, arising during the welding, and also their mathematical description with the purpose of obtaining optimal technological and design parameters.

In 1973 he defended a thesis for Doctor's degree, in 1978 he was elected as a correspondent-member and in 1990 as an academician of the AS of the UkrSSR.

The course of life of V.I. Makhnenko is closely connected with welding science. These are the years of fruitful fundamental investigations, when his inexhaustible diligence, purposefulness, sense of innovations and scientific intuition were fully revealed. V.I. Makhnenko together with his disciples founded a school on mathematic modeling of heat, diffusion, deformation, electromagnetic and other physical phenomena in welding and related technologies, which is well known both in his country and abroad.

The works of V.I. Makhnenko on prediction of the complex of physical parameters in welding of modern structural materials, which determine the quality of welded joint and operability of welded structure: sizes, shape, chemical composition and structure of penetration zone, thermal cycles, microstructure and properties of metal of heat-affected zone, kinetics of stresses, deformations and displacements in the process of welding heating, risk of cold and hot cracks formation, distribution of residual stresses and their influence on marginal state of welded units at static or variable external loads, were highly recognized in the world. Basing on these theoretic works together with different branch research institutes and industrial enterprises the optimal variants of design and technological solutions for a number of welded structures were developed.

In the recent years V.I. Makhnenko actively worked on the actual problem of evaluation of operability and life of safe operation of welded structures and constructions including objects of power engineering of Ukraine and main pipelines. The methods of evaluation of accessibility of revealed defects within the frames of ideology of «prediction and prevention» in the whole number of cases made it possible to refuse from untimely repairs of critical welded structures. In particular, he grounded the possibility of repair of main pipelines under their operating conditions. The result of fruitful developments in this direction is monograph «Life of Safe Operation of Welded Joints and Units of Modern Structures», published in 2006, and also the State Prize of Ukraine in science and technology of 2008.

Under the management of V.I. Makhnenko within many years the international conferences «Mathematical Modelling and Information Technologies in Welding and Related Processes» were

held, where specialists from different countries of the world took place.

V.I. Makhnenko is the author of more than 370 printed works, 112 of which are published in the journal «Avtomaticheskaya Svarka», 12 monographs. Many of his works were published in USA, England and Germany. Prof. Makhnenko lavishly shared his knowledge with youth and constantly paid attention to education of scientific staff. From the moment of foundation of the Chair of physical metallurgy and materials science of the Moscow Institute of Physics and Technology in 1988 Prof. Makhnenko delivered course of lectures «Strength of Welded Structures and Joints» to the students. Under his leadership 5 Doctors and 24 Candidates of Technical Sciences were prepared.

V.I. Makhnenko combined the fruitful scientific work with scientific-organizational and social activity, being the leader of section of the Scientific-Coordination Council on the problems of life and safe operation of structures, constructions and machines of the NAS of Ukraine, member of editorial board of the journal «Avtomaticheskaya Svarka».

V.I. Makhnenko was decorated with the awards of Friendship of Nations, For Merits of the III and II degrees and also medals. The international acknowledgement of merits of V.I. Makhnenko in welding science found the reflection in his election to the American Welding Society and member of International Federation of Quantity Non-Destructive Methods of Examination. In 2004 V.I. Makhnenko was decorated with the merit award «Merit worker of science and technology of Ukraine» for significant investment into development of national science and technology in the direction of creation of modern welded structures and guarantee of life of their operation.

Due to his talent, spiritual warmth and tenderness, benevolence and modesty, the scientist gained authority and respect among the welding society. Many disciples, friends and colleagues take this loss with deep sorrow, express sincere condolence to family and relatives of Vladimir I. Makhnenko everybody who was acquainted with him, loved and respected him. Bright memory shall always remain in their hearts.

*E.O. Paton Electric Welding*
*Institute of NASU*
*Editorial Board*
*of «The Paton Welding Journal»*

## *NEWS*

### *Glass Backing for Weld Back Bead Formation in Manual and Mechanized Arc Welding*

Glass backing is used for submerged-arc, stick-electrode and gas-shielded arc welding of root welds. Sticke-lectrode and gas-shielded welding can be performed in site in various positions.

*Applications*. Site welding in construction, shipbuilding, tank and bridge construction and other sectors.

*Technical and economic advantages*. The cost is reduced through application of glass as backing material instead of the regularly applied more expensive ceramic backing. Glass backing does not absorb moisture from the atmosphere, unlike the ceramic one, and, therefore, it has no limitations on storage conditions and does not require preliminary baking before welding. Replacement of two-sided welding by welding with application of glass backing allows improvement of welded joint quality due to prevention of burns-through and lacks-of-penetration. An improvement of labour conditions is achieved owing to elimination of welding in closed volumes under constrained conditions.

*Efficiency*. An improvement of welding efficiency is achieved due to elimination of the operation of gouging the root part of the first weld, which is used in welding from both sides.

*Return-on-investment*. Introduction of welding with application of glass backing, instead of welding from both sides with intermediate gouging of the root weld, allows saving 43.2 UAH per one running meter of weld owing to reduction of labour consumption of the operations, reduction of deposited metal volume, and shortening of construction time. Replacement of ceramic backing by glass one allows saving 42.6 UAH per one running meter of weld through lowering of backing cost.

*State of development*. Ukrainian specification was developed, manufacturing of commercial batches of backing is organized. Testing of welded joints made with application of glass backing was conducted. Charpy impact bending tests showed that at −20 °C testing temperature the impact energy is not less than 52 J.

# NEWS

## *Technology and Equipment for Continuous Ultrasonic Welding of Polymeric Materials*

In manufacture of products of polymeric film materials it is necessary to provide their rapid and reliable joining. The most effective method of joining these materials is the continuous ultrasonic welding (USW). It guarantees the producing of continuous long welds by a relative movement of material being welded and a waveguide (tool). As to the degree of mechanization, the continuous USW is divided into manual and mechanized. Here, depending on the method of a relative movement of material and waveguide the step-seam and seam welding are distinguished. In its turn the seam welding can be performed by a rotating waveguide for pulling or at the rotating roller-support.

*Manual welding*. To produce welds of any extension and configuration, an acoustic head is moved manually and the workpiece remains fixed. As in USW a local heating of the welding zone is occurred, then the given method is effective in sealing the tare with food products or highly inflammable substances, and also in welding of products, whose edges to be welded are covered with oil, solutions of salts, acids and others. In this case, there is no need in preliminary cleaning of the surfaces being welded due to a specific effect of ultrasound on welding zone.

Installation for manual USW consists of an ultrasonic generator and acoustic head, composed of a piezo-electric converter and waveguide with changeable tips. Tips have a special sharpening that allows producing welds of different width, making cutting of several layers of synthetic fabrics or films; simultaneous cutting through and welding of materials in production of clothes elements. The output capacity of the installation is 200 W, operating frequency is 20 kHz.

This installation makes it possible to join polypropylene and polyamide films, multilayer packs of polyethyleneterephthalate, and also films, having metallized, photoemulsion or ferrovarnish coating without their preliminary removal. The obtained width of weld is 1–5 mm at thickness of films from 10 up to 500 μm.

**Figure 1**

*Step-seam welding*. The material being welded is moved per one step of welding after completion of an operating cycle and each next weld overlaps previous weld partially. This technology is effective in welding of polymeric films, synthetic textures, and also sheet polymeric blanks of up to 3 mm thickness.

The installation for step-seam welding (Figure 1) consists of a pneumatic welding press, ultrasonic generator, control system, control panel, support with a mechanism of fixation and movement of a material being welded, and also a switching unit for the installation connection to electric and pneumatic mains. The installation is equipped with a sensor of linear movements, located by the design on the support of pneumatic press, that makes it possible not only to measure the initial thickness of blanks being welded and residual thickness of weld, but also to use the deformational criteria of dosing the input energy.

The presence of control system allows presetting and control of the following operations and values:

- welding with fixed time of energy input into material being welded;
- welding with use of a deformational criterion of control;
- welding with a dynamic switching on of ultrasound;
- welding with guarantee of constancy of energy supplied into material being welded taking into account the losses of acoustic head at idle operation;
- welding «for pulling» (material is pulled between the oscillating waveguide and support);
- speed of feeding the materials being welded depending on the type of polymer, thickness, number of layers, etc.;
- presetting of upper and lower values of technological parameters;
- recording of parameters of each cycle of welding on printer;
- control of quality of welded joints by determination of deviation from allowable values of main parameters of the USW conditions;
- possibility of inclusion of the installation into the production line.

The output power of the installation is adjusted smoothly within the 100–630 W ranges, operating frequency is 20 kHz. Depending on the technological task the installation is completed with plastic waveguides having the length of an operating surface from 10 up to 300 mm. The installation provides up to 40 welds per minute.

*Seam welding*. The seam welding is realized on the rotating roller-support and can produce rectilinear welds of the unlimited length. The welding speed and weld width

**Figure 2**

are defined by the physical-mechanical properties of the material being welded, number of its layers, requirements to welded joint, etc.

The designed installation represents a functionally-completed unit and consists of:

- a working table;
- pneumatic press;
- rotating acoustic head, composed on the base of a high-quality piezo-ceramics;
- ultrasonic generator, system of feeding the materials being welded, roller-support;
- system of monitoring and control of the technological process.

General view of the installation is shown in Figure 2.

The distinguish feature of the installation is the presence of a rotating acoustic head. This made it possible to widen greatly the assortment of polymeric materials being welded, as there is no sticking of softened polymer on the operating surface of the waveguide during welding that provides in its turn the high quality of welded joints due to absence of burns, weld undercuts, overlaps, etc. in them. Moreover, the presence of a rotating acoustic head and active (resonance) roller-support makes it possible to obtain high strength characteristics of the weld along the entire its length in the multi-layer welding of films, in particular, polyethylene films (Figure 3).

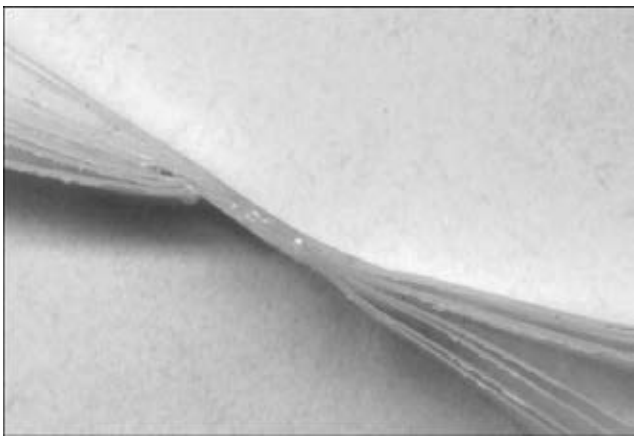

**Figure 3**

The output power of the installations is adjusted smoothly within the ranges of 100–630 W, operating frequency is 20 kHz. Depending on the technological task the installation is completed by changeable waveguides and necessary technological fixture. In USW of laminated polyethyleneterephthalate film of 200–300 μm the welding speed can reach 5–8 m/min.

*Field of application*. The developed technology and equipment provide welding of polyethylene, polyethyleneterephthalate, polyvinylchloride films of 50–1000 μm, used in packing of food products and chemical substances, and also in manufacture of polymeric filters, raincoats, capes, tents, structures of agricultural purpose, etc.

Efficiency of installation for manual USW depends on skill of the operator. The efficiency of step-seam installation is up to 30 welds per minute. The speed of seam USW is 5–10 m/min.

*Status of development*. Installations have been implemented at a number of enterprises of Russia and Ukraine.

# RULES FOR JOURNAL AUTHORS

*«Avtomaticheskaya Svarka» is Published Monthly Since 1948 in Russian, ISSN 005-111X;*
*«The Paton Welding Journal» is Published Since 2000 in English, ISSN 0957-798X*
*(Translation of «Avtomaticheskaya Svarka» Journal Into English)*

**Publication of Articles in Journal is Free of Charge, the Fee is not Paid**

**1.** Standard volume of article shall be 8–10 pages of text including tables, references, 5–6 figures (the volume of review article can be increased up to 12–14 pages). Text shall be printed at 1.5 spacing by Times New Roman, 12 type size.

Information should be described briefly, without repetition of data of tables and figures in the text. References should be given for literature, tables and figures.

Figures should not have the data of secondary importance. Physical units and symbols should be presented using International System of Units SI.

Publication of article will be accelerated if to send it in electron form by E-mail in Word for Windows format. Illustrations shall be presented in separate files in format *.tif (300 dpi) for raster graphics or *.cdr (versions of not higher than 11.0, 600 dpi) for vector graphics.

**2.** The article should not have more than 5 authors (the rest ones, participating in the work, can be mentioned in footnote). Information about author should include affiliation and address, position, scientific title, address, telephone. In addition, the postal address of organization should be given in Russian and English (to take better from official site) and E-mail of one of authors (organization).

**3.** The article should be added with abstract and key words (from 7 to 10). The abstract (of 1400–1600 characters at a single space between words) should completely enough to describe the article content. It should include the aims and tasks, methods, results, field of application, conclusions.

**4.** Each article should have a bibliography list, including of not less than 8–10 references (own works of authors should amount to not more than one/fourth of the list; references to sources since 2000 are obligatory).

The literature cited in the article should be prepared in the following way:

*for books*: name, initials of author(s), full title, city, publishing house, year of edition, total number of pages;

*for journal articles*: name, initials of author(s), title of article, journal, year of publication, number, volume or issue, pages; foreign publications should be given in the language of original;

*for articles in collection*: title of article, authors, name of collection, number of issue (or volume), place of publication, publishing house (or publishing organization), pages of beginning and end of article; for internet-references: name of resource, access mode.

**5.** Manuscript of article should be signed by all the authors (or by one author on behalf of author's group). Manuscript should enclose the license agreement for transfer of the author's rights to the editorial board for the article publication. Form of agreement is given on site: www.paton.kiev.ua or can be sent by the editorial board by E-mail (by request). Non-conformity of materials to the above-mentioned requirements (items 1–5) may serve a reason to refuse a manuscript for publication.

**6.** Authors of the article can receive free of charge one copy of appropriate numbers of journals «Avtomaticheskaya Svarka» and «The Paton Welding Journal» (by request).

Contacts of Editorial Board of Journal «Avtomaticheskaya Svarka» and «The Paton Welding Journal»:
Tel.: (38044) 200-63-02, 200-82-77
E-mail: journal@paton.kiev.ua; www.paton.kiev.ua; www.rucont.ru